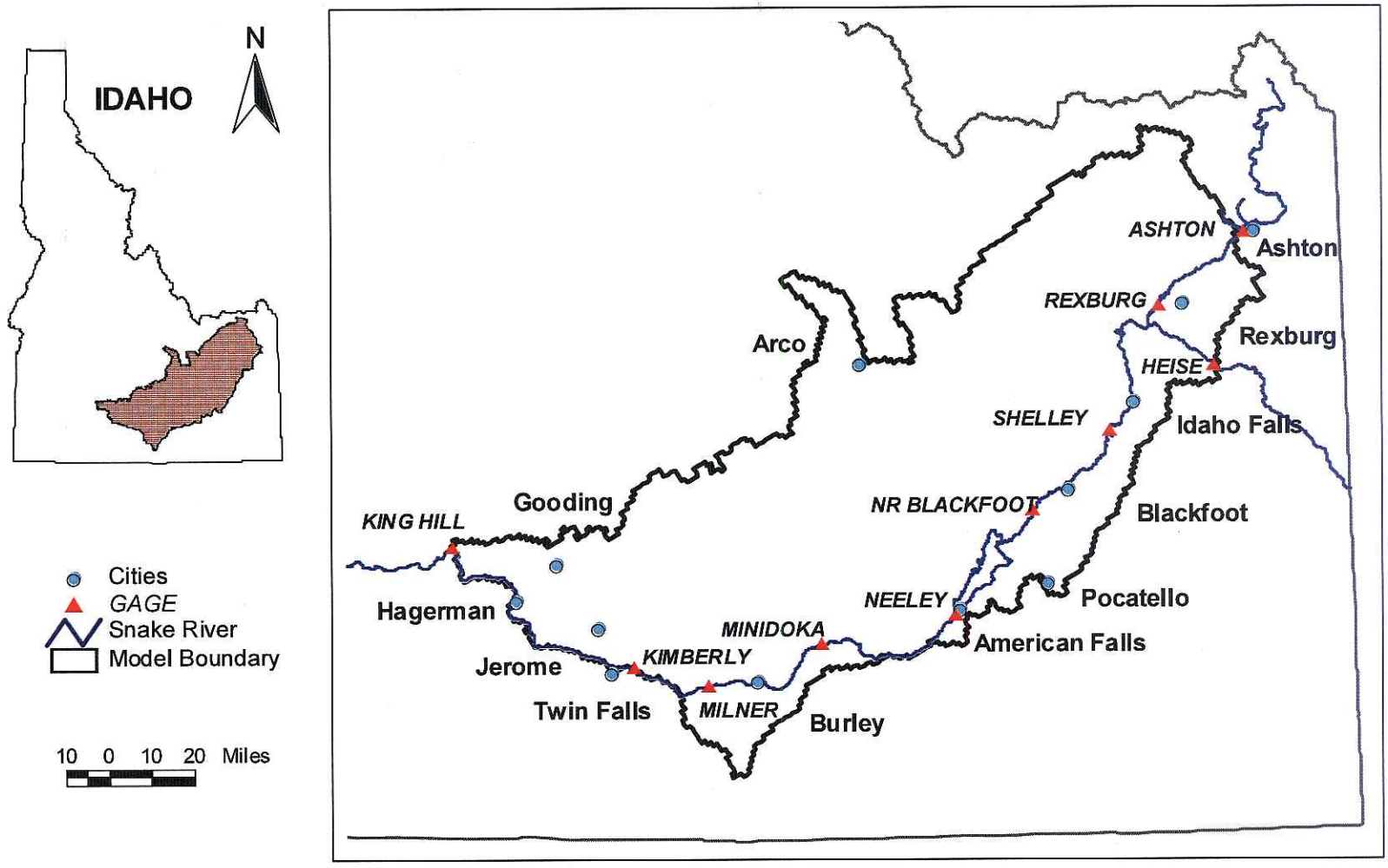


Figure 1. Study area and ESPA model boundaries.

A&B 2930

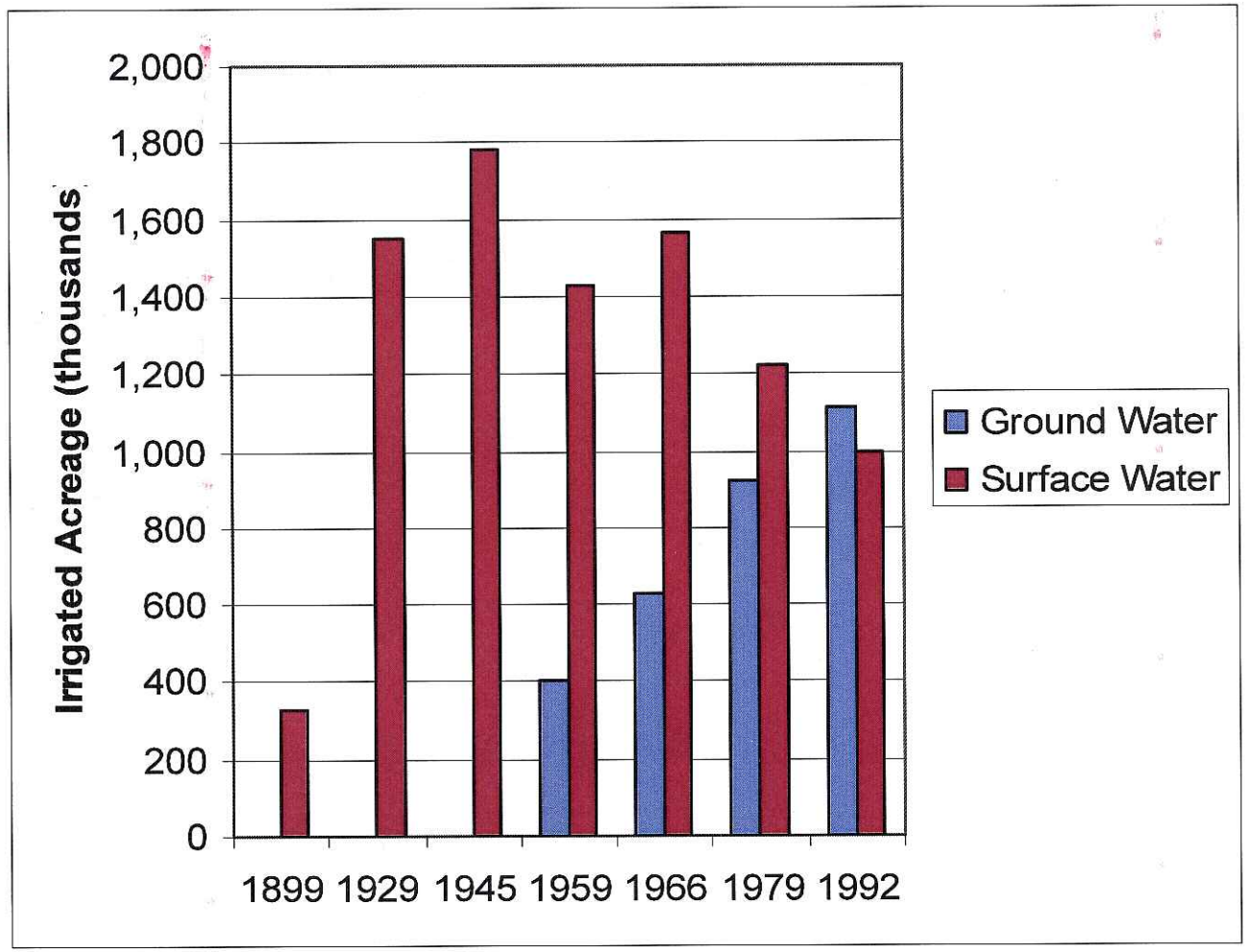


Figure 2. Changes in surface and ground water irrigated acres on the eastern Snake River Plain (after Garabedian, 1992).

A&B 2931

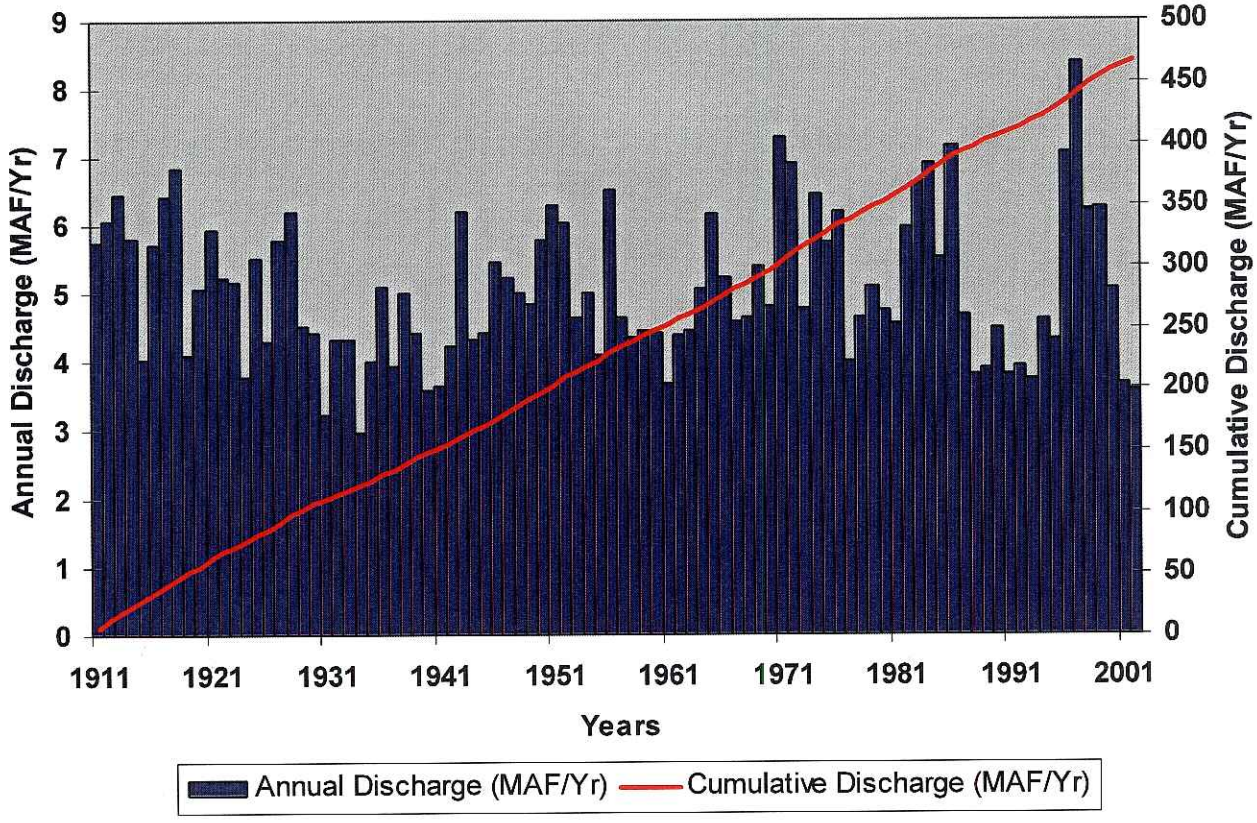


Figure 3. Annual and cumulative discharge of the Snake River near King Hill (U.S. Geological Survey data).

A&B 2932

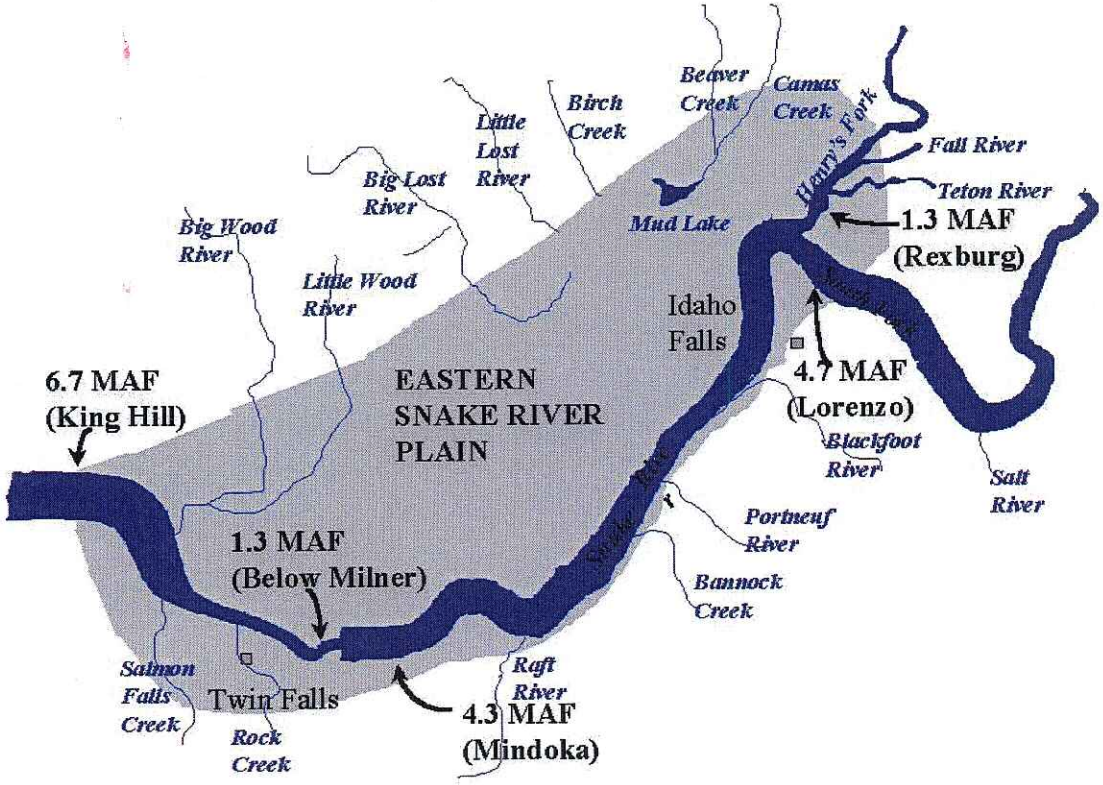


Figure 4. Conceptual illustration of variation in average annual flow of the Snake River (after the U.S. Bureau of Reclamation, 1996).

A&B 2933

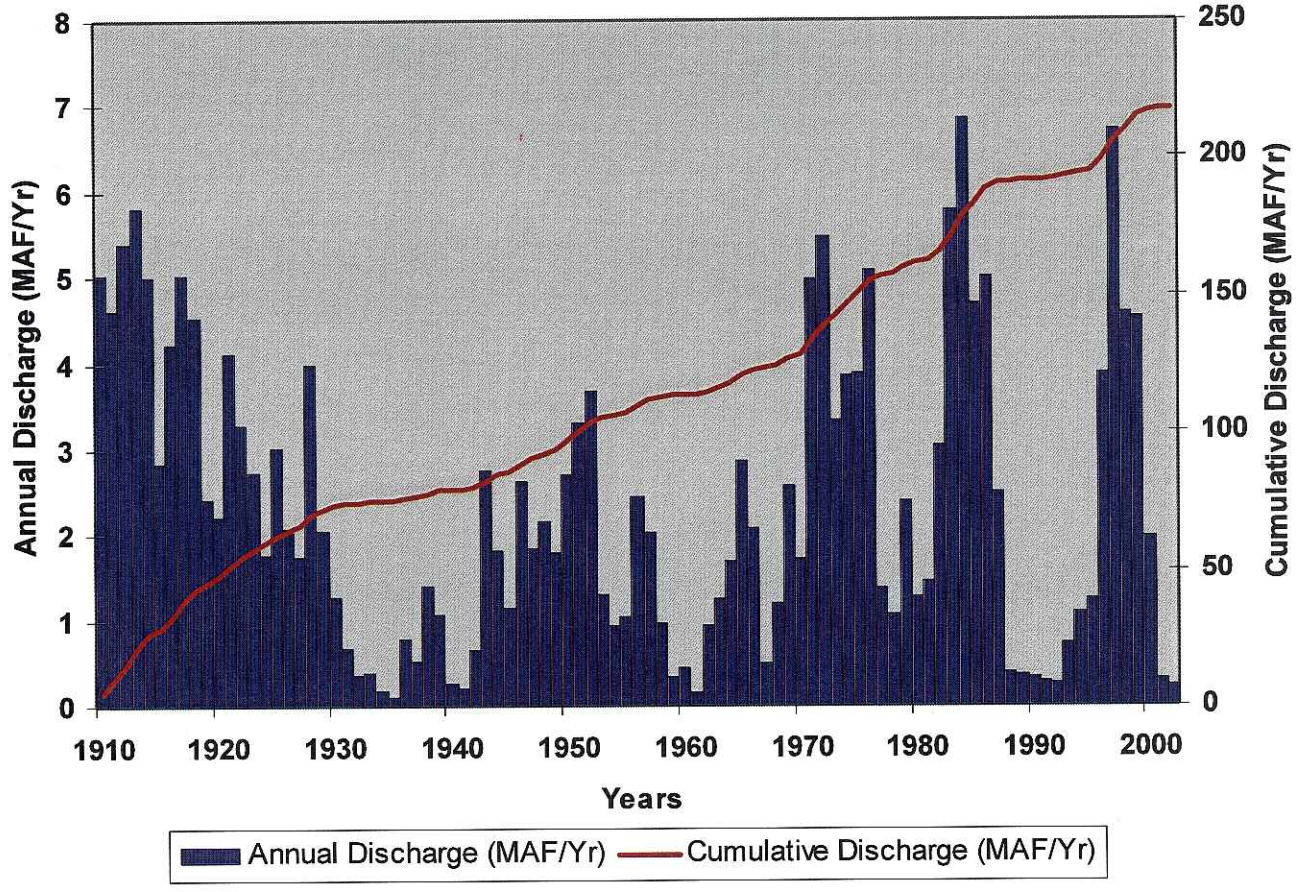


Figure 5. Historic discharge of the Snake River at Milner Dam (U.S. Geological Survey Data).

A&B 2934

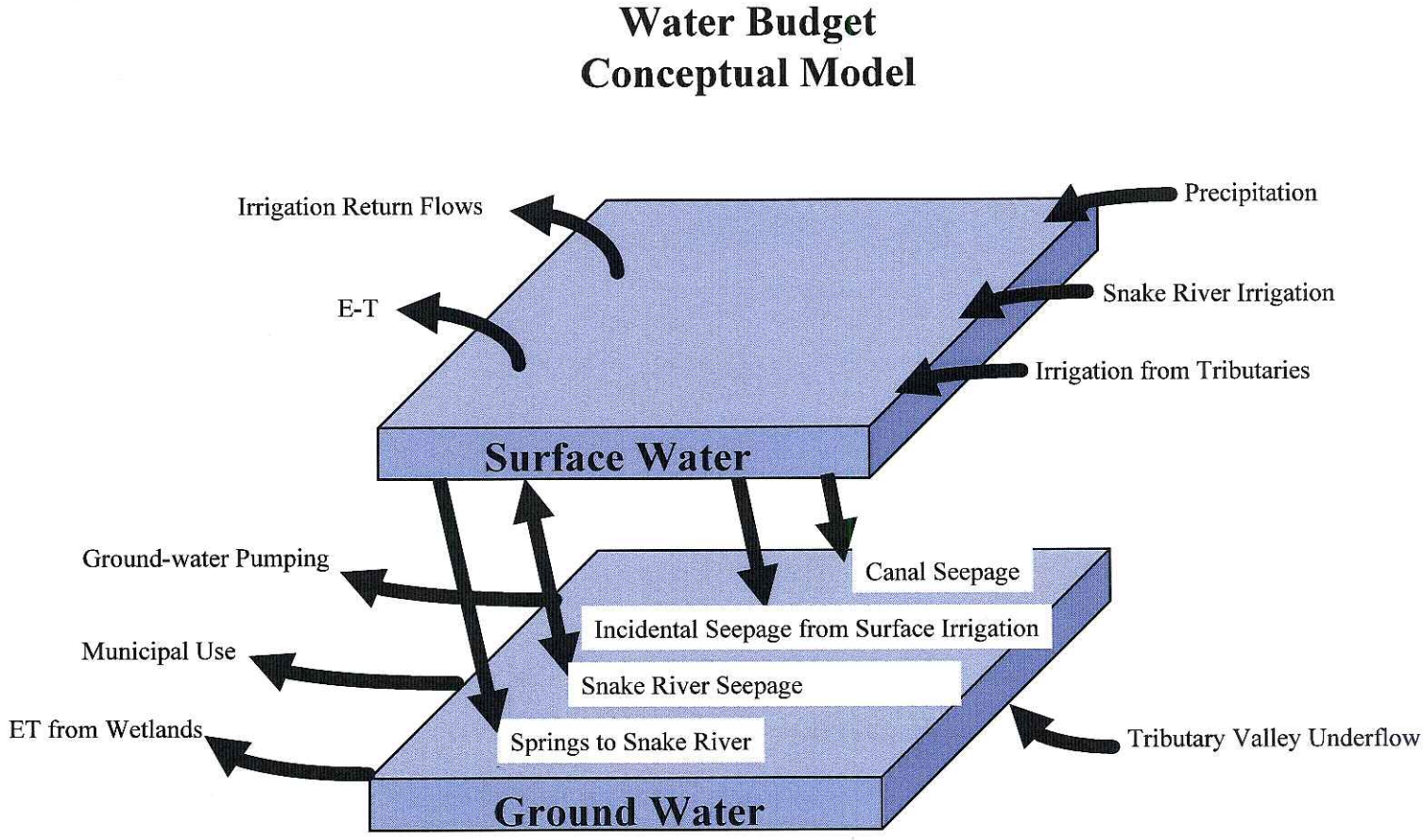


Figure 6. Conceptual water budget for eastern Snake River Plain aquifer.

A&B 2935

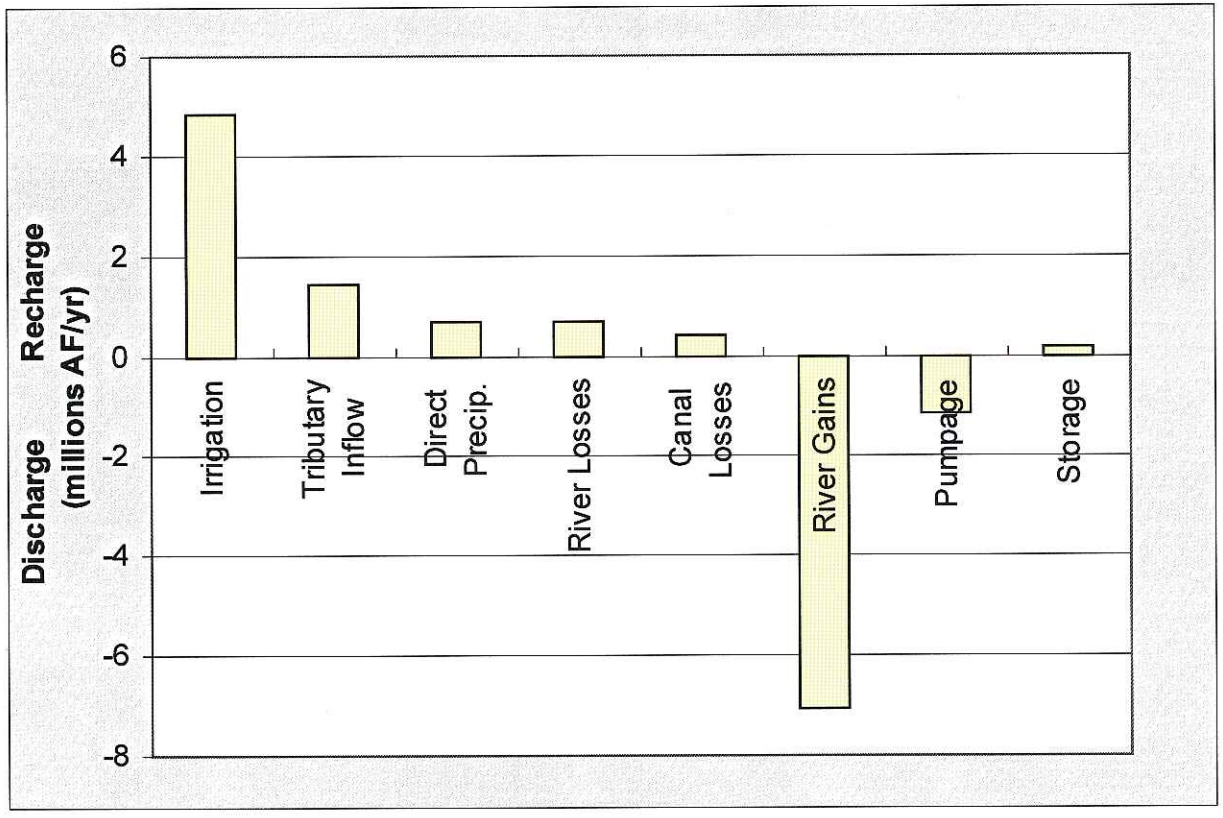


Figure 7. Snake River Plain Aquifer estimated annual recharge and discharge from April 1980 through March 1981 (after Garabedian, 1992).

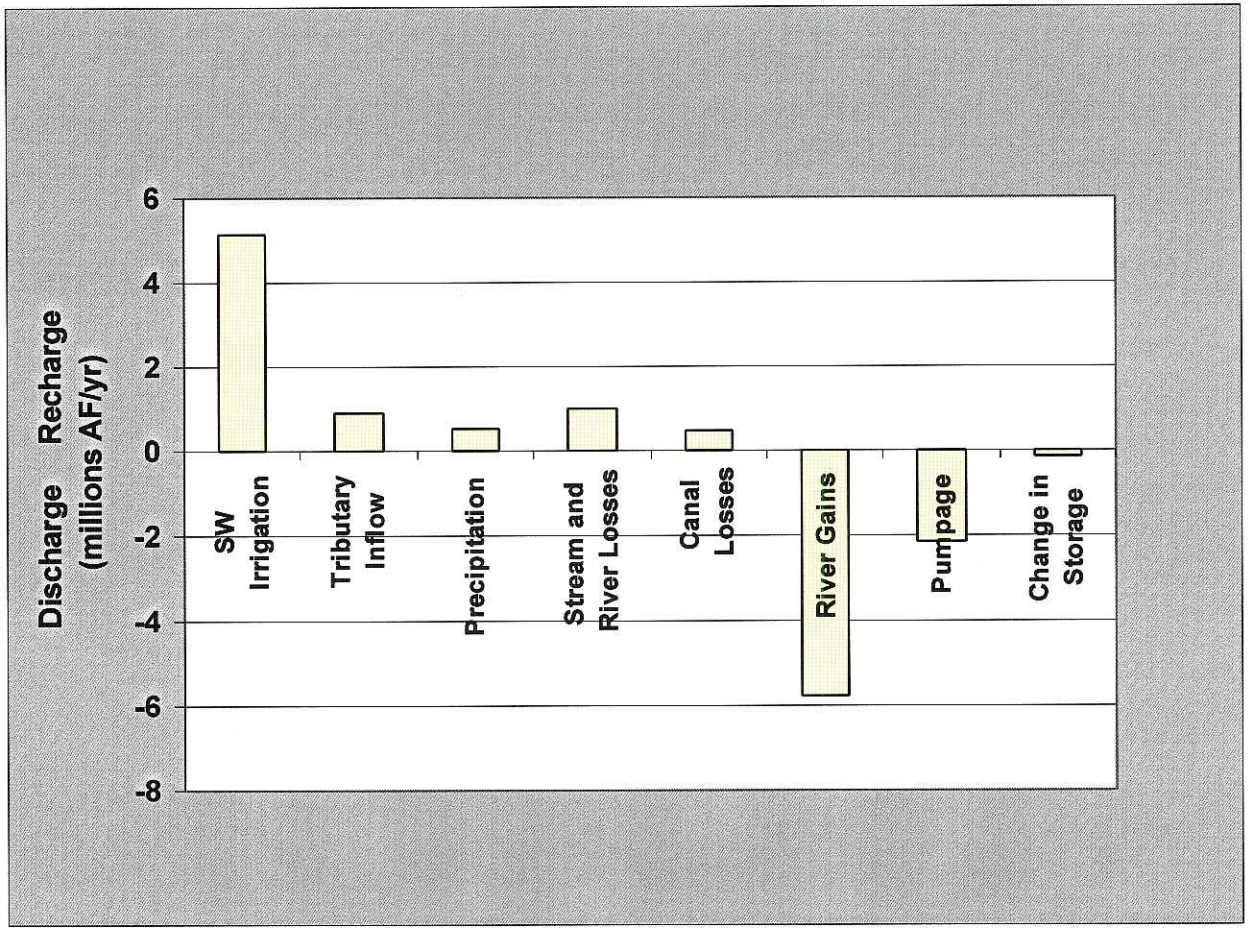


Figure 8. Snake River Plain Aquifer estimated annual recharge and discharge assuming the average irrigation development level of 1980 through 2001 (after IDWR, 1997).

A&B 2937

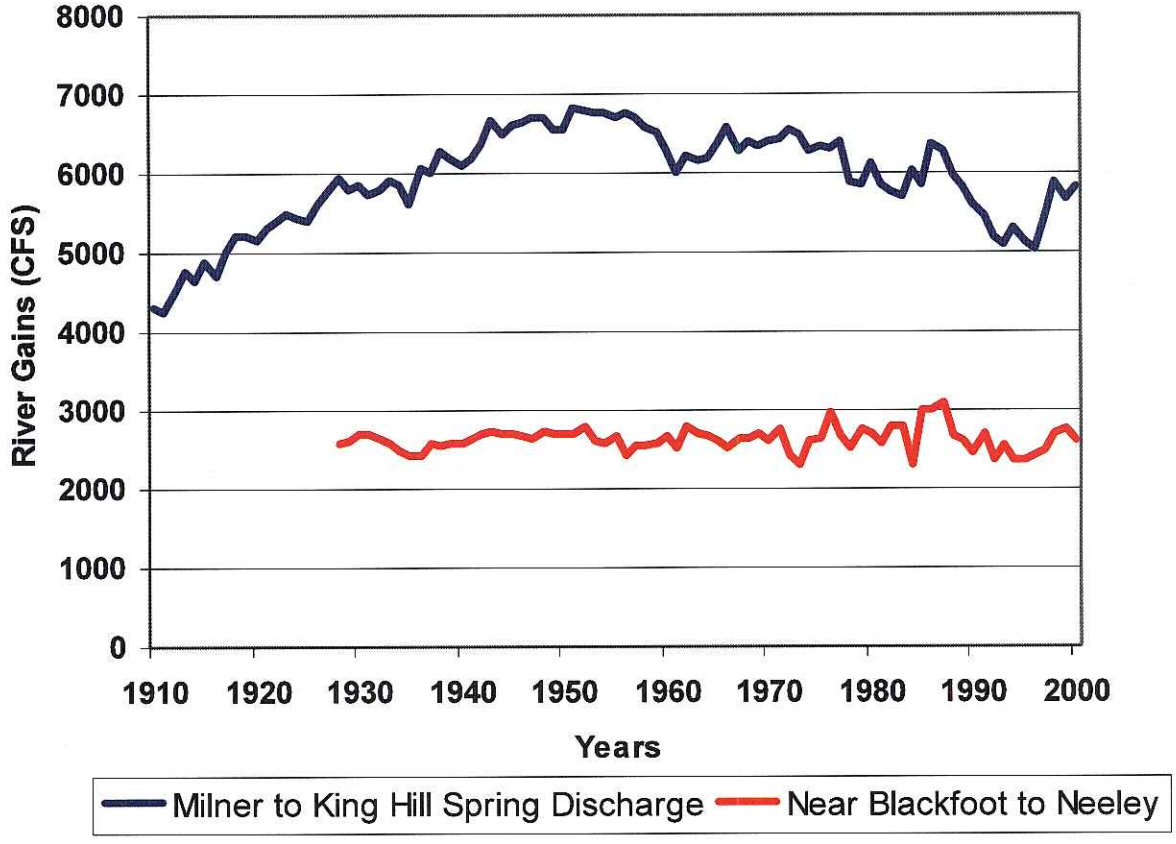


Figure 9. Average annual Snake River gains in the Milner to King Hill and Blackfoot to Neeley reaches. (From IDWR data.)

A&B 2938

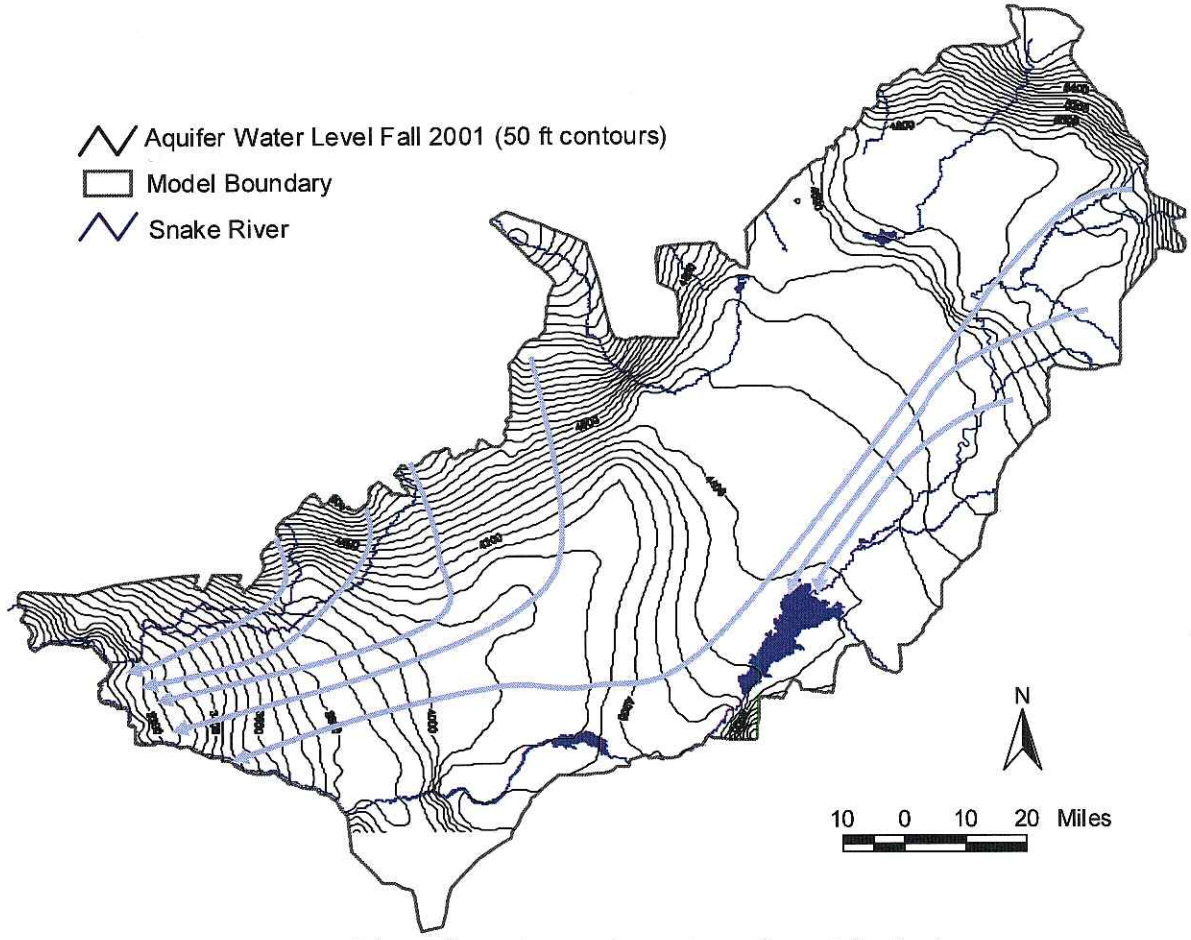


Figure 10. Contours of the Fall, 2001potentiometric surface of the Snake River Plain Aquifer and estimated aquifer flow lines.

A&B 2939

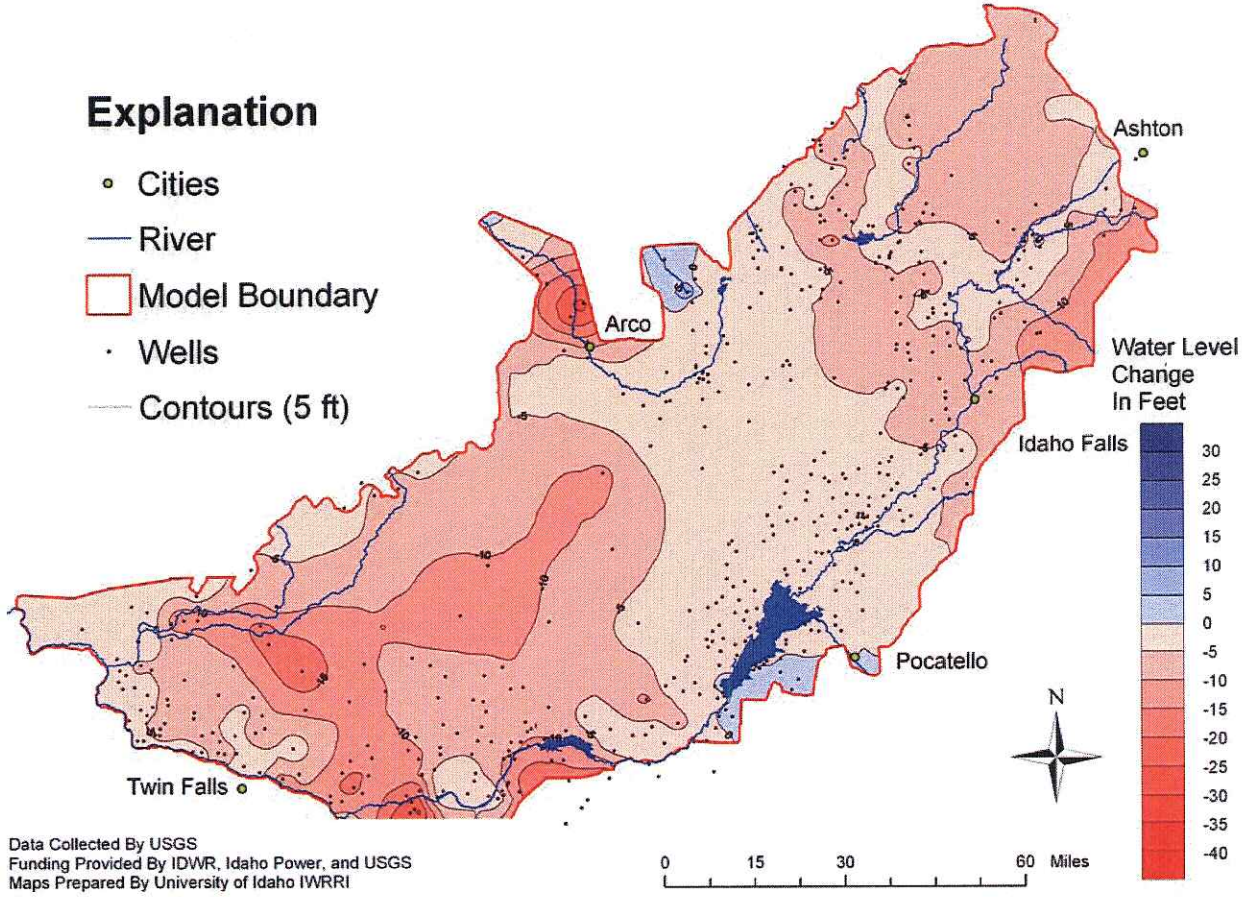


Figure 11. Water level change map spring, 1980 to spring, 2002.

A&B 2940

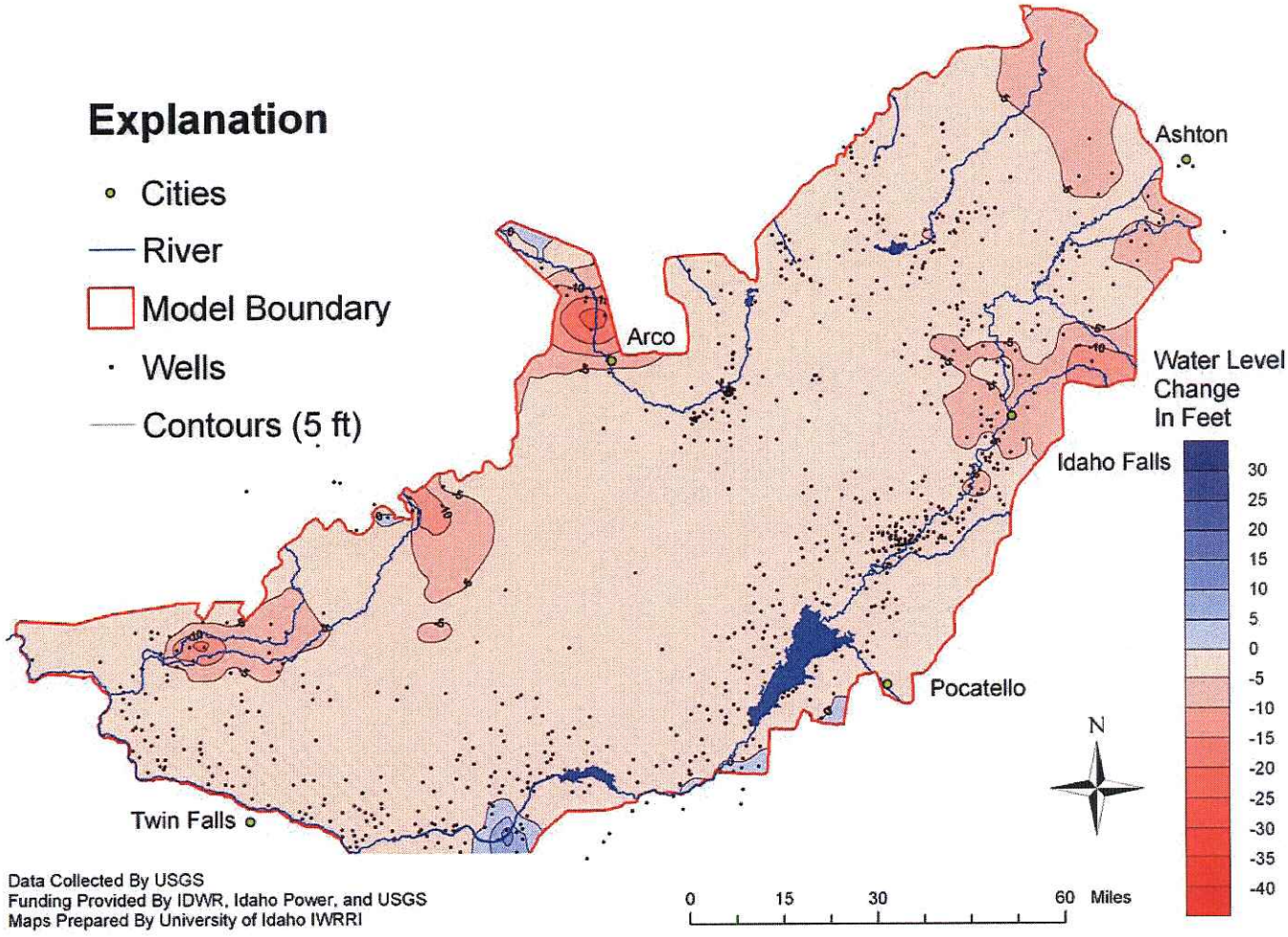


Figure 12. Water level change map spring, 2001 to spring, 2002.

A&B 2941

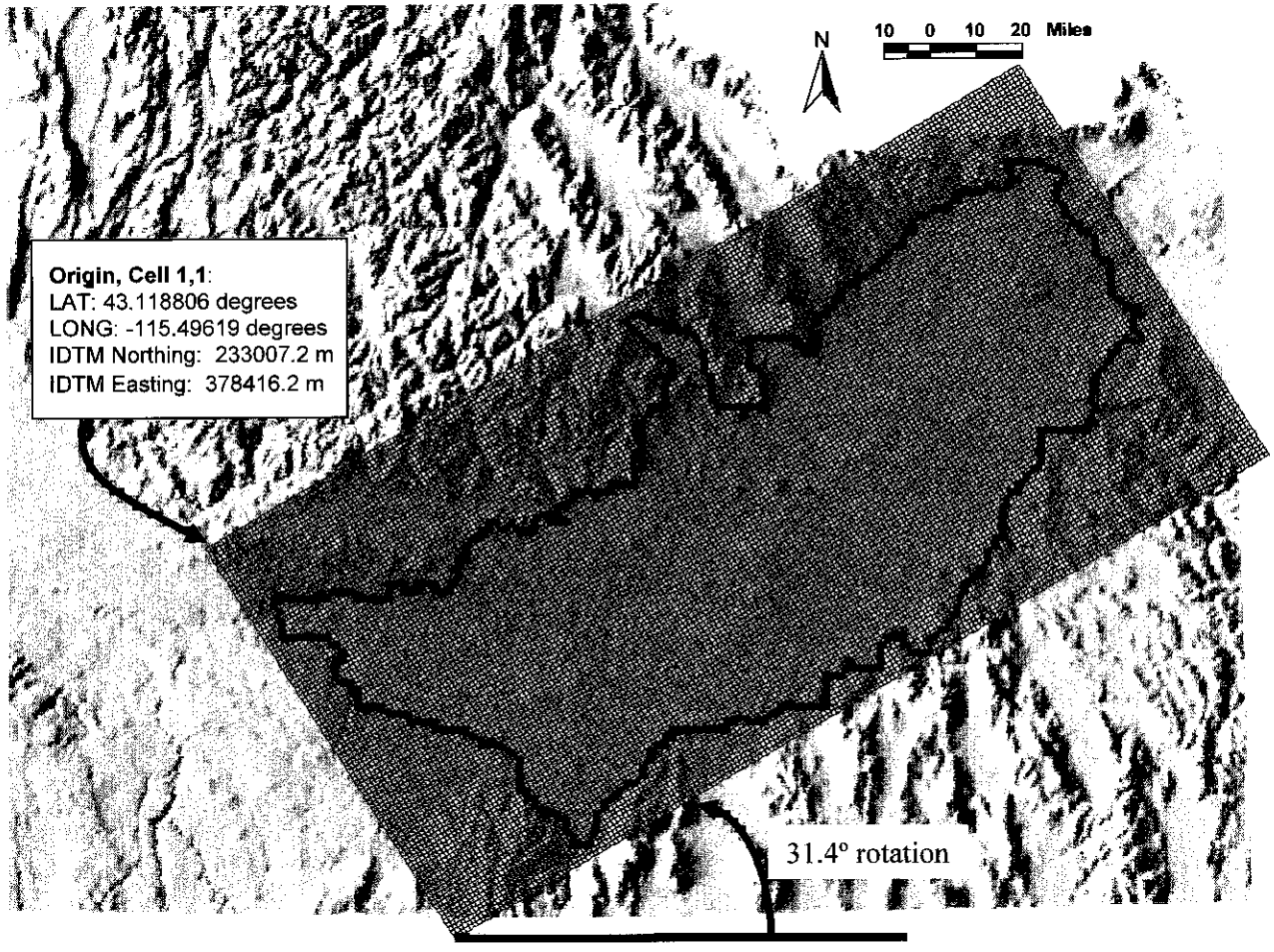


Figure 13. Model grid and origin.

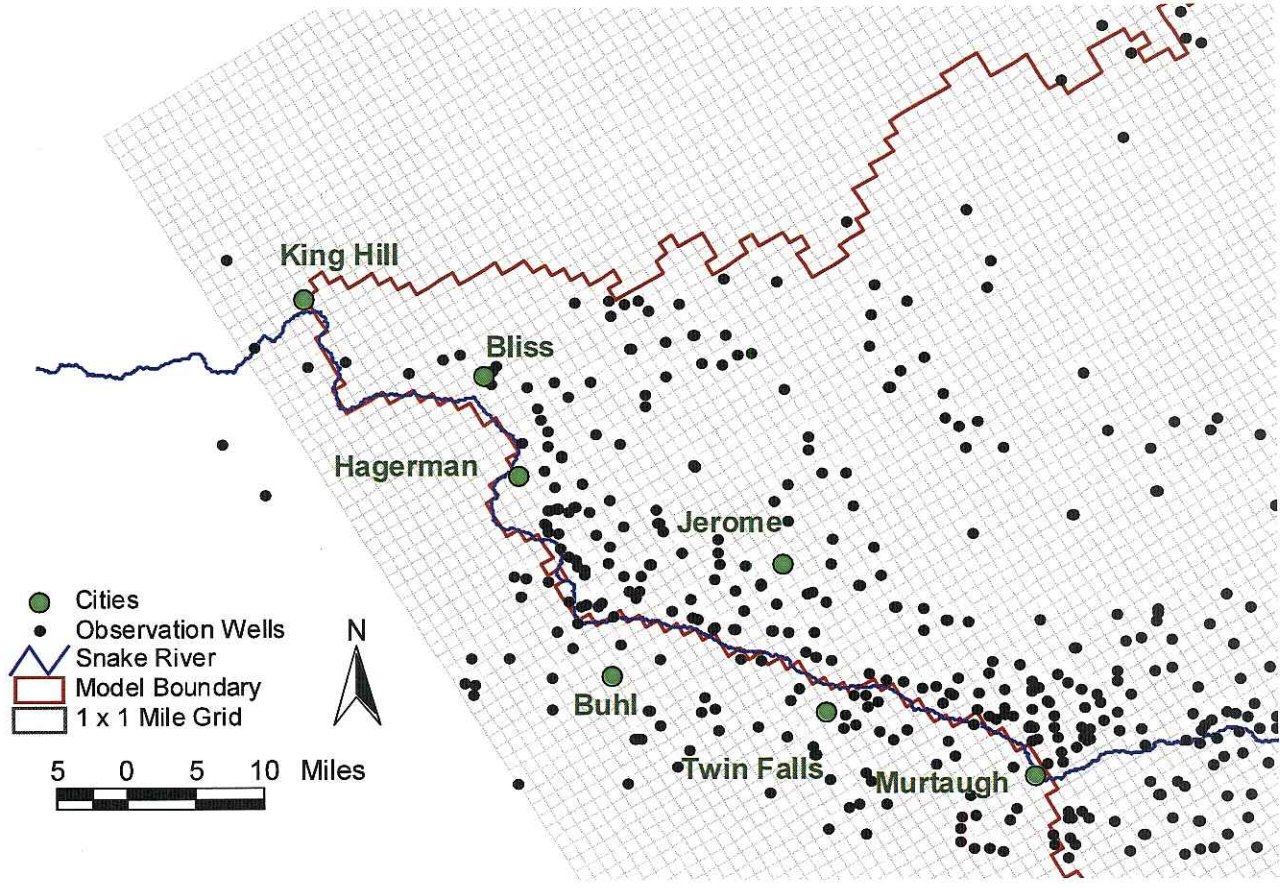


Figure 14. Close-up of model grid in the Thousand Springs area.

A&B 2943

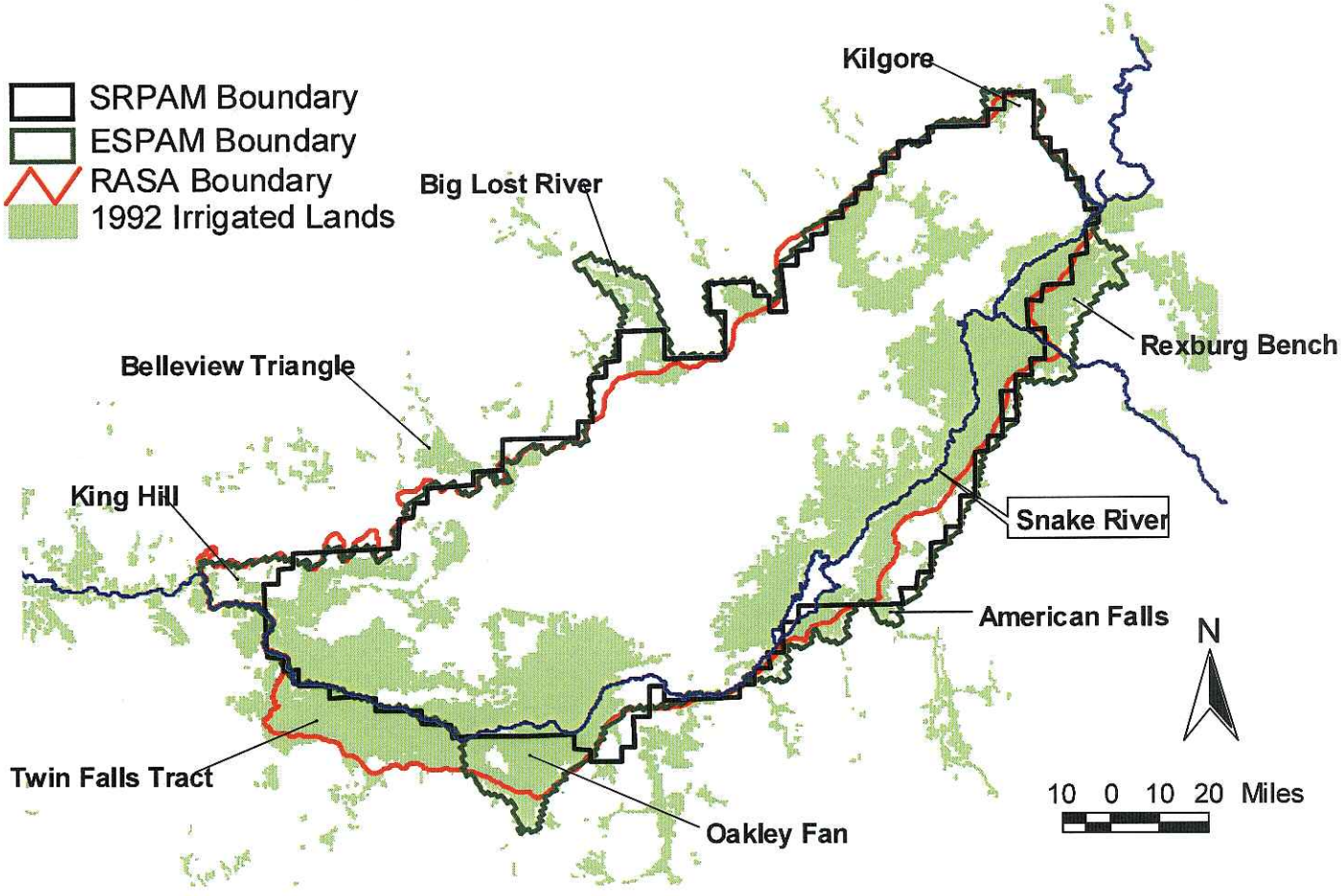


Figure 15. ESPAM model boundary compared with SRPAM and RASA boundaries.

A&B 2944

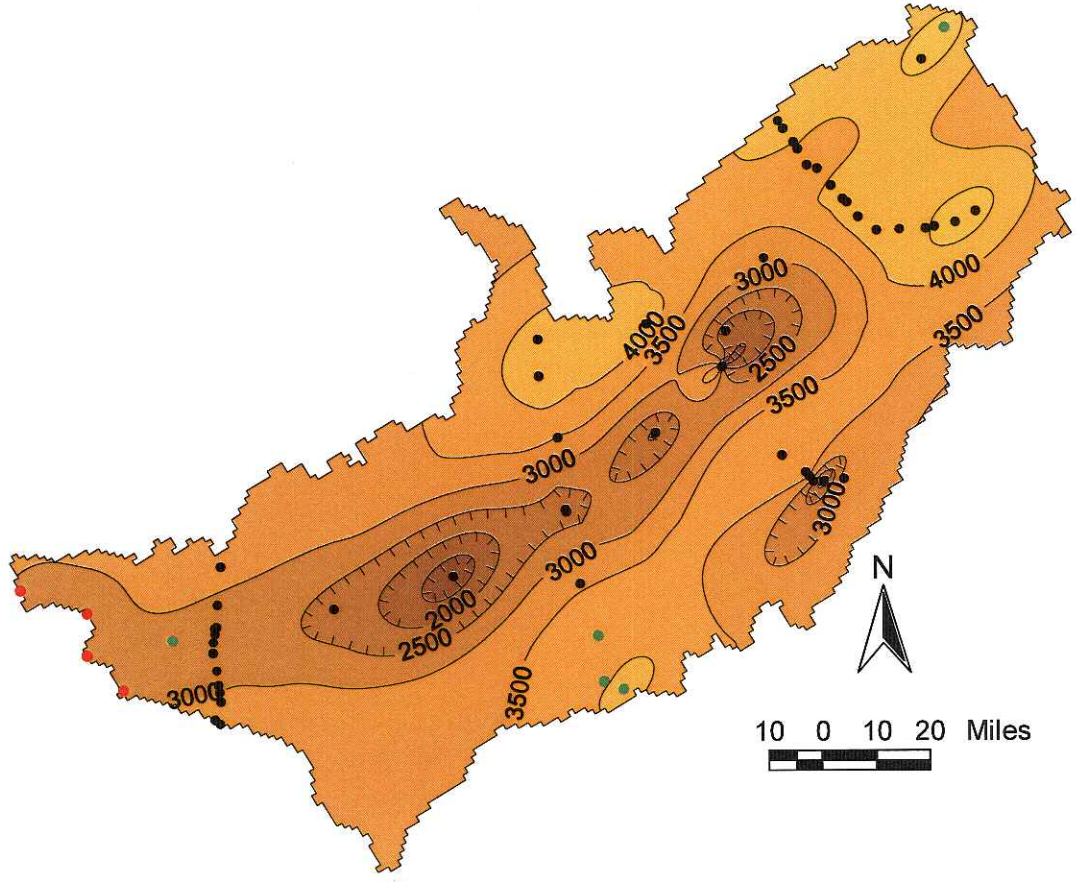


Figure 16. Aquifer bottom elevations with estimated elevation points. Based on modified Whitehead (1986) data. Black dots represent locations used by Whitehead, green dots represent modified Whitehead data points, red dots represent points added to anchor kriged surface.

A&B 2945

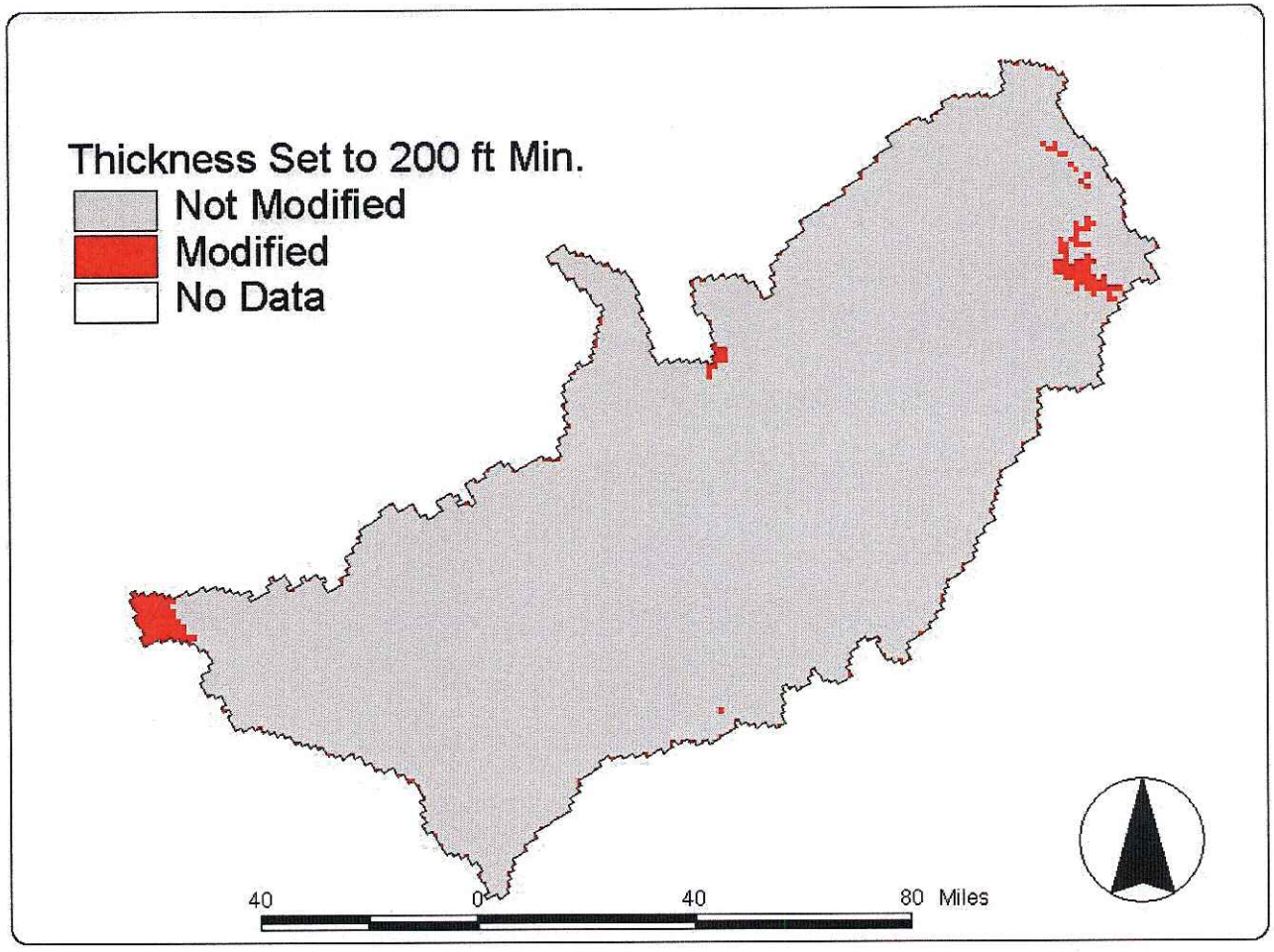


Figure 17. Areas where aquifer thickness was adjusted to 200 feet.

A&B 2946

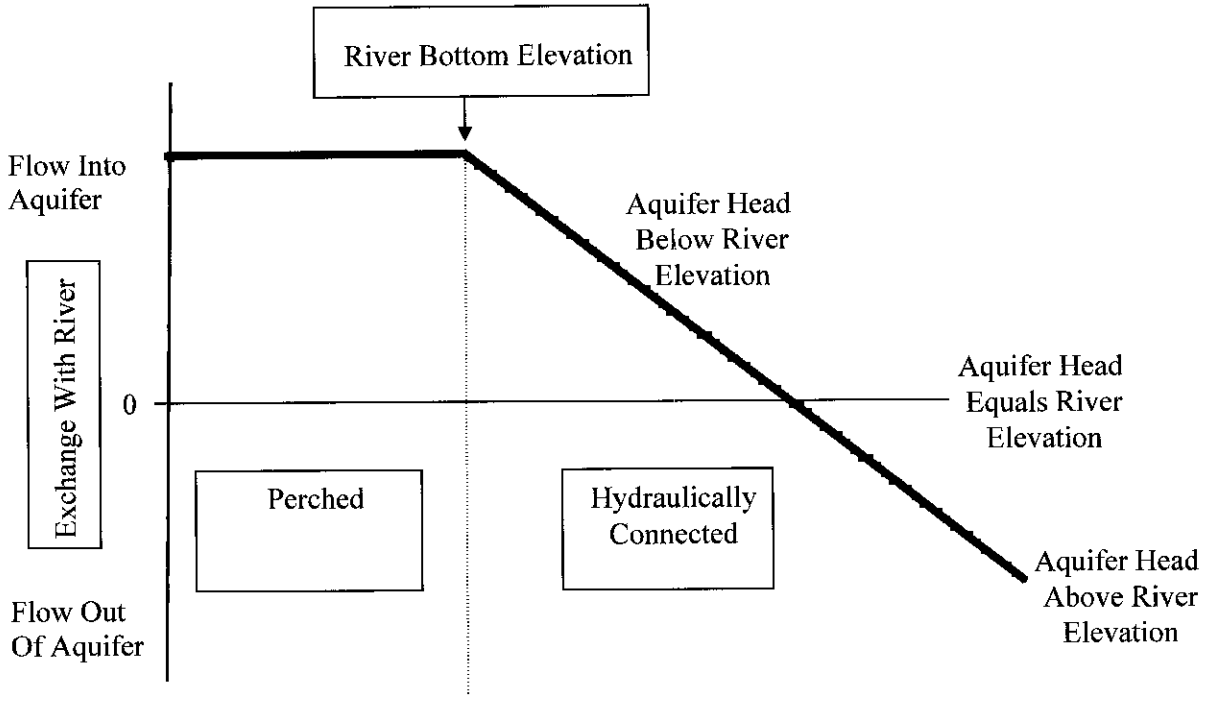


Figure 18. Conceptual illustration of river leakage computation (after McDonald and Harbaugh 1988).

A&B 2947

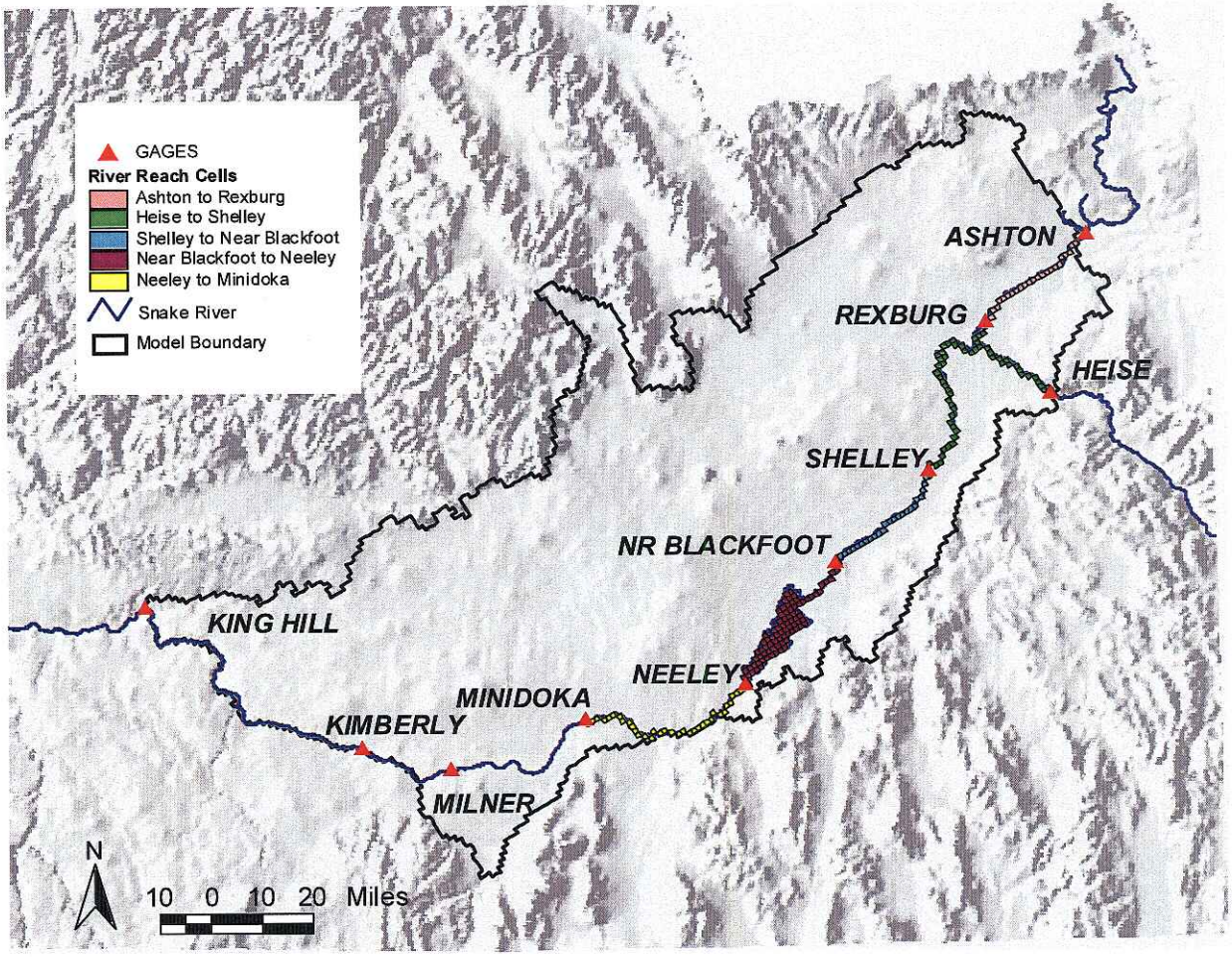


Figure 19. Head-dependent river reaches.

A&B 2948

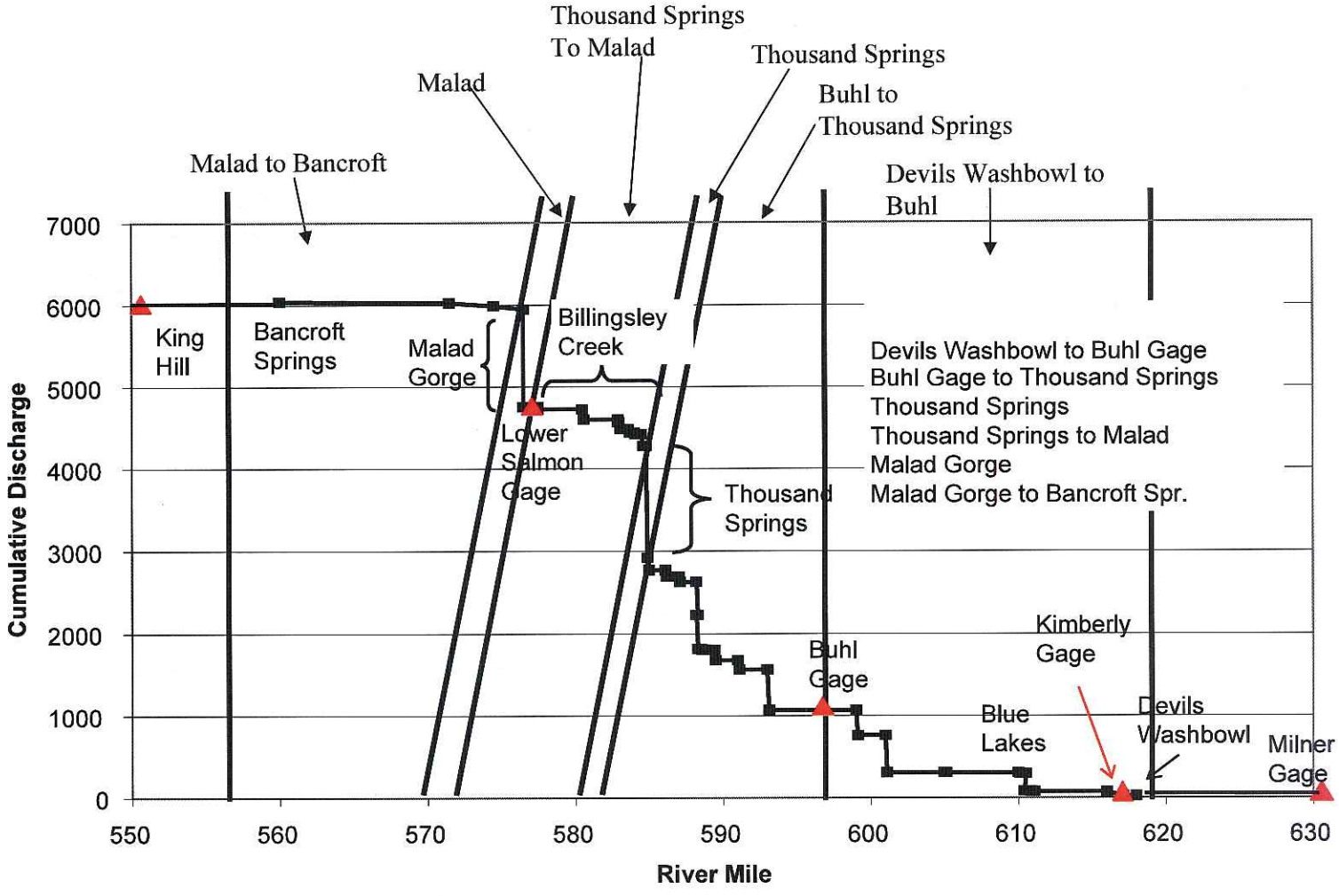


Figure 20. Cumulative spring discharge progressively from Milner Dam to King Hill. River miles are from Covington and Weaver, 1990.

A&B 2949

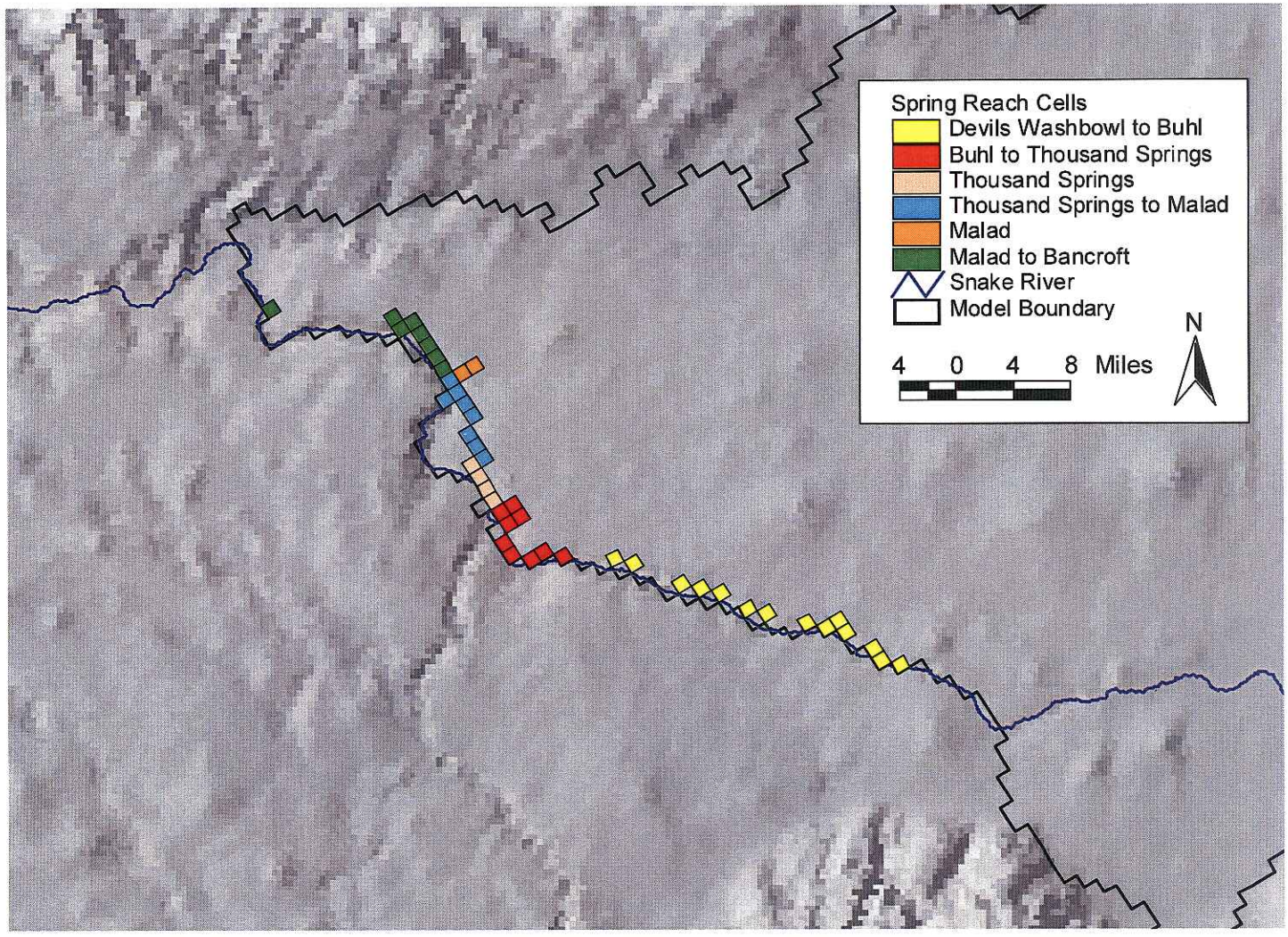


Figure 21. Head-dependent spring reaches.

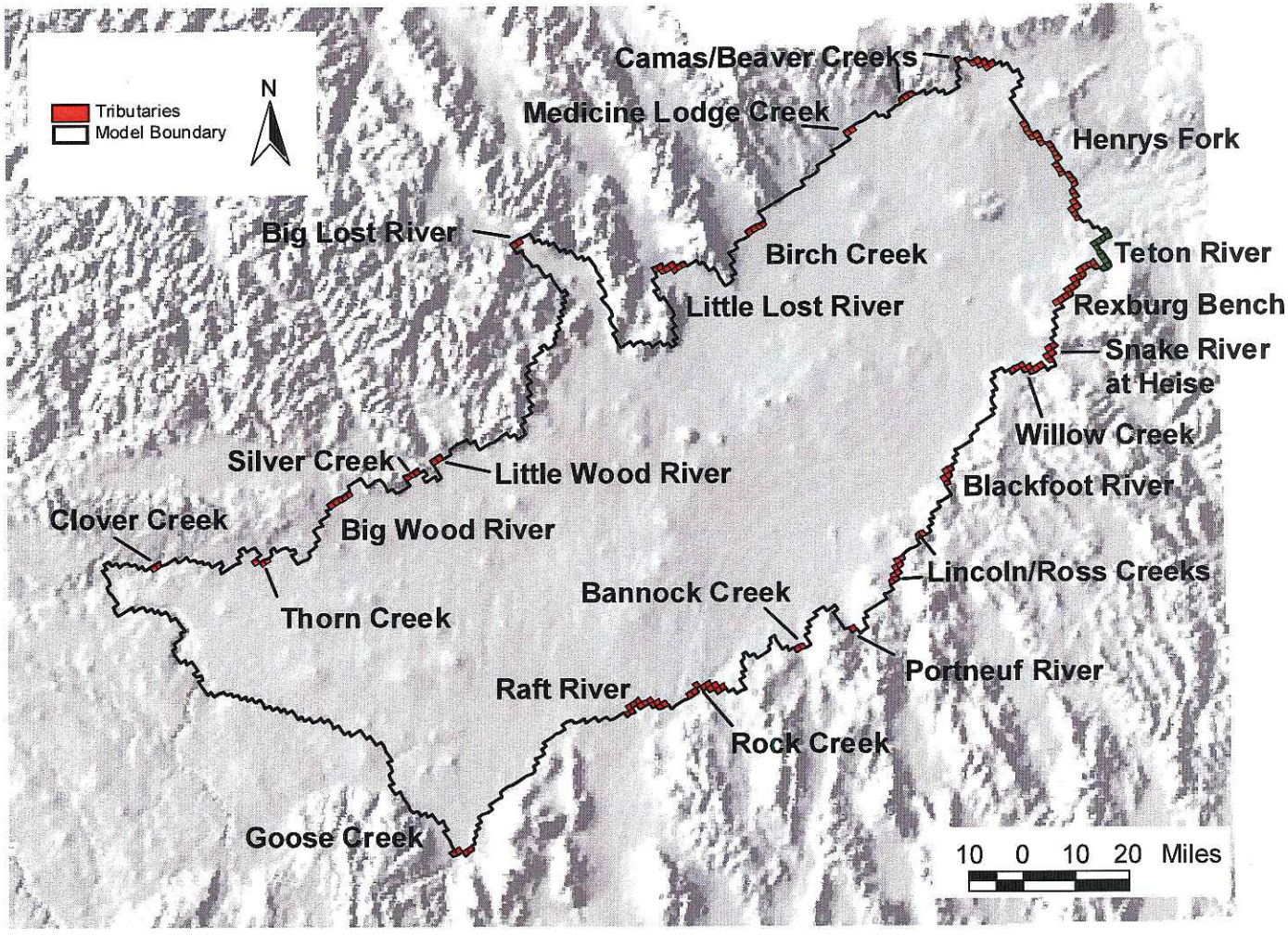


Figure 22. Specified flux tributary underflow locations.

A&B 2951

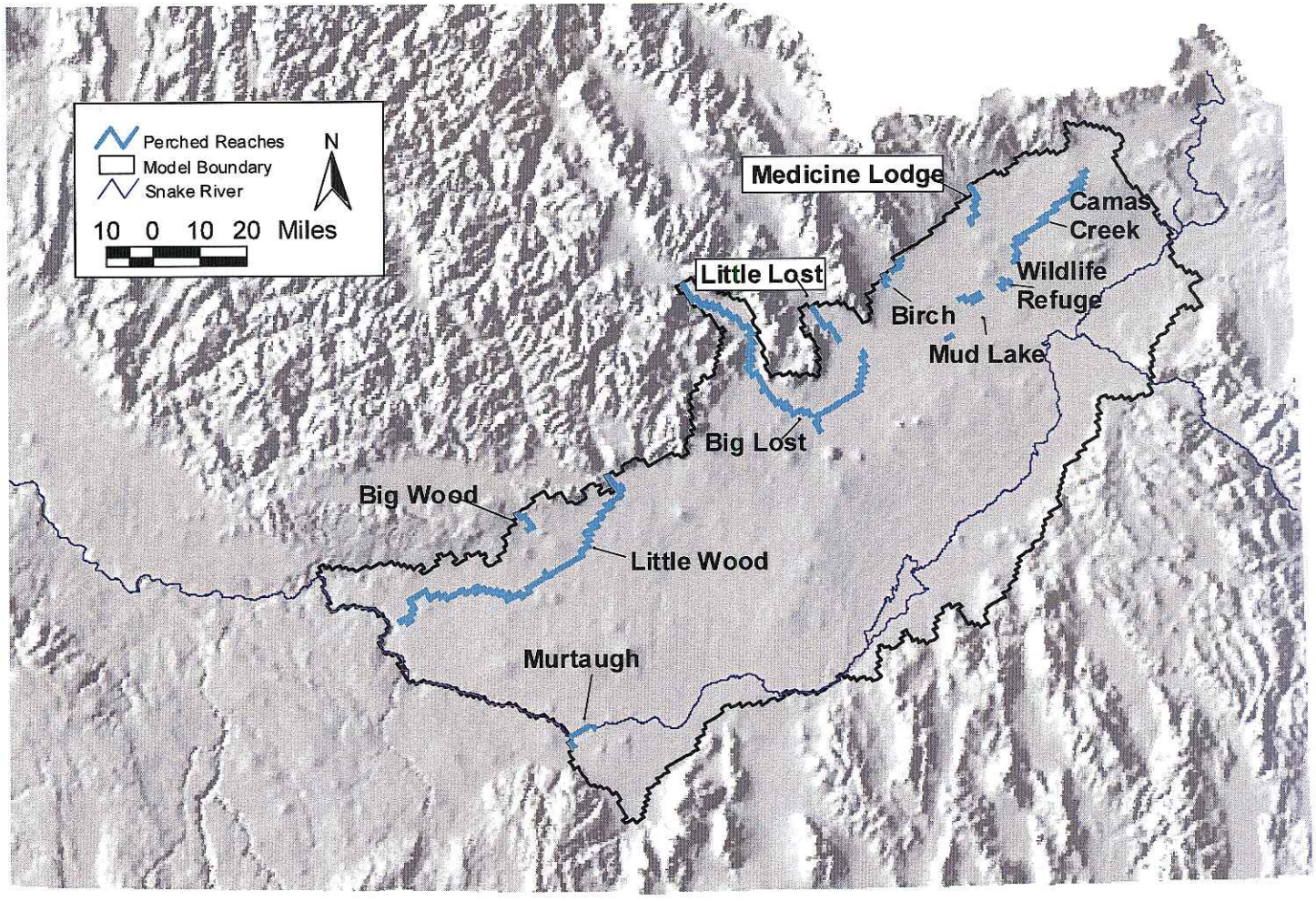


Figure 23. Non-Snake River perched reaches.

A&B 2952

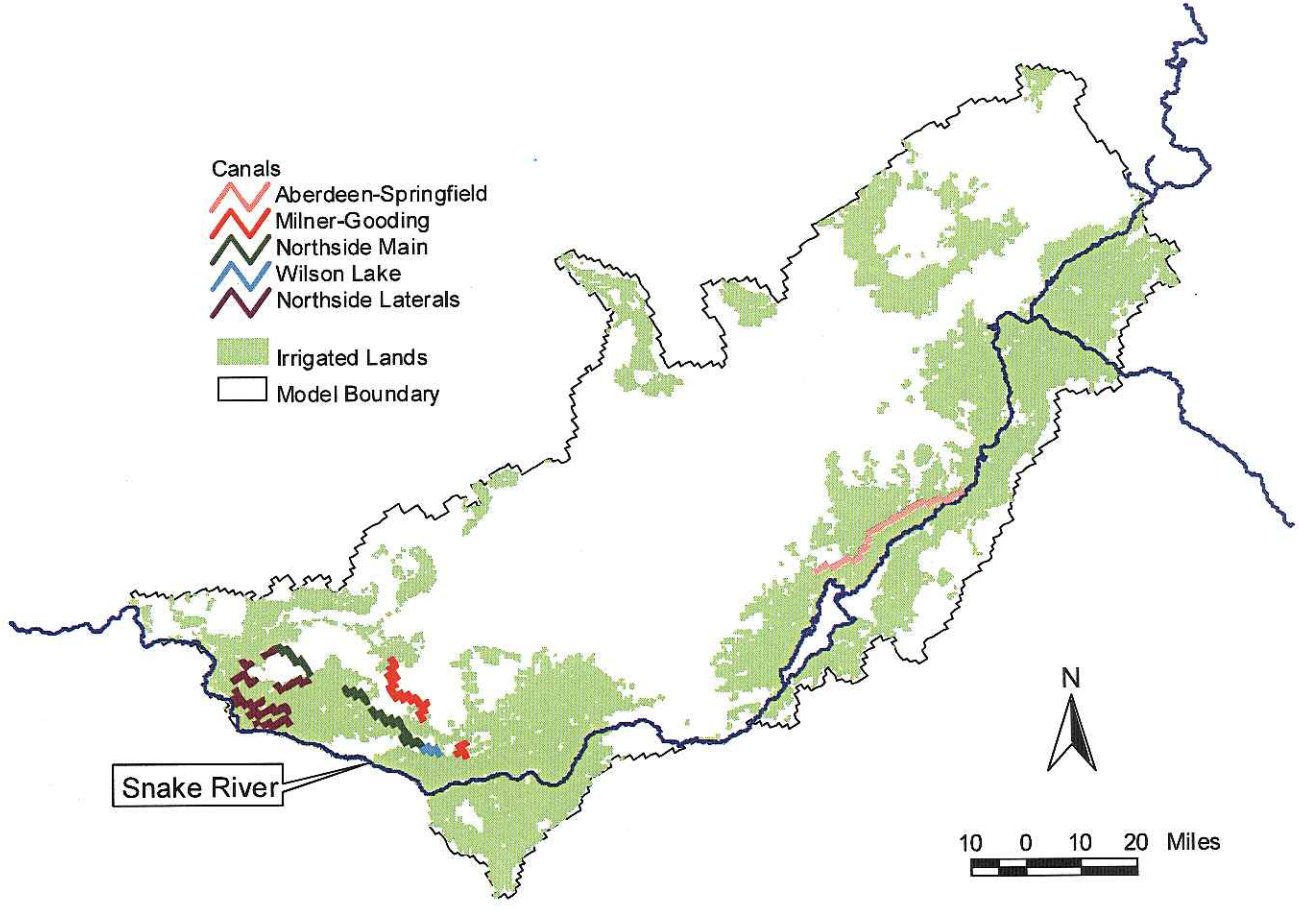


Figure 24. Locations of canals where leakage is explicitly represented.

A&B 2953

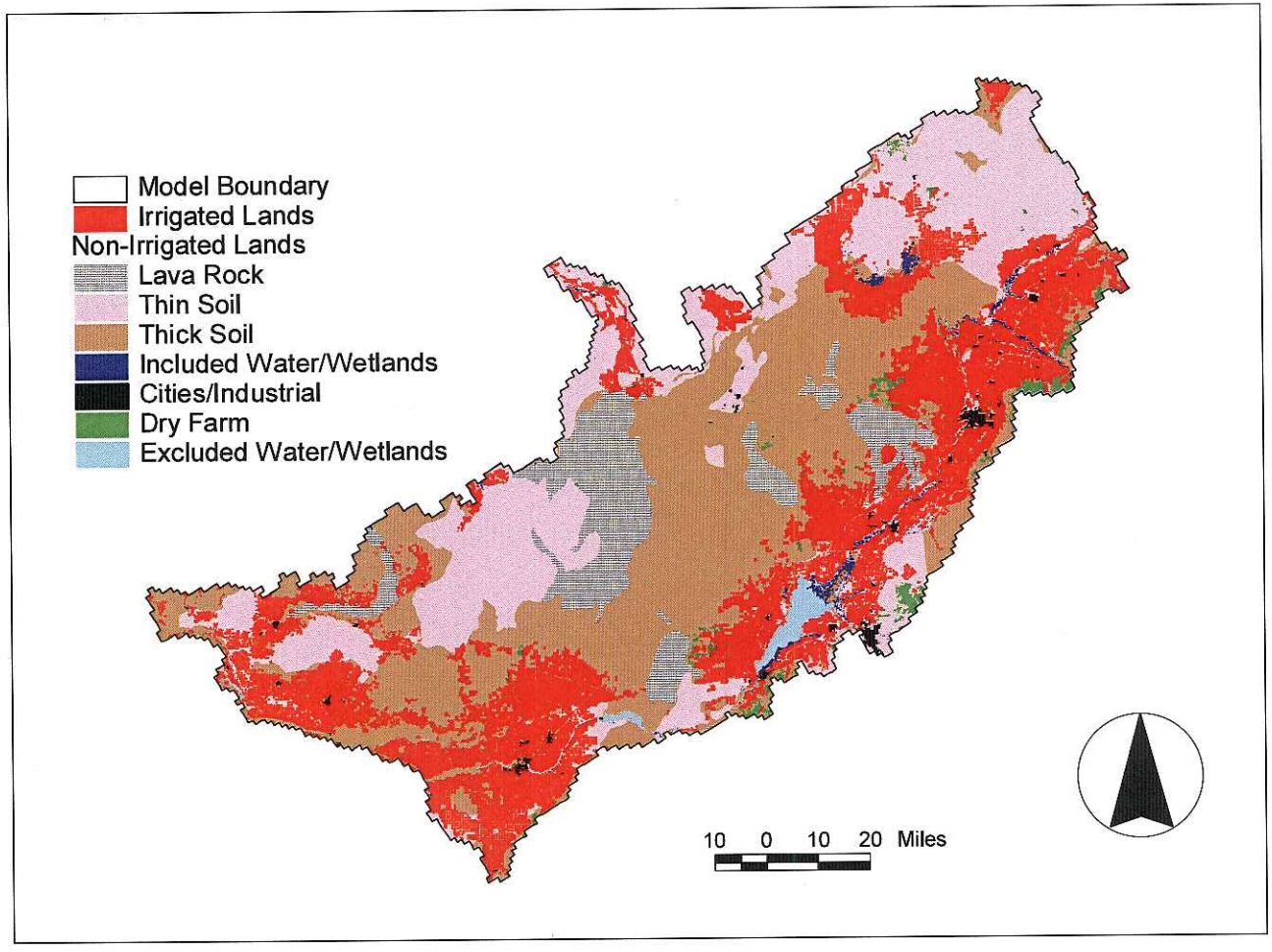


Figure 25. Generalized soil cover and land use map after Garabedian (1992) refined with aerial photography and ground truthing circa 1992 (IDWR 1997b).

A&B 2954

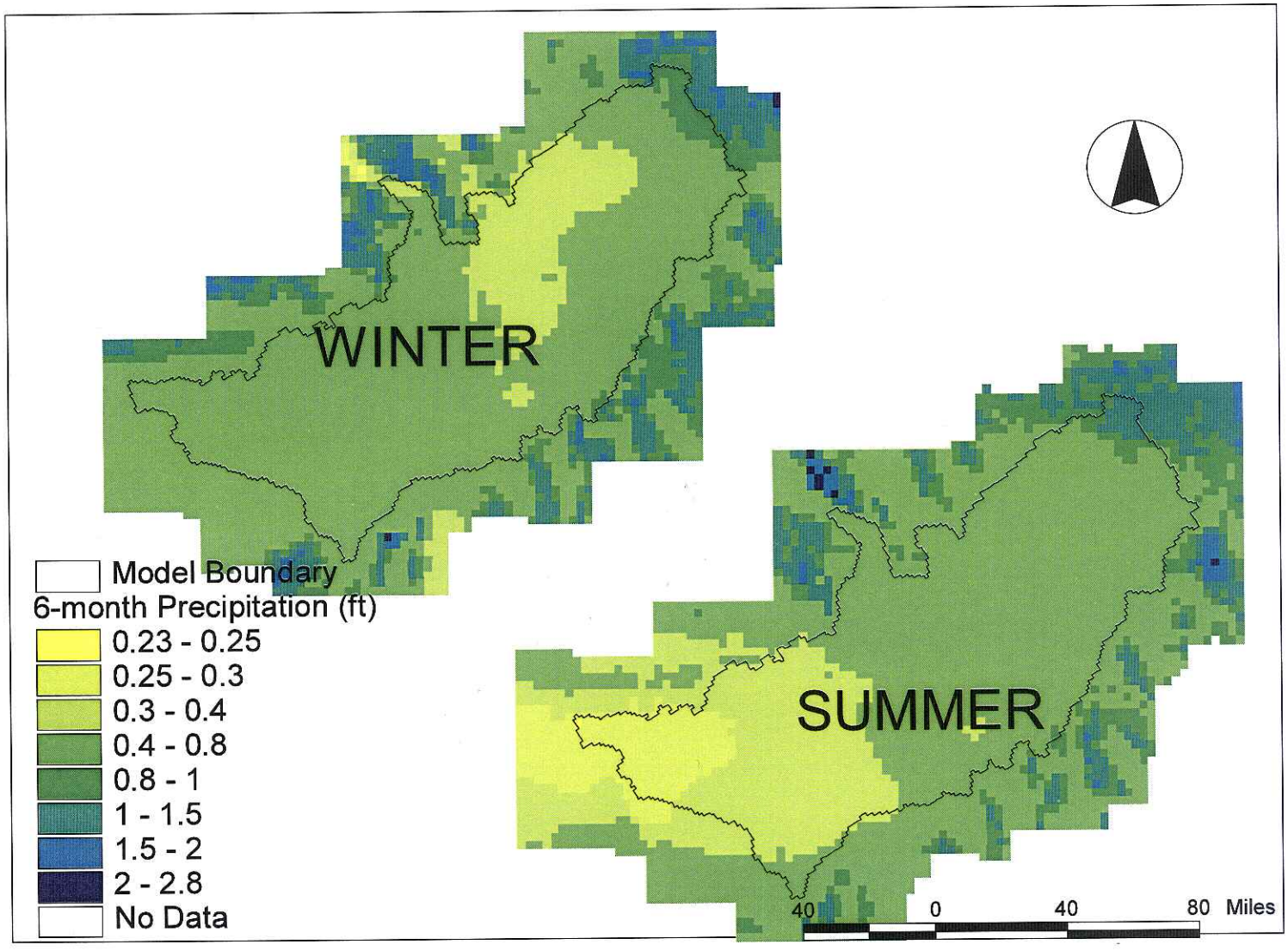


Figure 26. PRISM precipitation maps for the irrigation season and non-irrigation season, based on average precipitation for model period.

A&B 2955

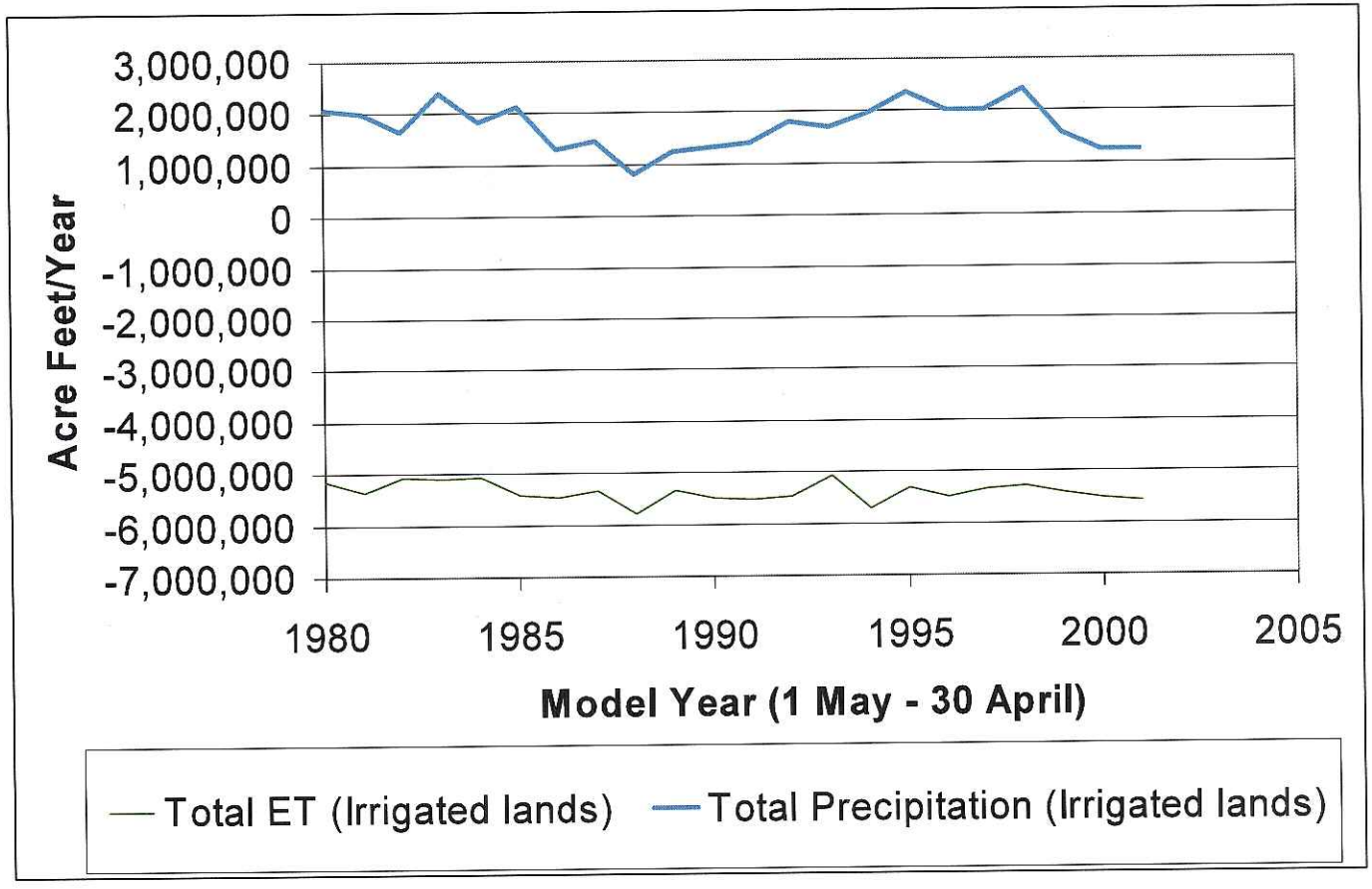


Figure 27. Annual precipitation and evapotranspiration for irrigated lands for the model study period.

A&B 2956

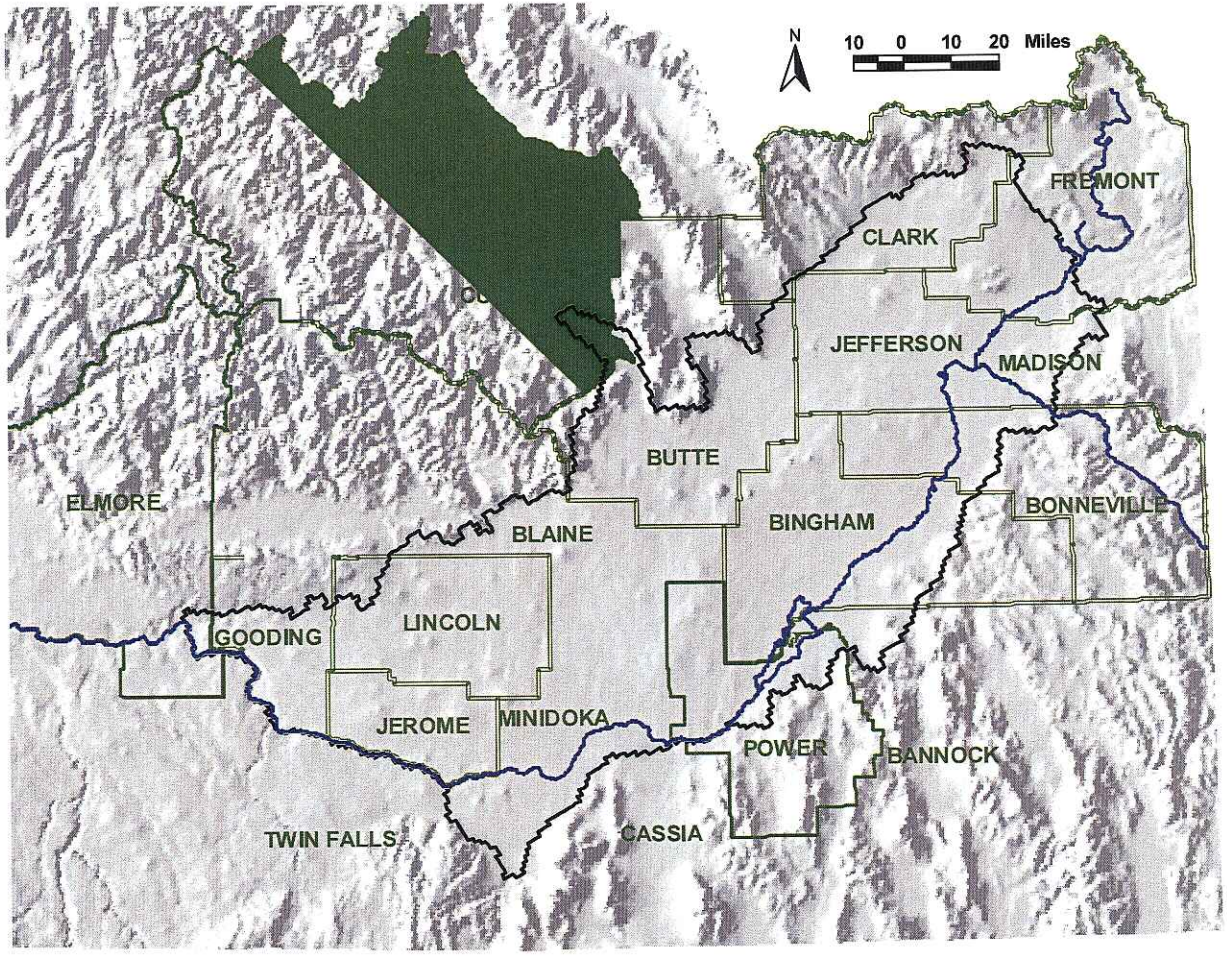


Figure 28. Idaho counties in the study area.

A&B 2957

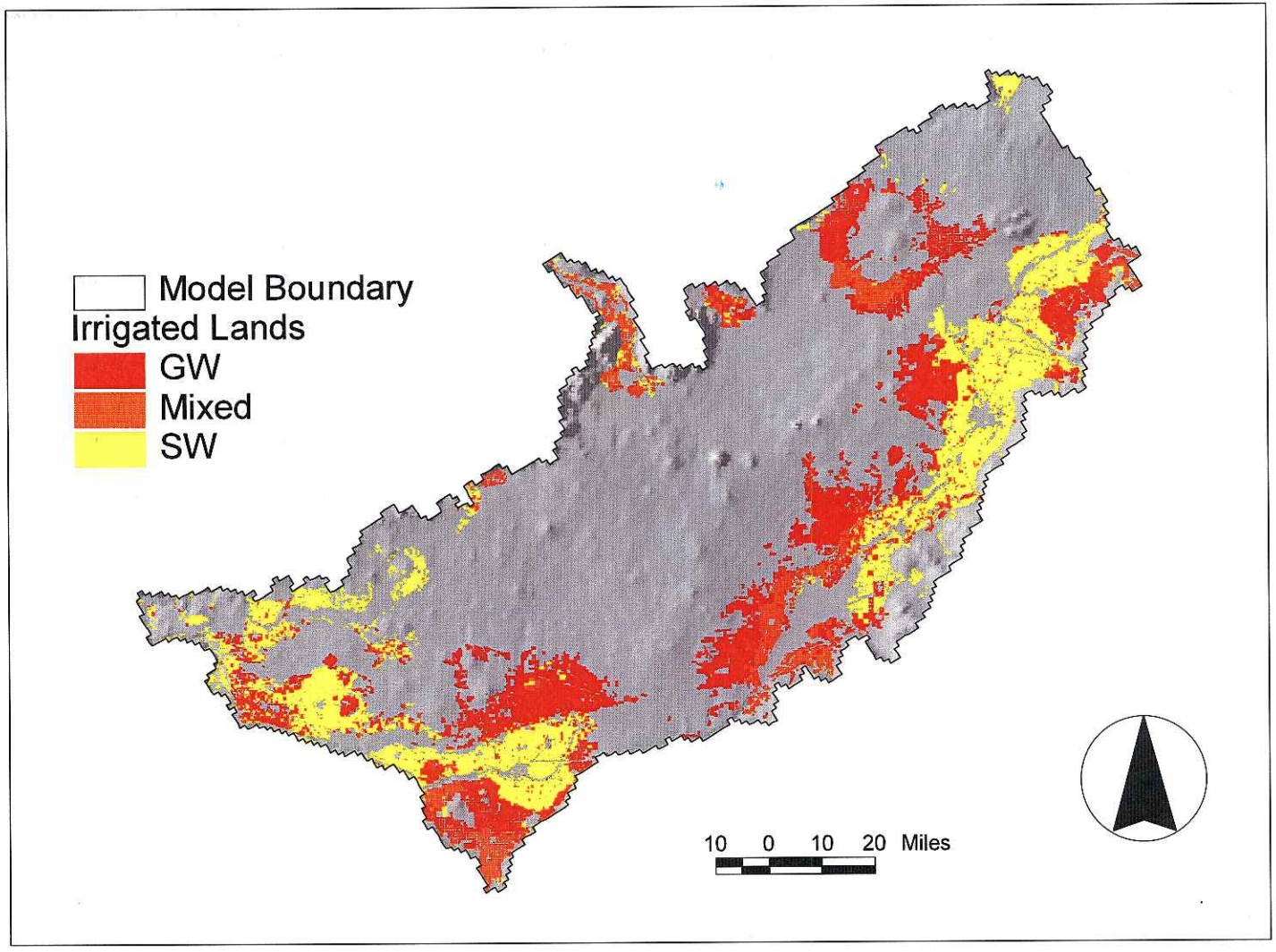


Figure 29. Irrigation water source determined from adjudication data.

A&B 2958

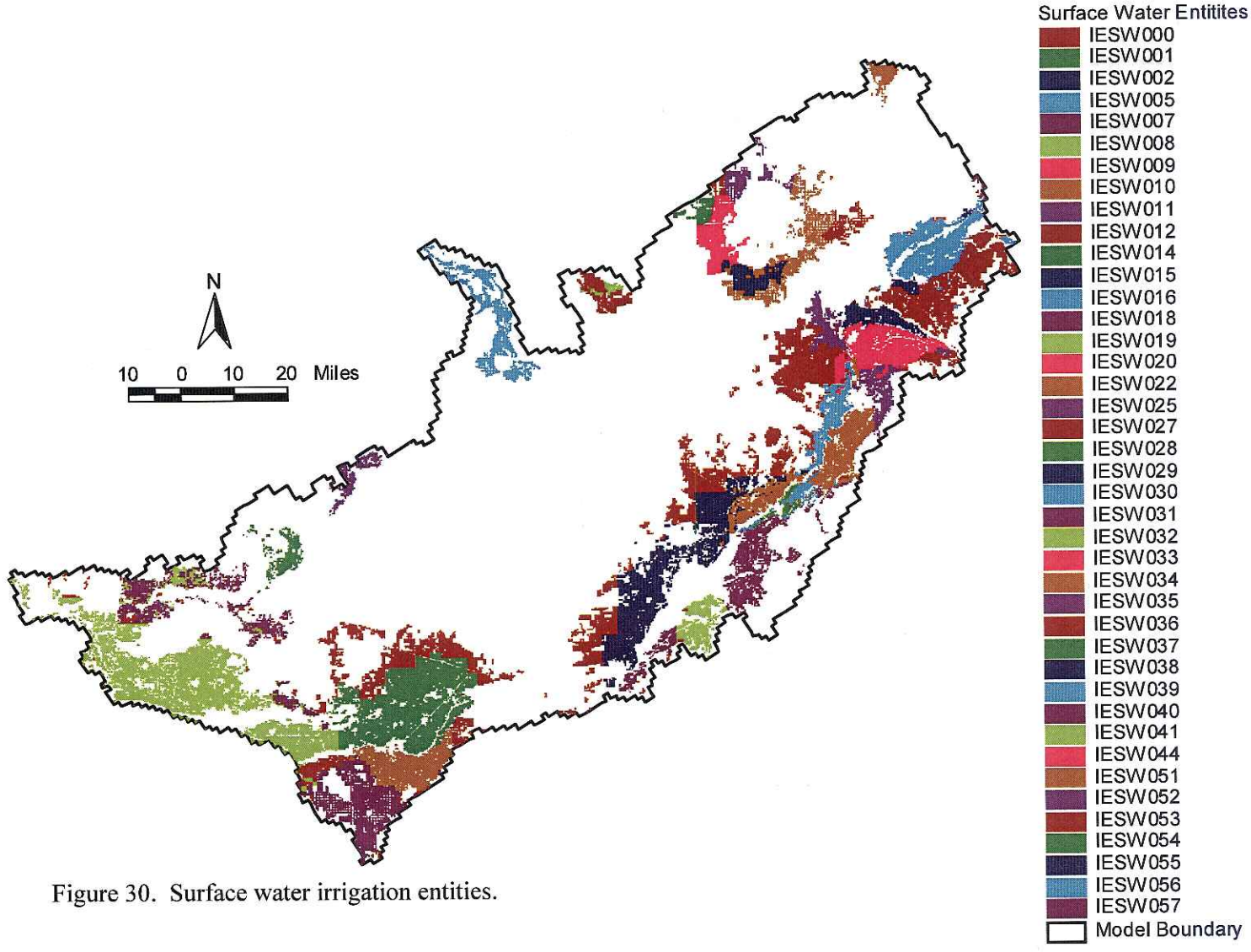


Figure 30. Surface water irrigation entities.

A&B 2959

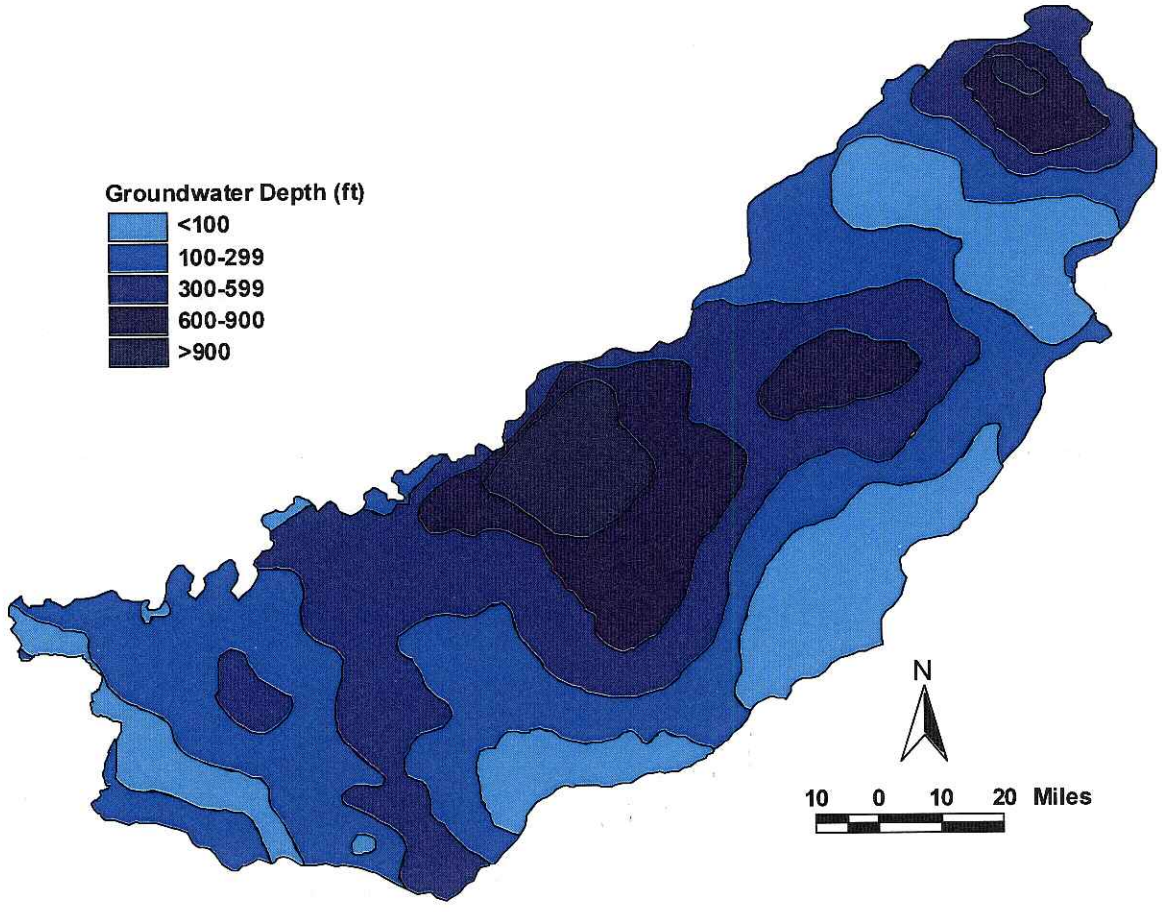


Figure 31. Depth to water (after Lindholm and others, 1988).

A&B 2960

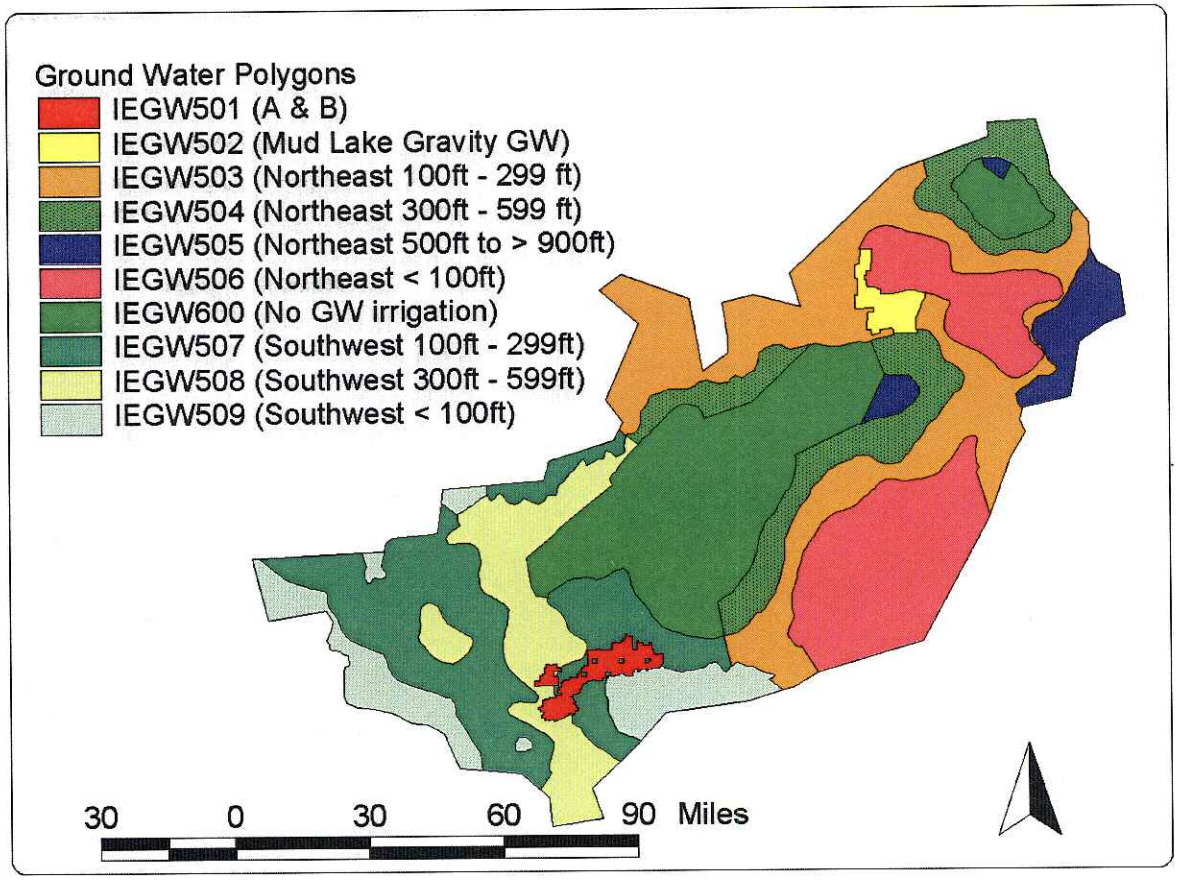


Figure 32. Ground-water polygons (based on depth to ground water).

A&B 2961

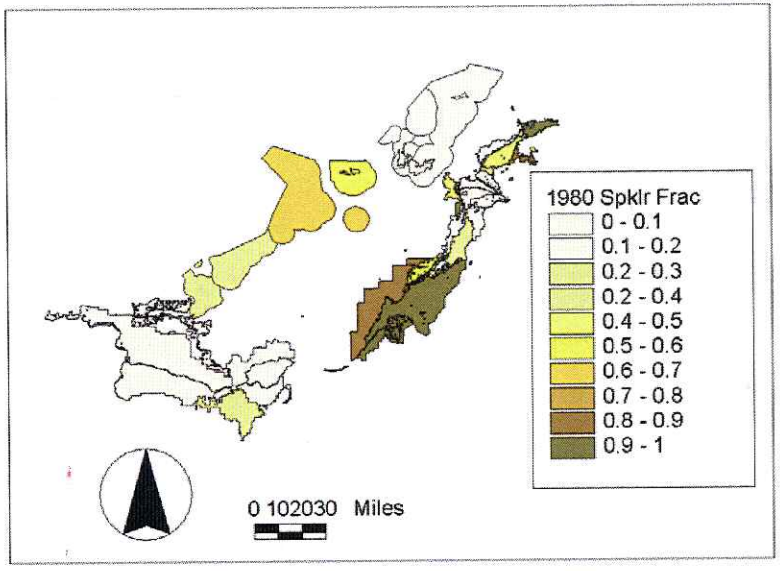


1980

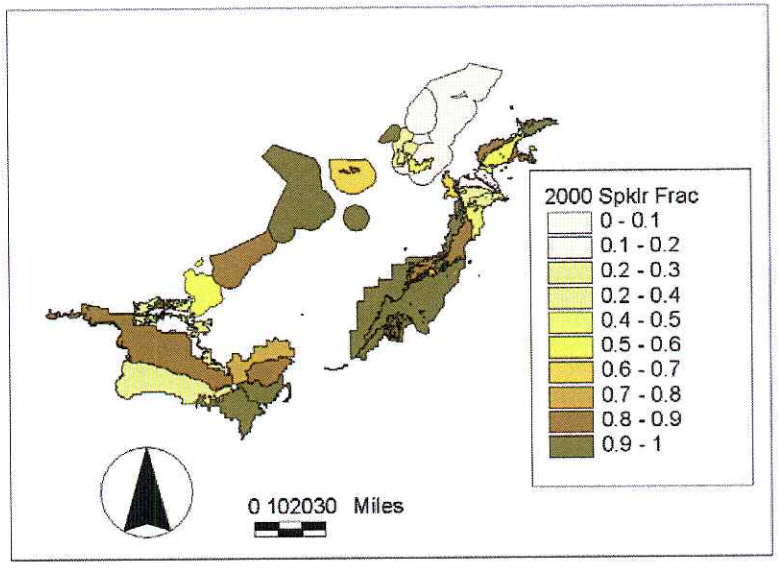


2000

Figure 33. Sprinkler fraction by surface-water entity, 1980 and 2000.

A&B 2962

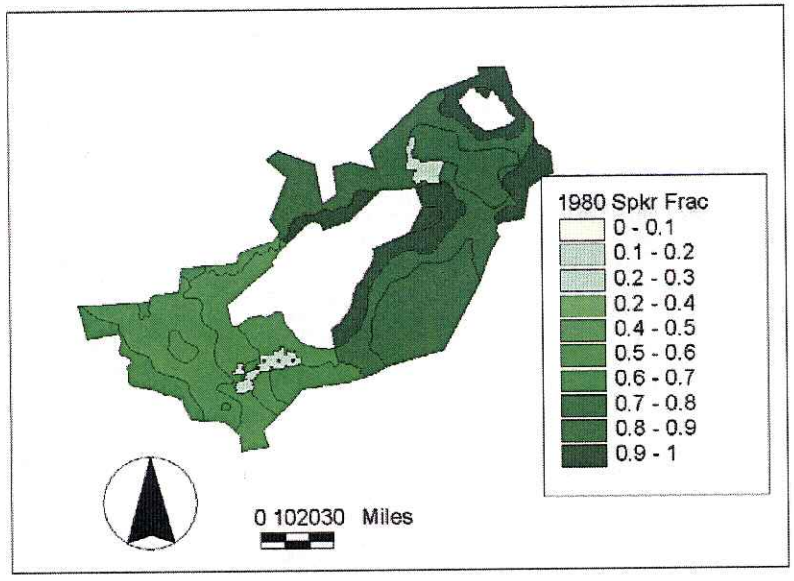


1980

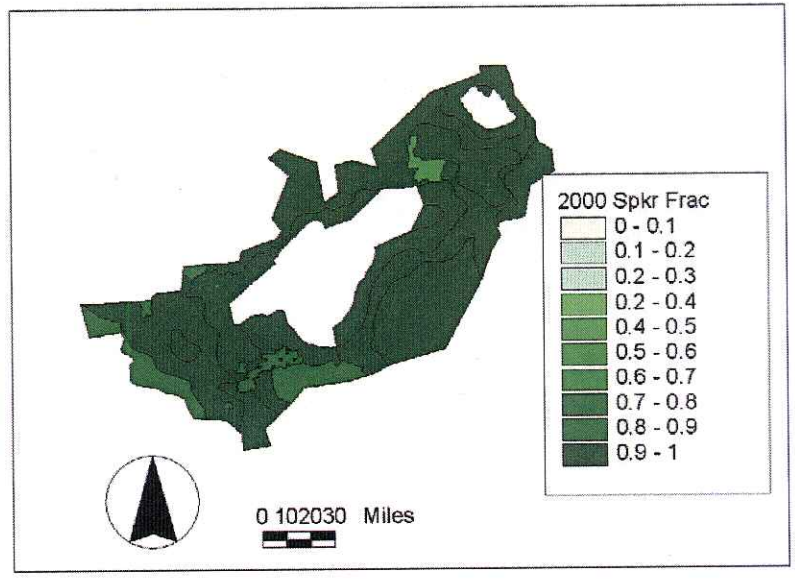


2000

Figure 34. Sprinkler fraction by ground-water polygon, 1980 and 2000.

A&B 2963

A&B 2964

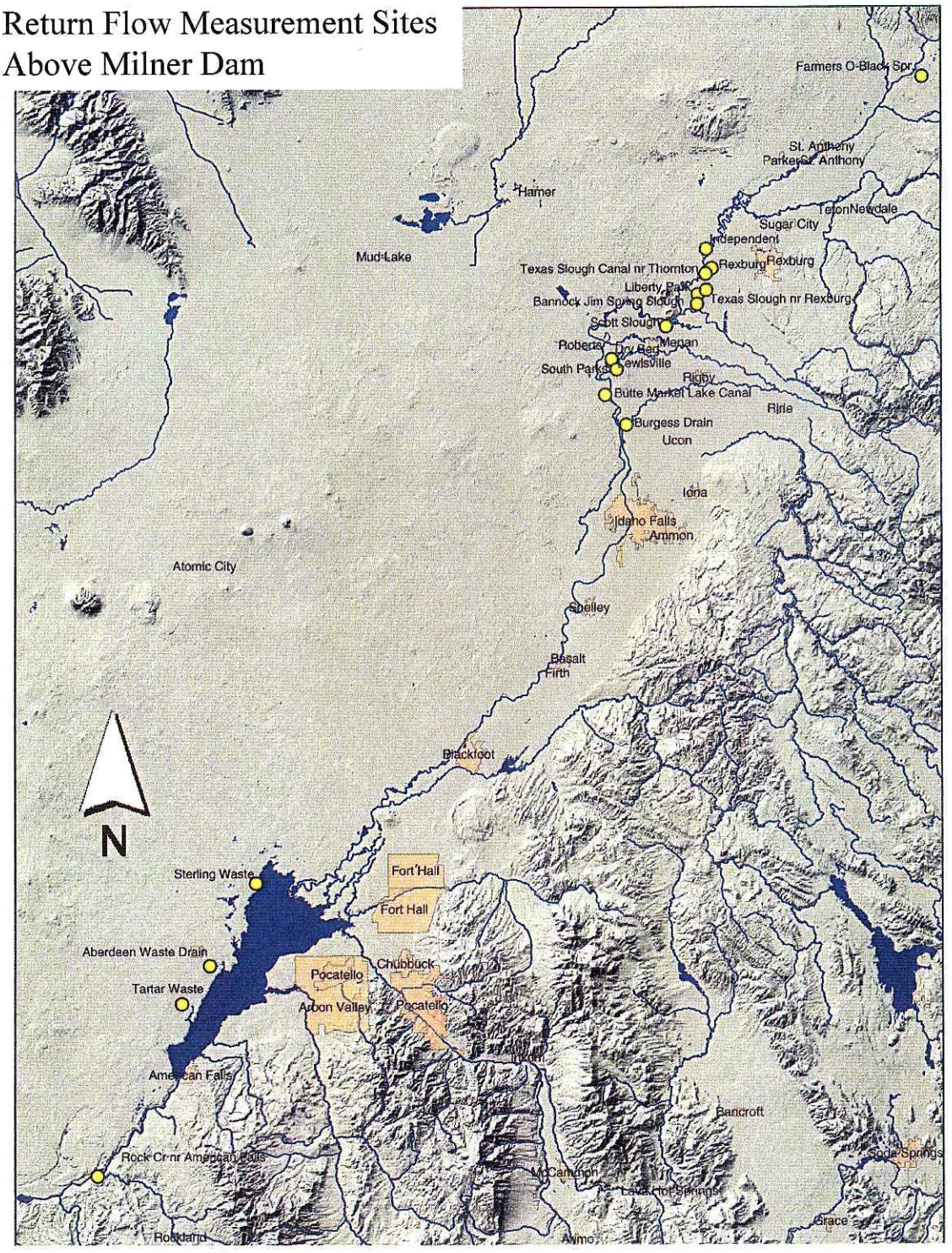


Figure 35. Return flow measurement sites above Milner Dam.

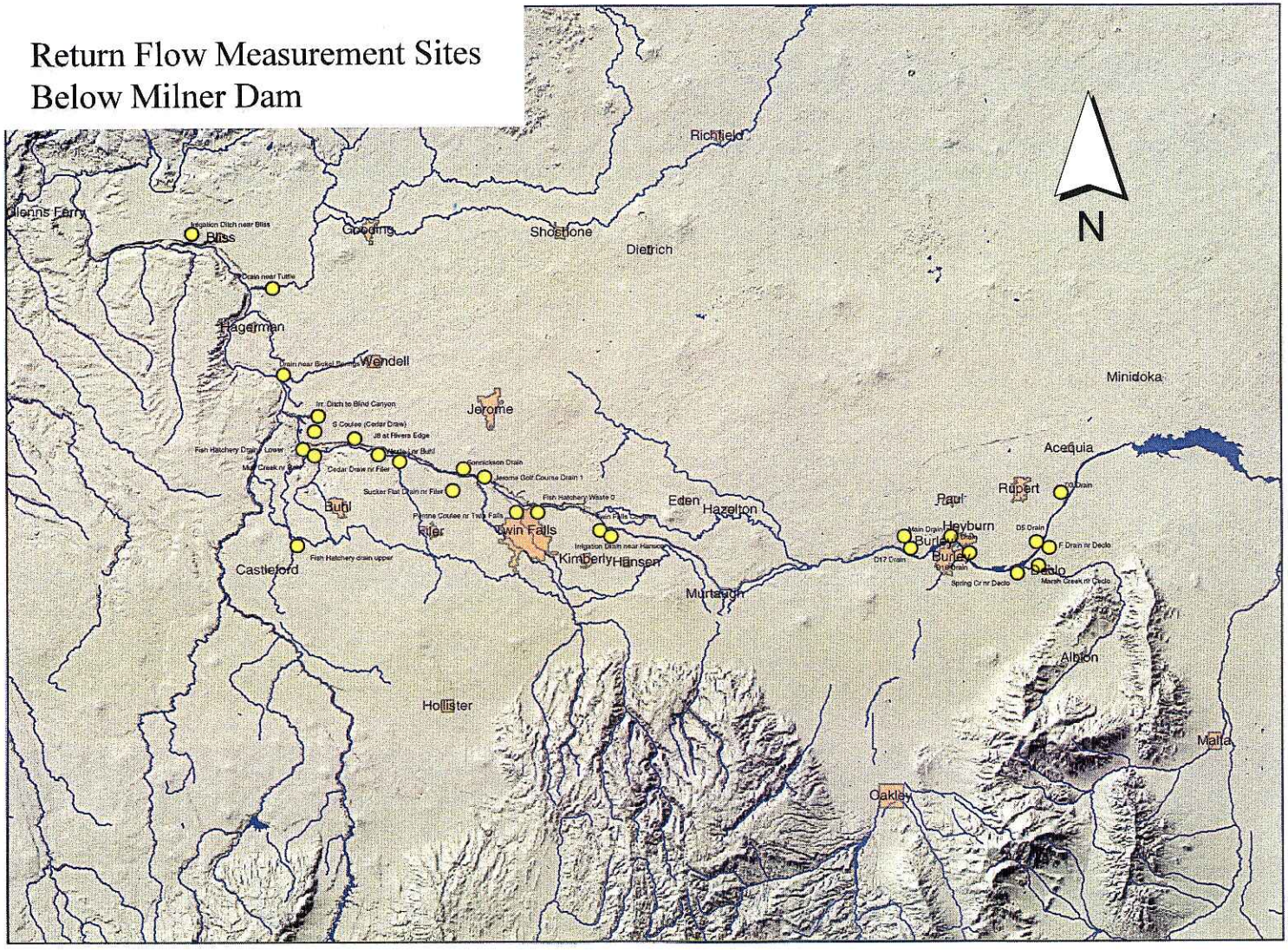


Figure 36. Return flow measurement sites below Milner Dam.

A&B 2965

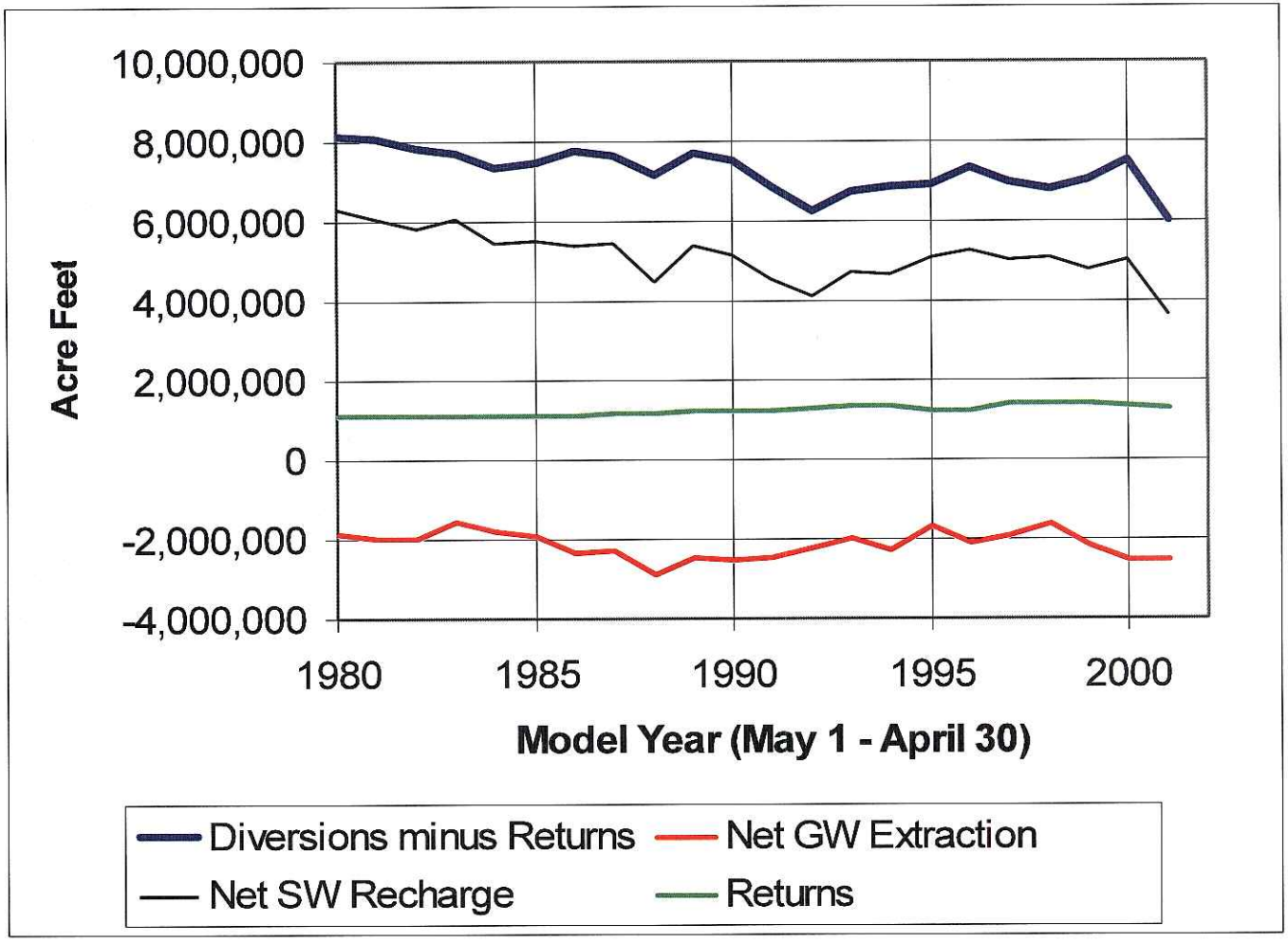


Figure 37. Diversion volume less return flow volume, return flow volume, net ground-water extraction and net recharge due to surface water irrigation.

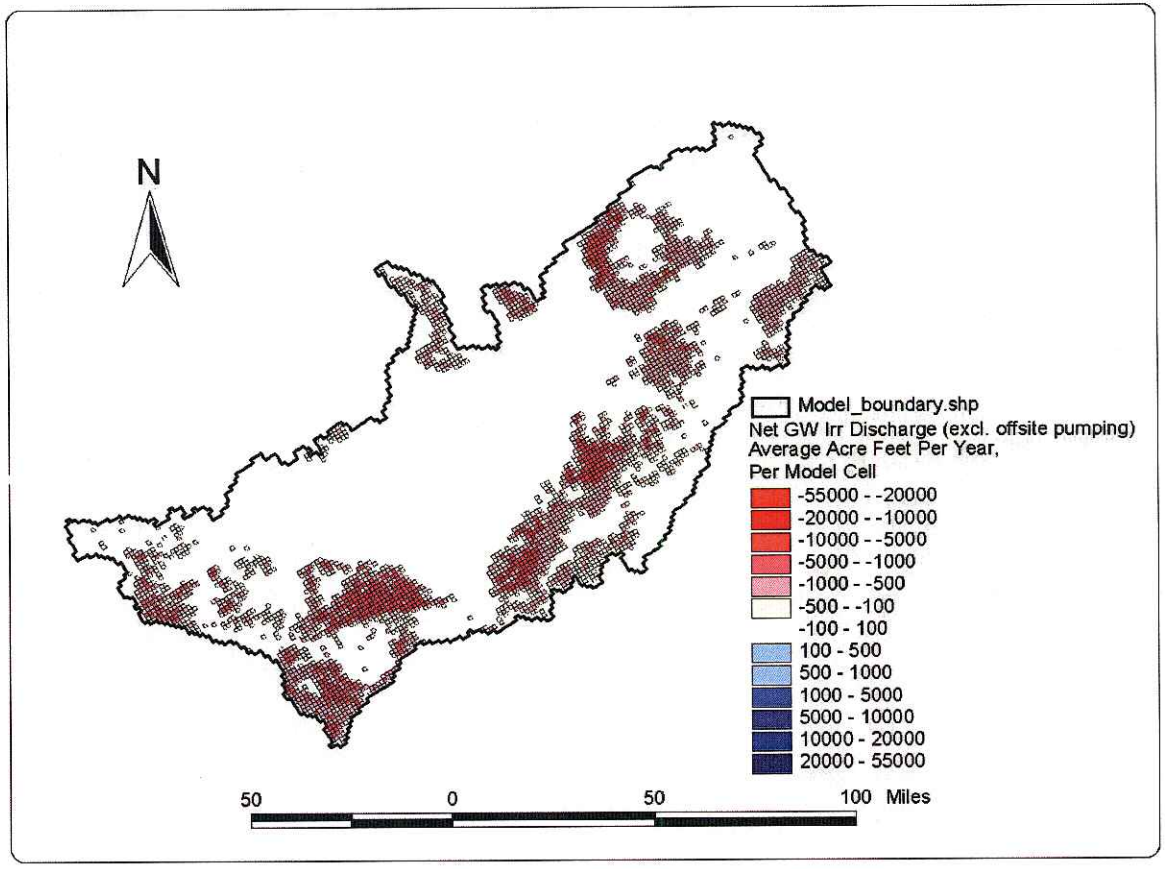


Figure 38. Areal distribution of net ground-water extraction averaged for the 22-year model calibration period.

A&B 2967

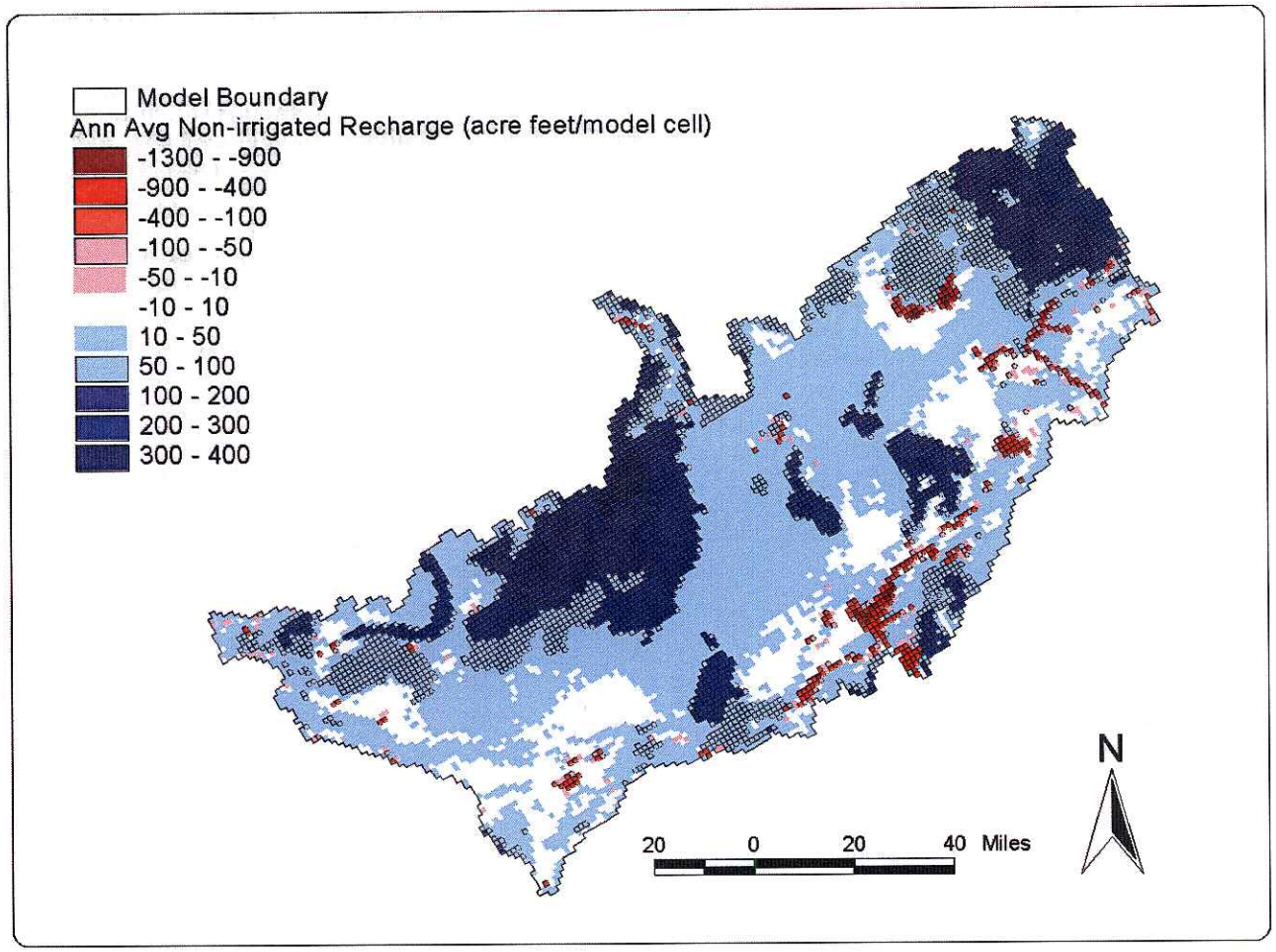


Figure 39. Spatial distribution of non-irrigated recharge averaged for the 22-year calibration period.

A&B 2968

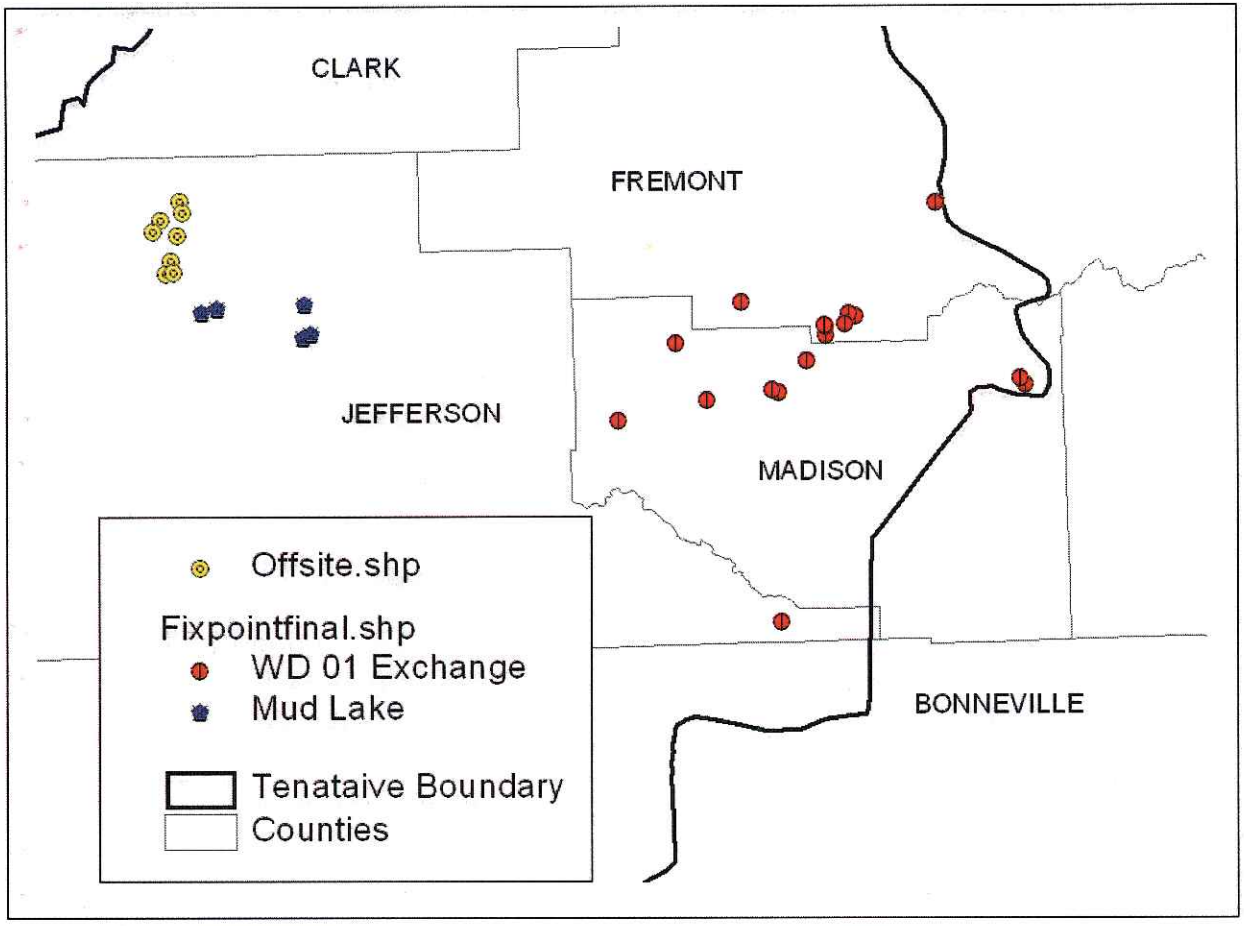


Figure 40. Exchange wells represented as fixed point pumping.

A&B 2969

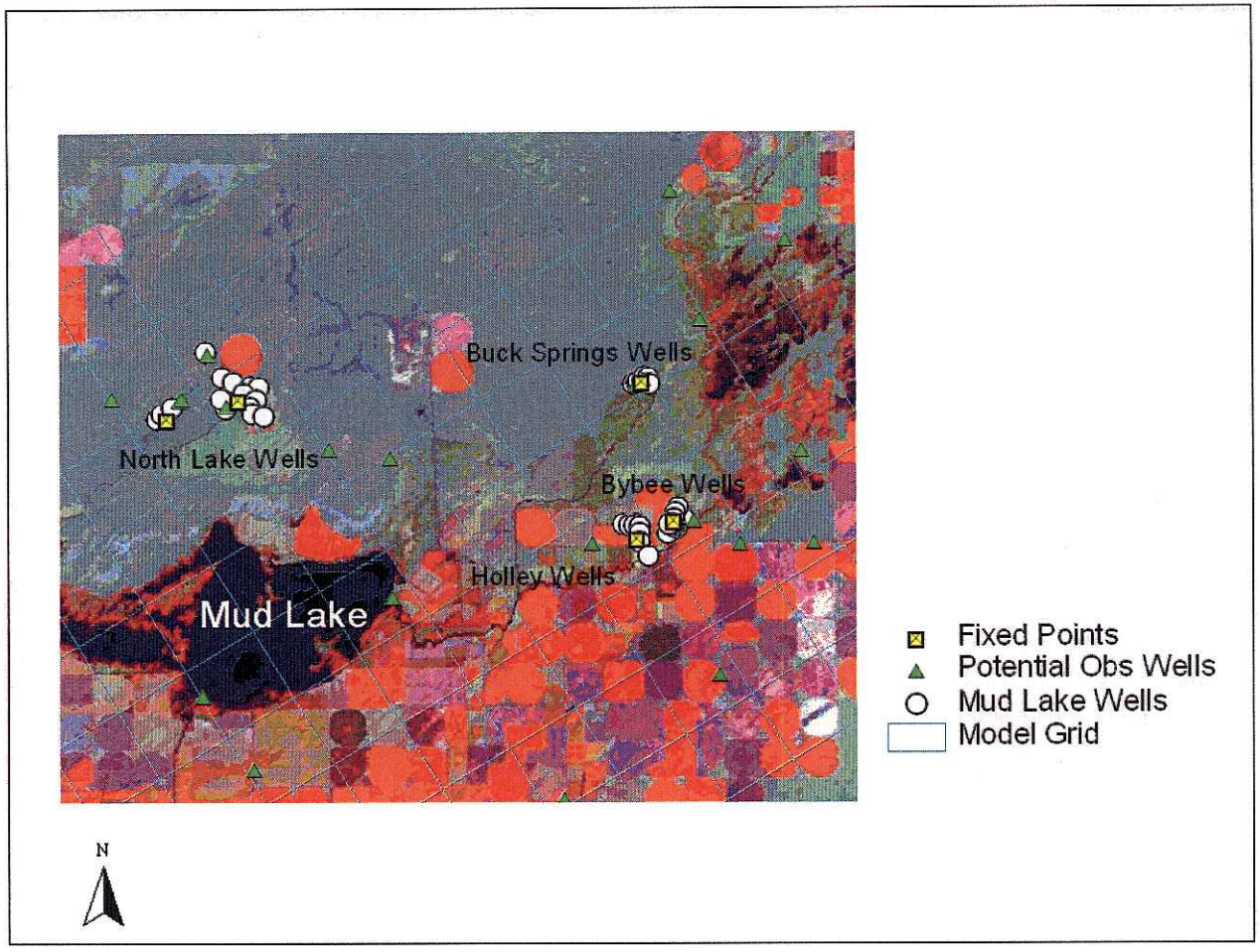


Figure 41. Fixed point wells in the Mud Lake area.

A&B 2970

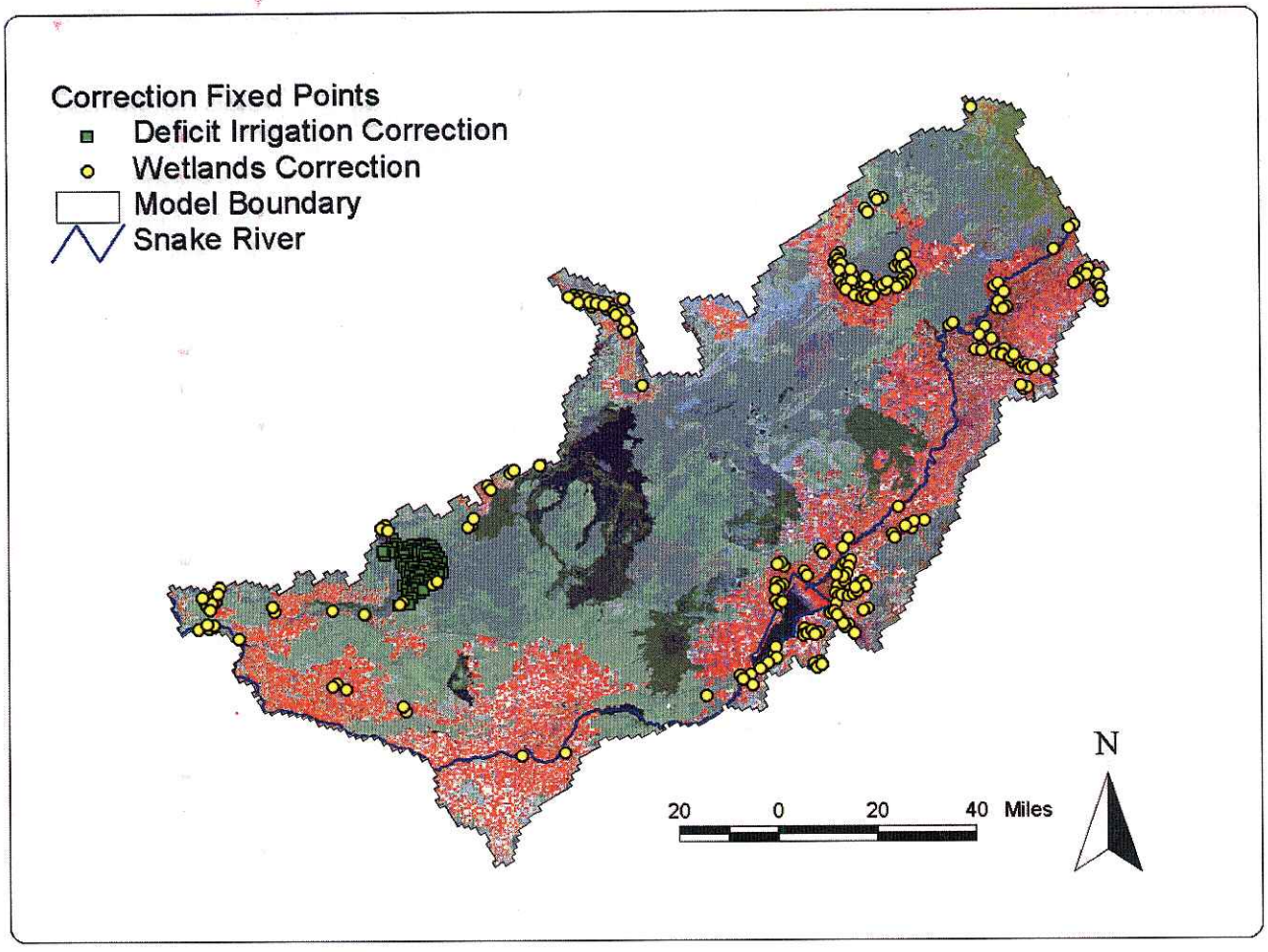


Figure 42. Location of wetlands and deficit irrigation correction fixed point wells.

A&B 2971

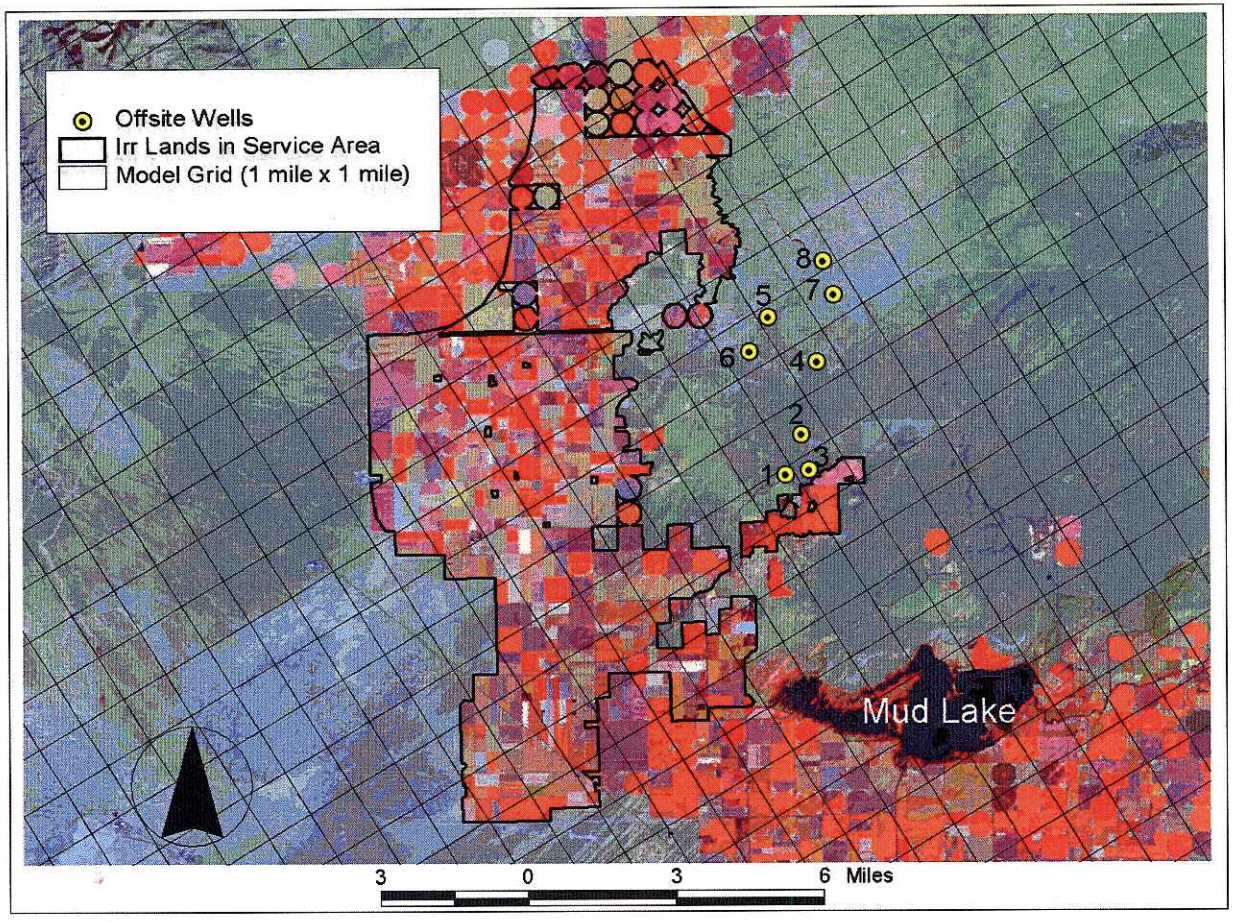


Figure 43. Location of off-site wells and destination irrigated areas.

A&B 2972

Figure 44. Bar graph of the components of recharge for steady state model.

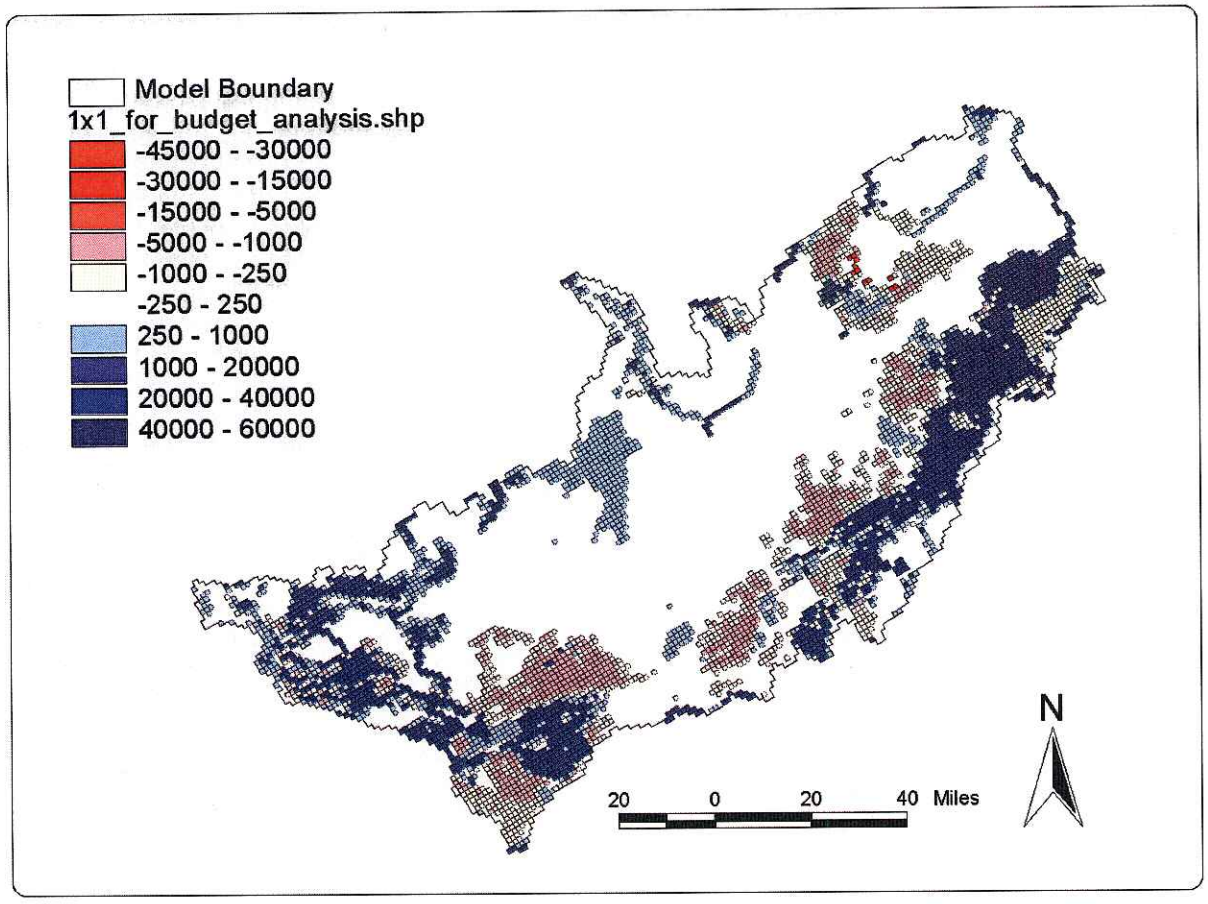


Figure 45. Areal distribution of recharge for steady state model (AF/yr).

A&B 2974

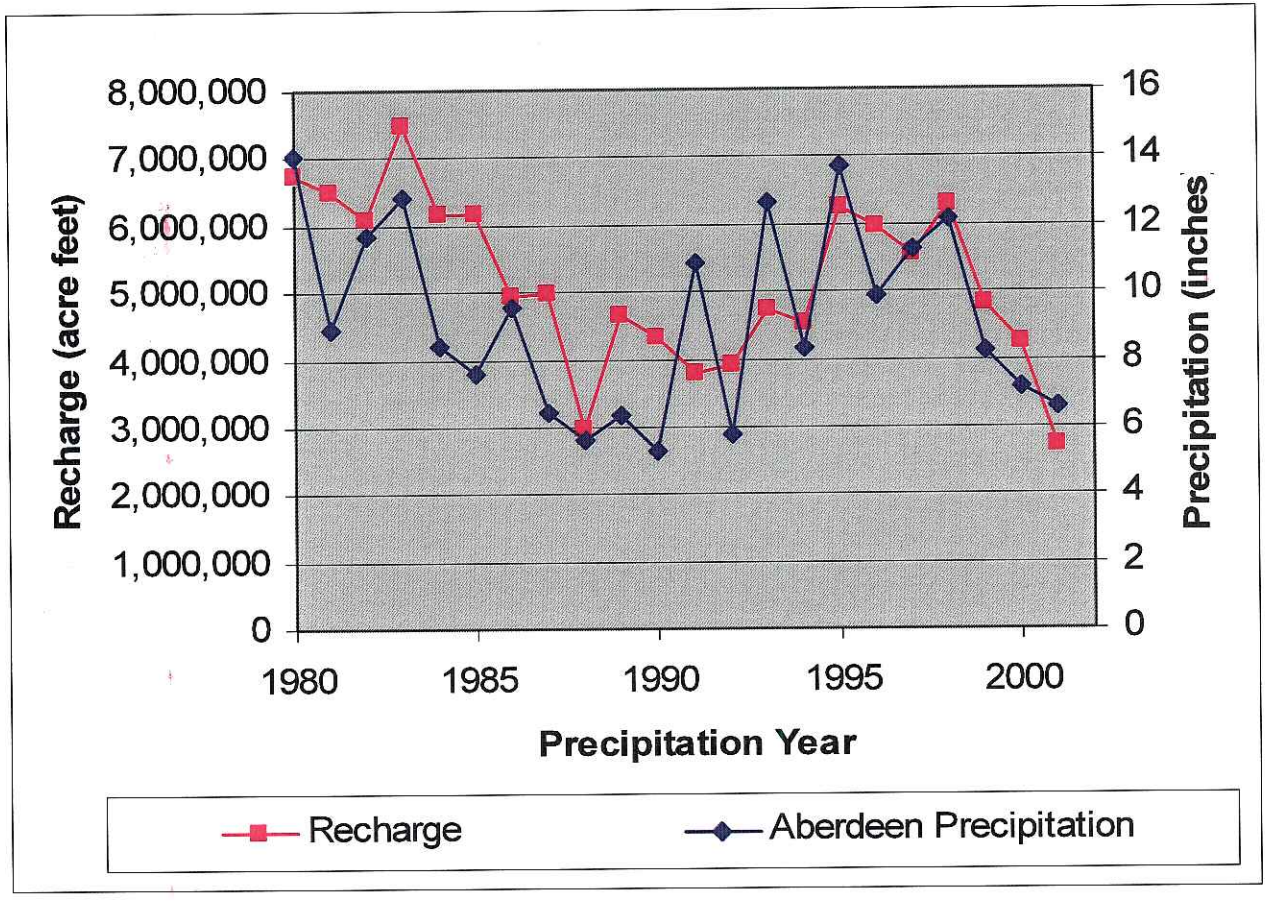


Figure 46. Recharge variation with time compared with precipitation at Aberdeen, Idaho for the transient ESPAM model.

A&B 2975

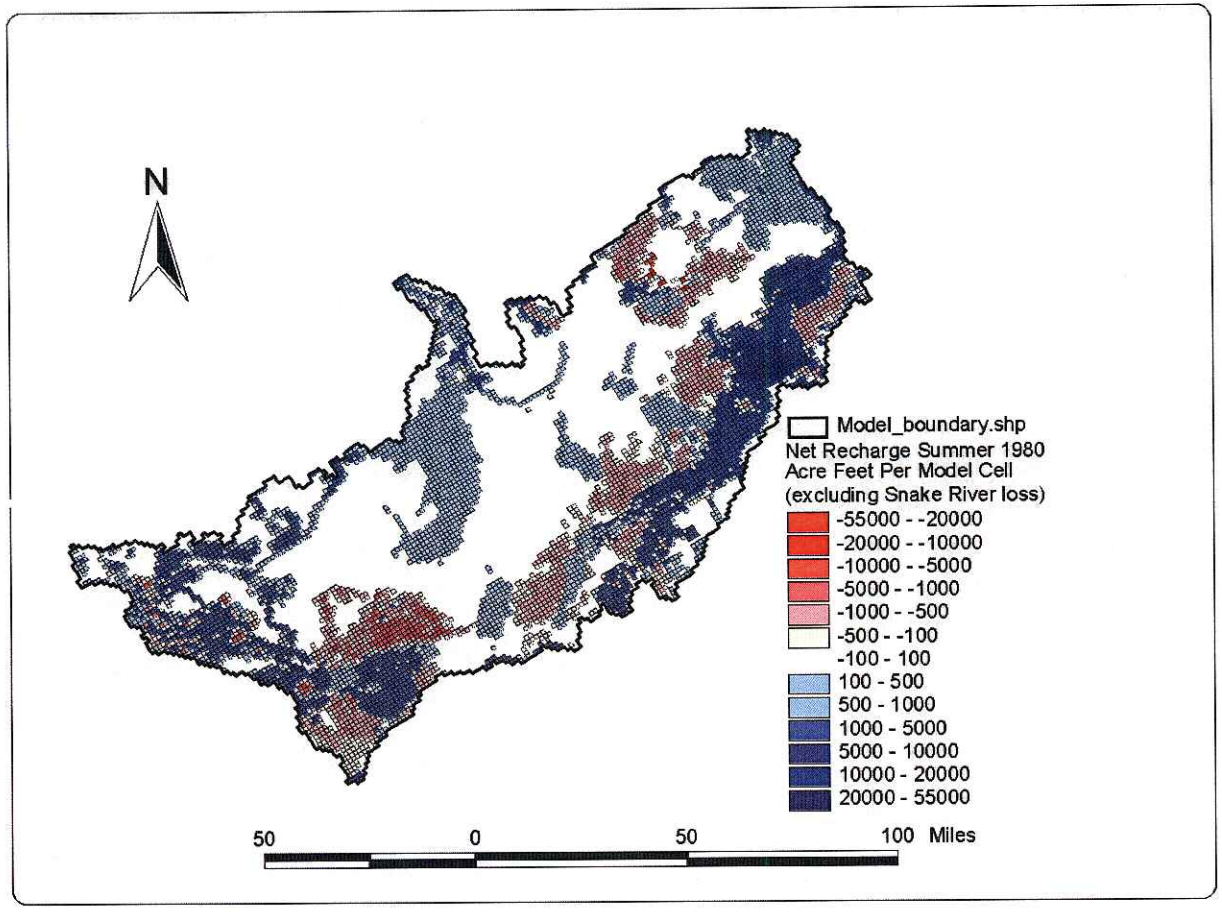


Figure 47. Areal distribution of transient recharge for 1980-1981 irrigation season (AF/stress period).

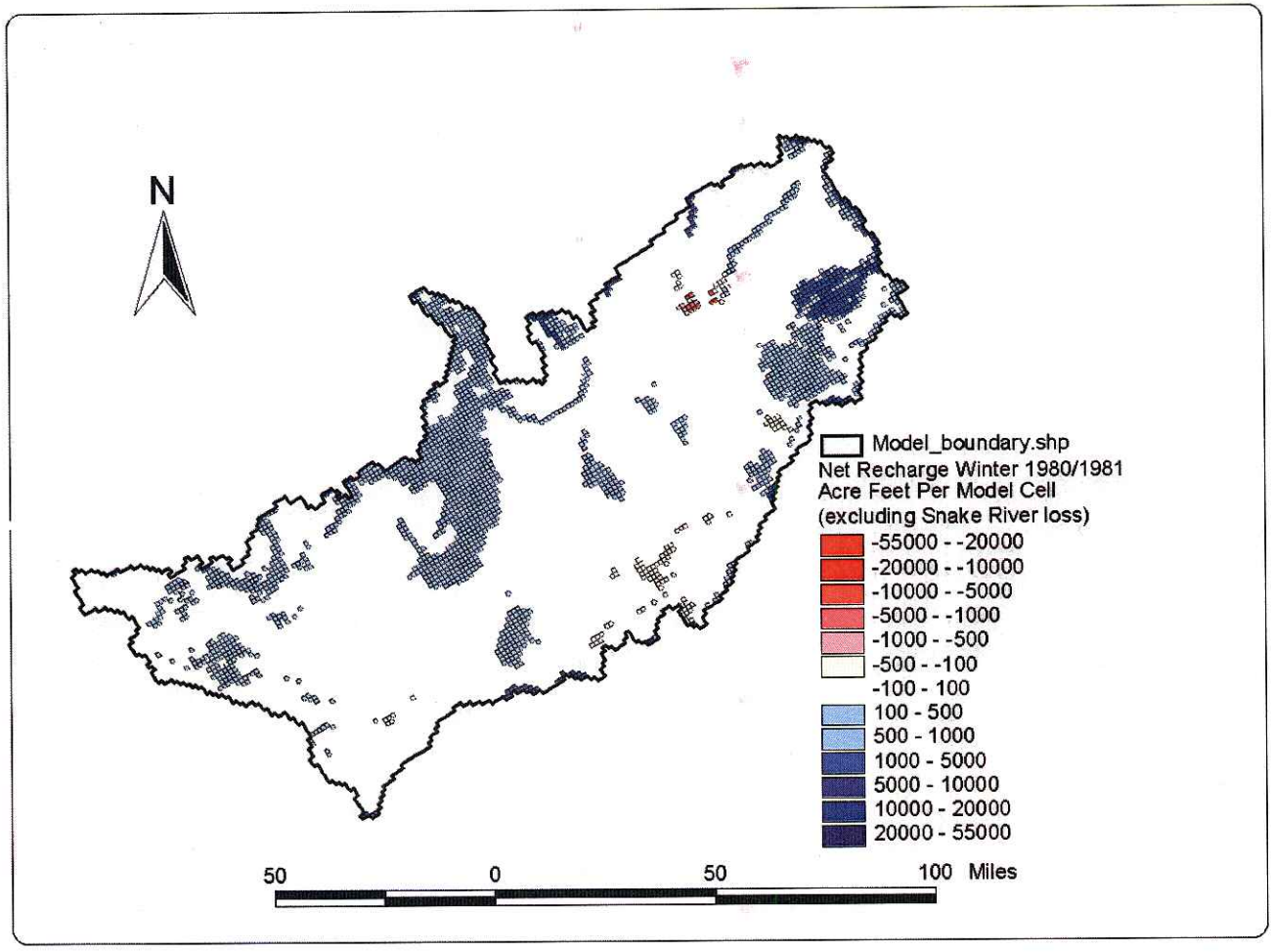


Figure 48. Areal distribution of transient recharge for 1980-1981non-irrigation season (AF/stress period).

A&B 2977

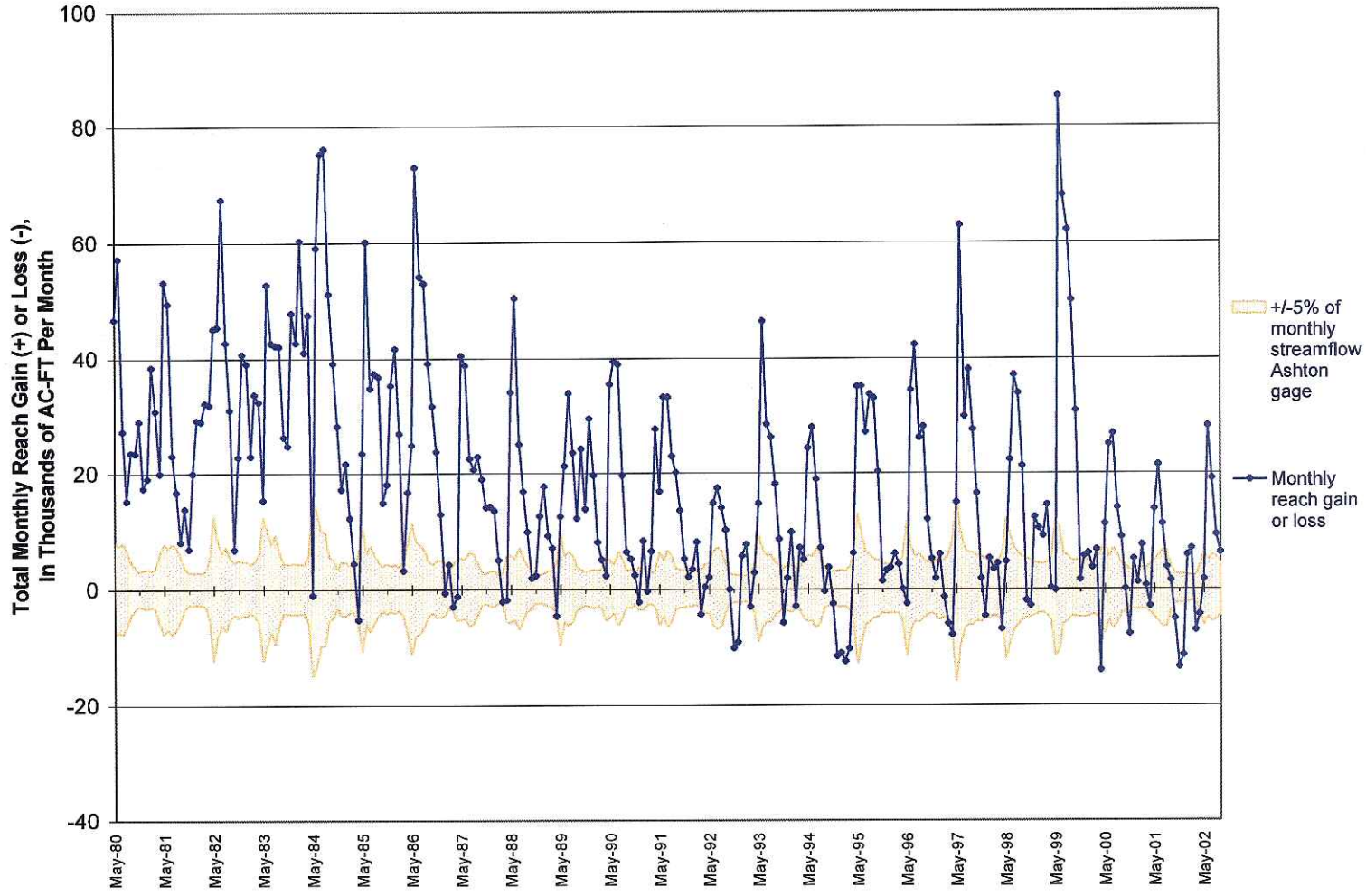


Figure 49. Monthly Snake River gains and losses: Ashton to Rexburg reach.

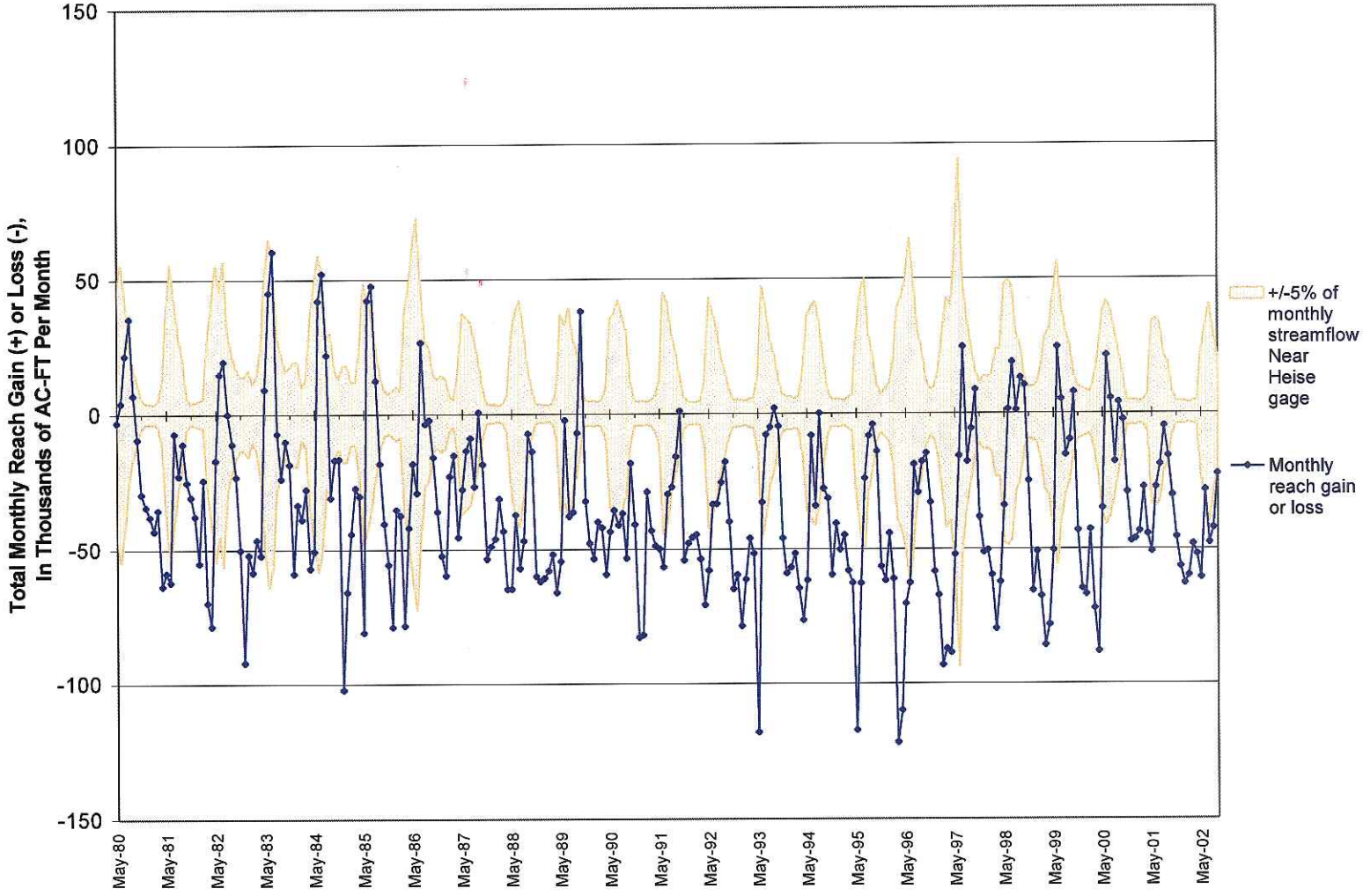


Figure 50. Monthly Snake River gains and losses: Heise to Shelley reach.

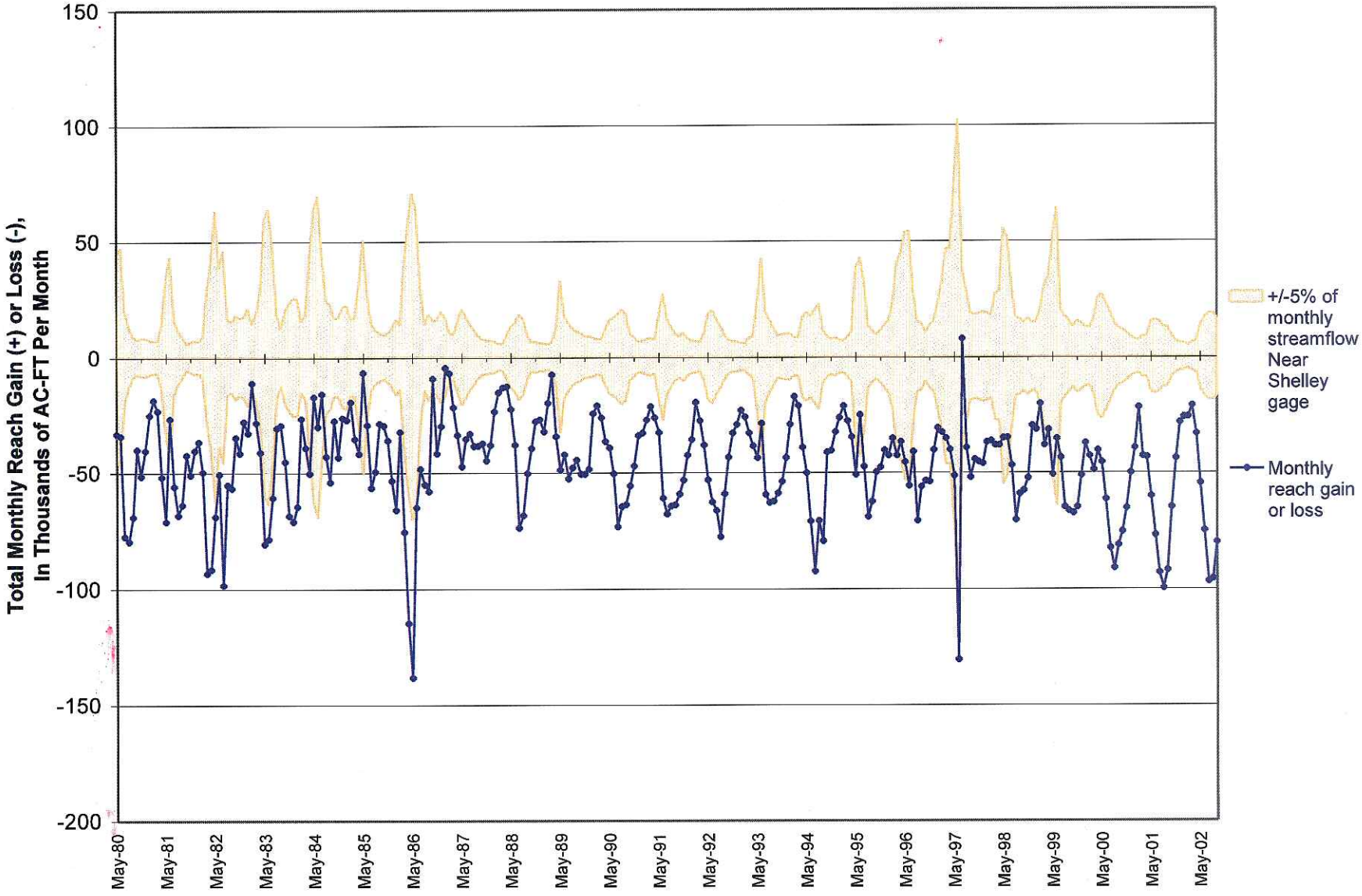


Figure 51. Monthly Snake River gains and losses: Shelley to Near Blackfoot reach.

A&B 2980

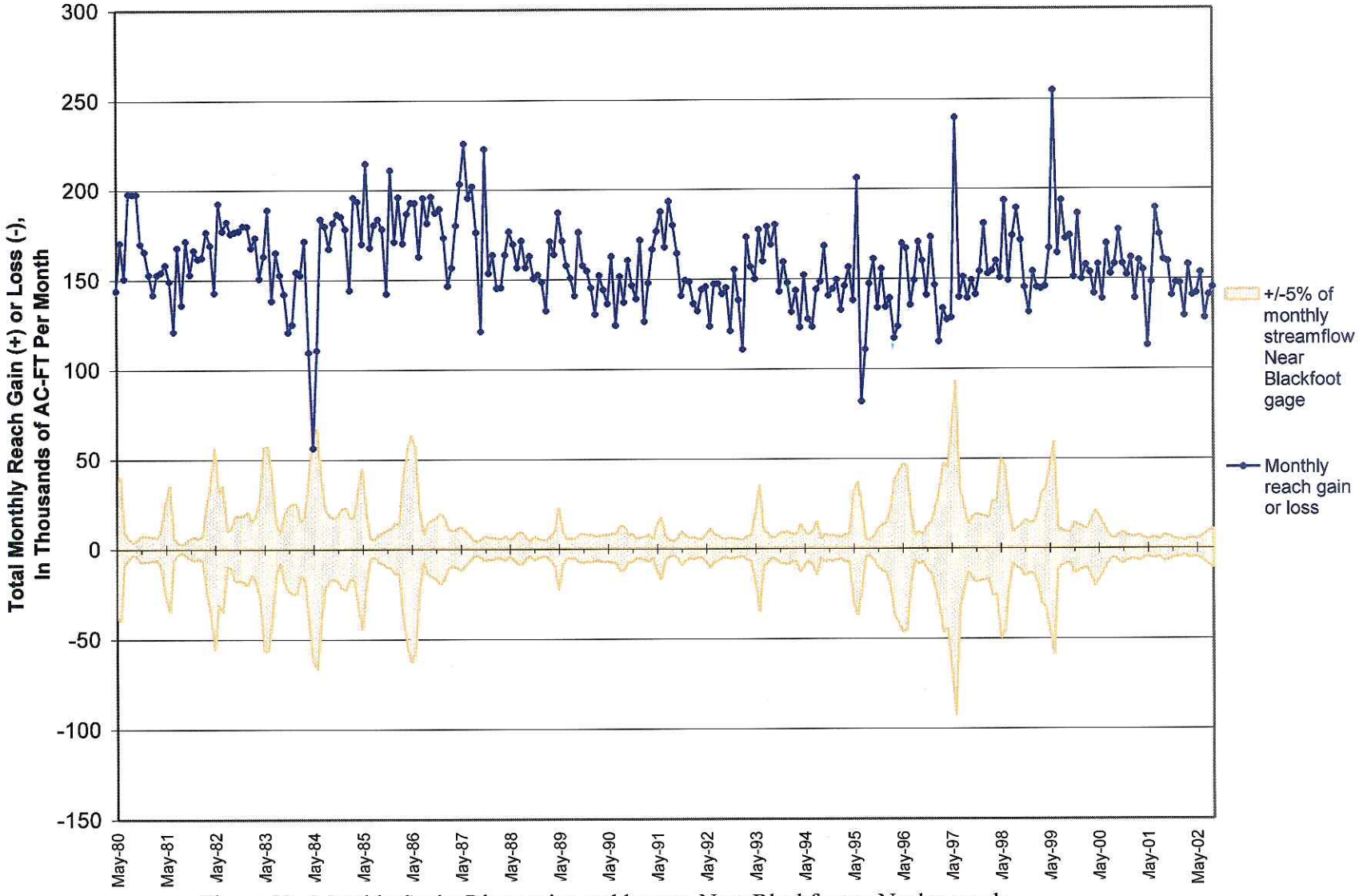


Figure 52. Monthly Snake River gains and losses: Near Blackfoot to Neeley reach.

A&B 2981

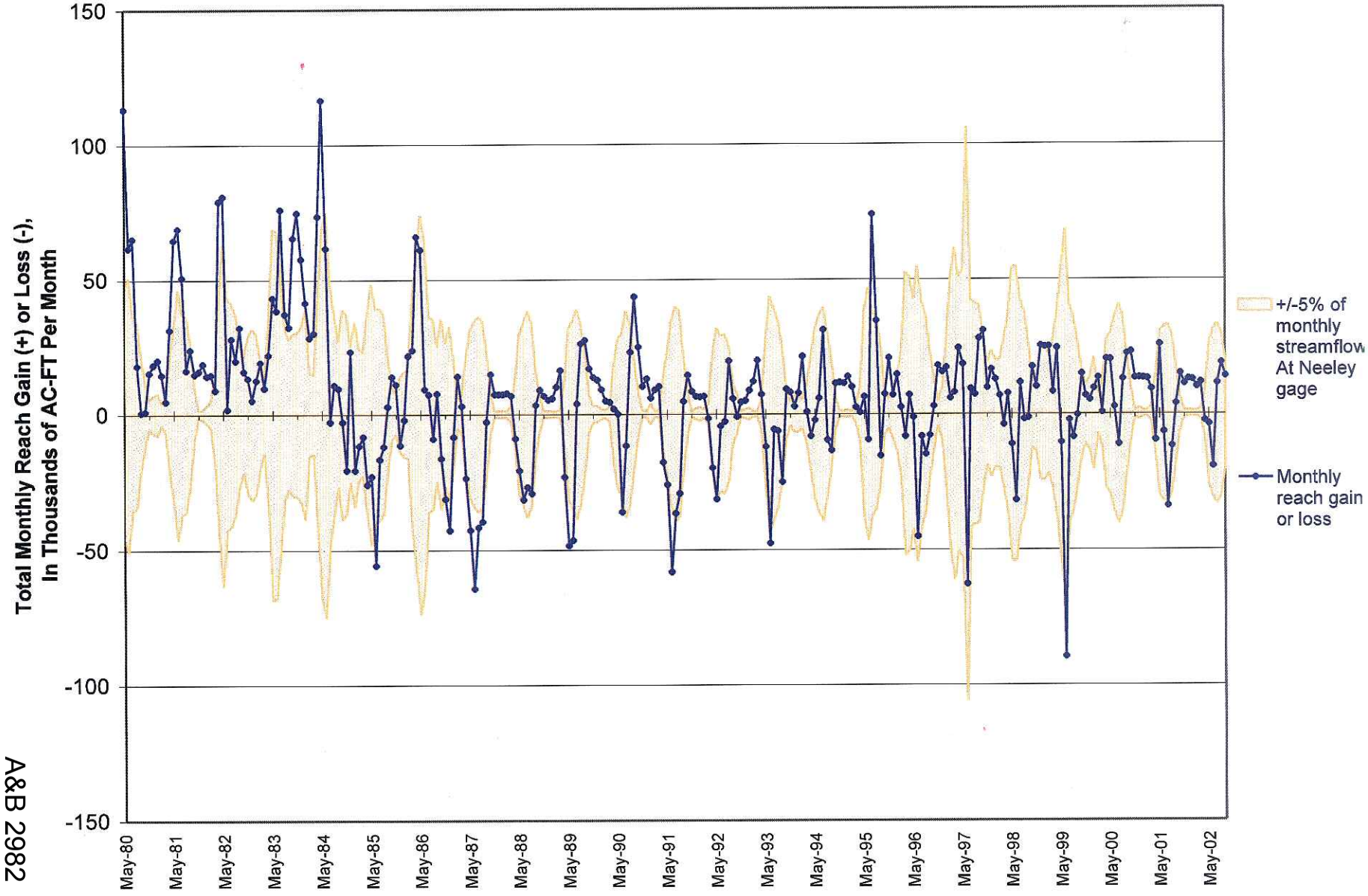


A&B 2982

Figure 53. Monthly Snake River gains and losses: Neeley to Minidoka reach.

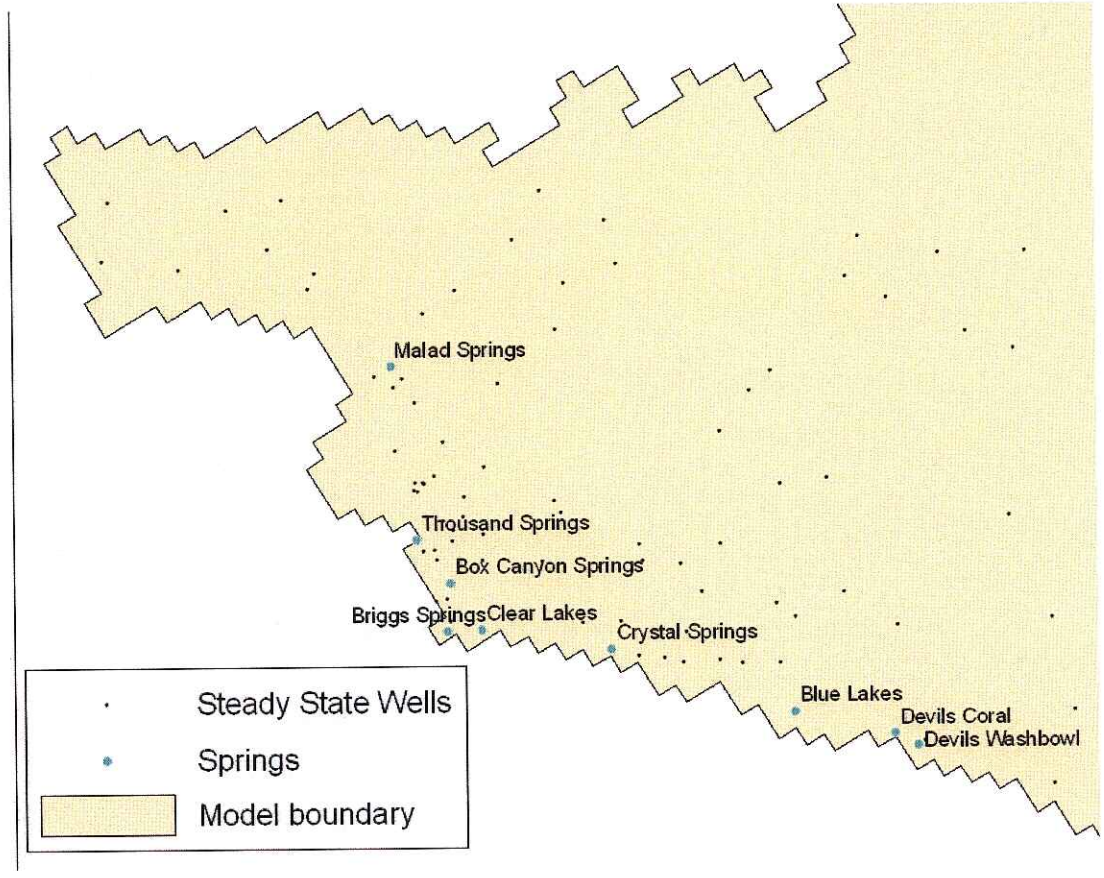


Figure 54. Location of springs used as calibration targets.

A&B 2983

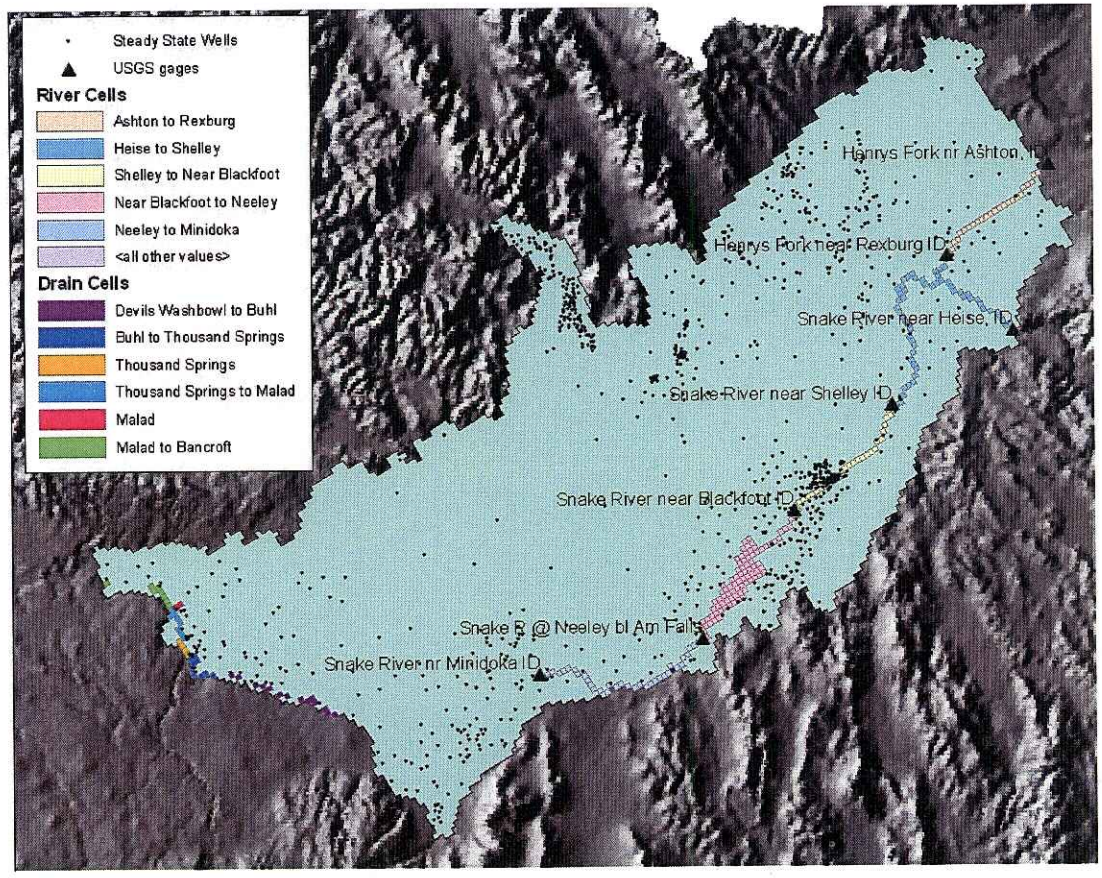


Figure 55. Location of steady state calibration water level targets.

A&B 2984

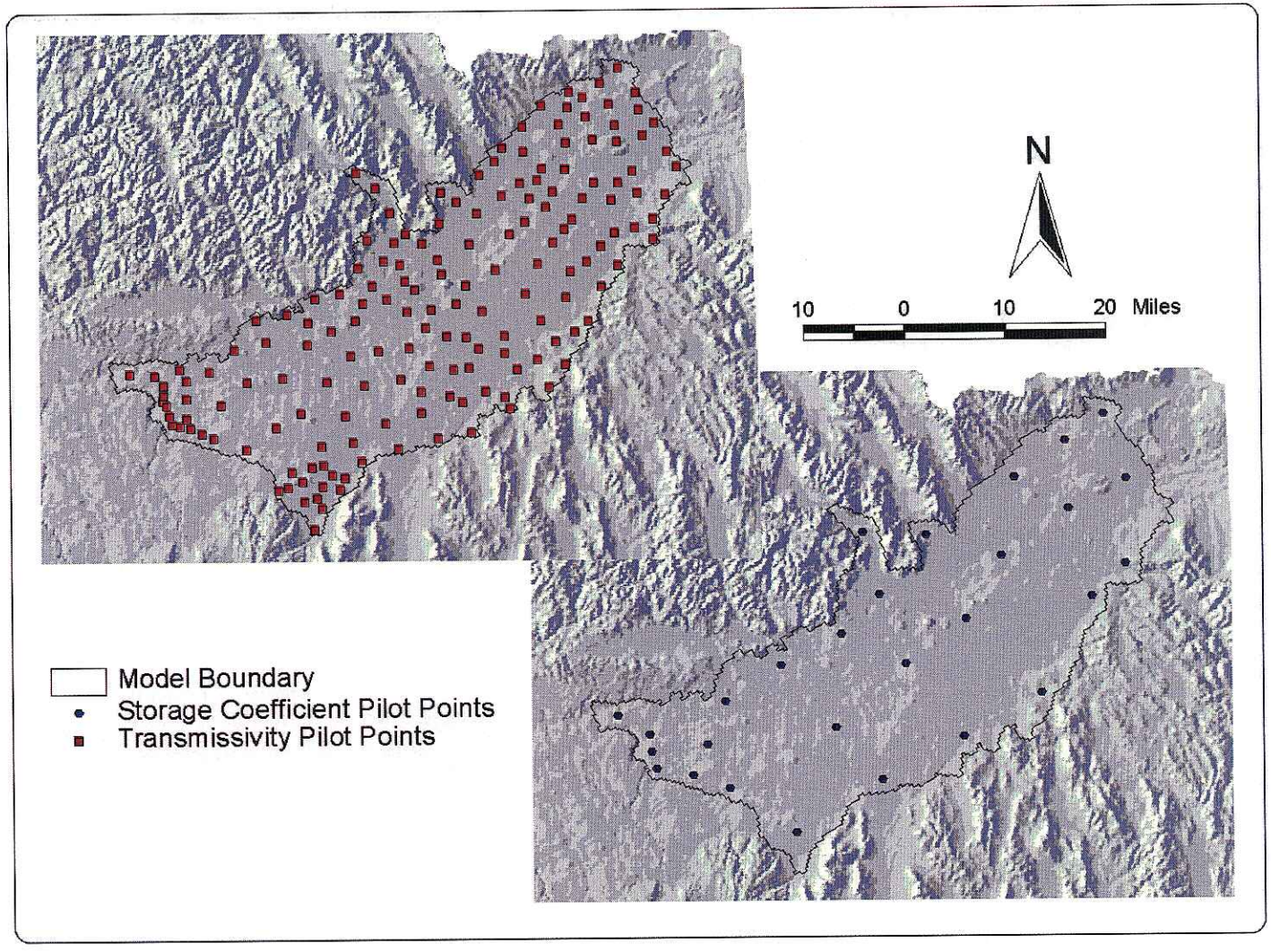


Figure 56. Location of pilot points used for calibration of transmissivity and aquifer storage.

A&B 2985

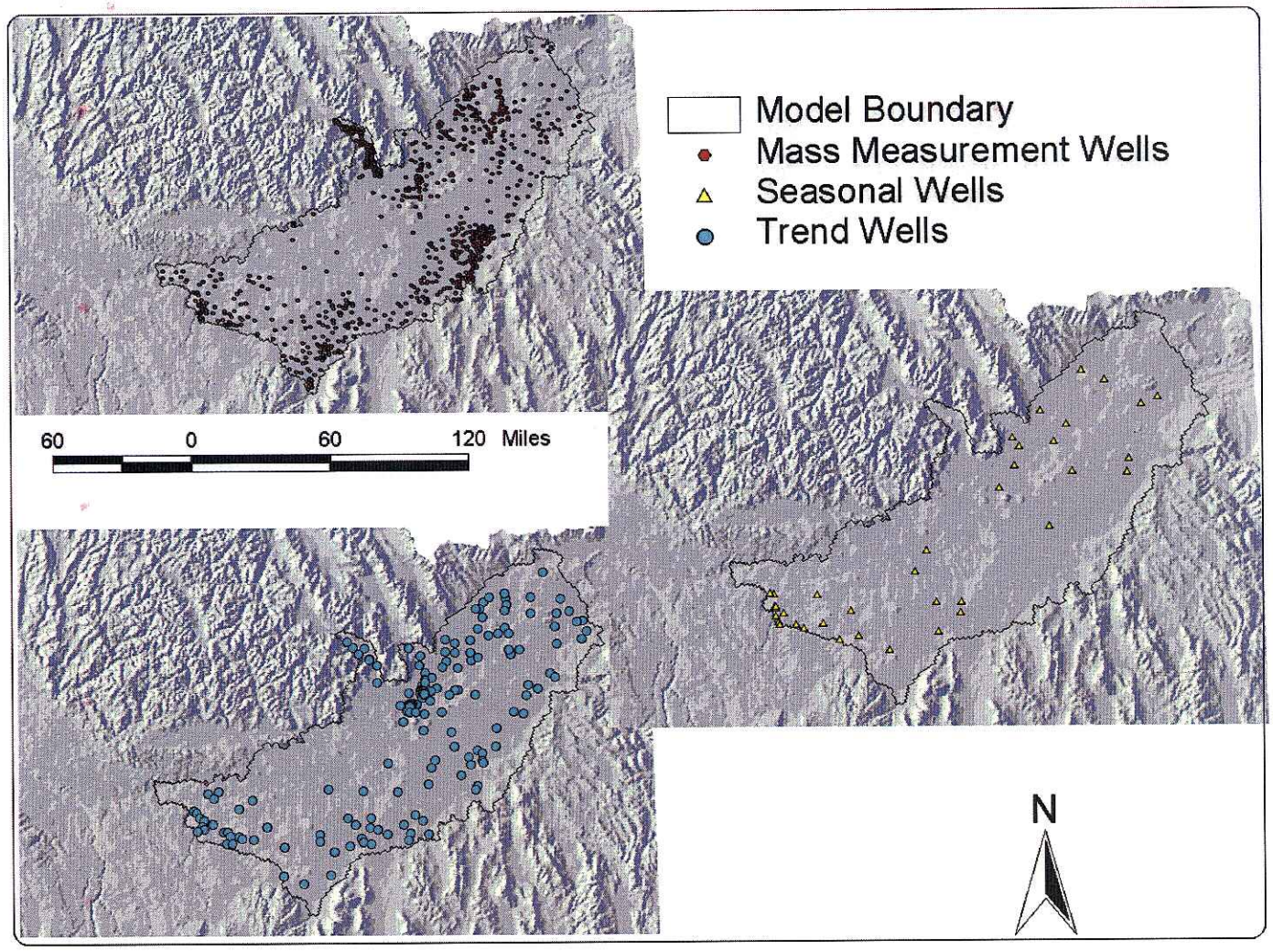


Figure 57. Location of transient aquifer water level observation well locations.

A&B 2986

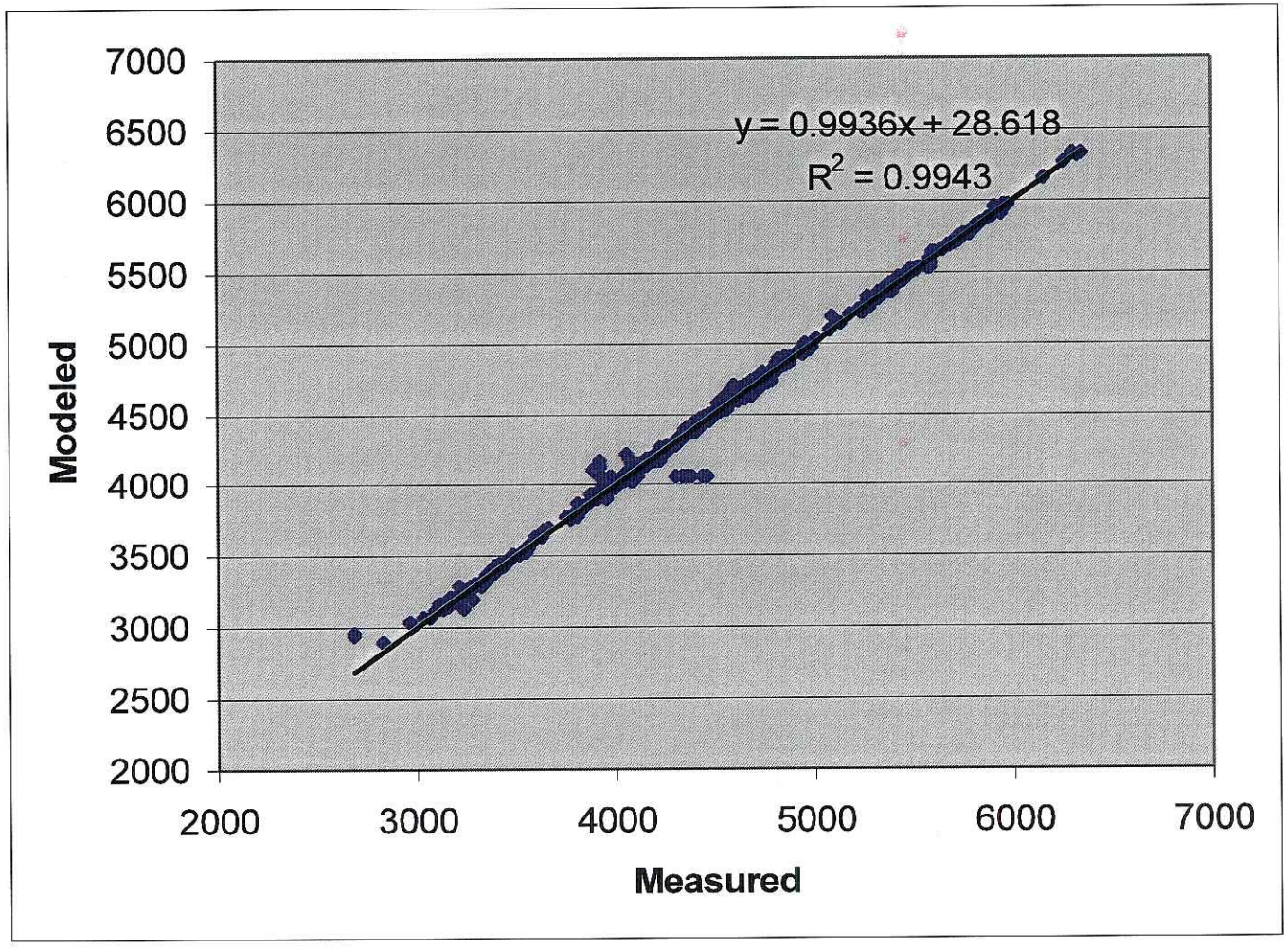


Figure 58. Scatter plot of model-predicted versus observed steady aquifer water levels (ft).

A&B 2987

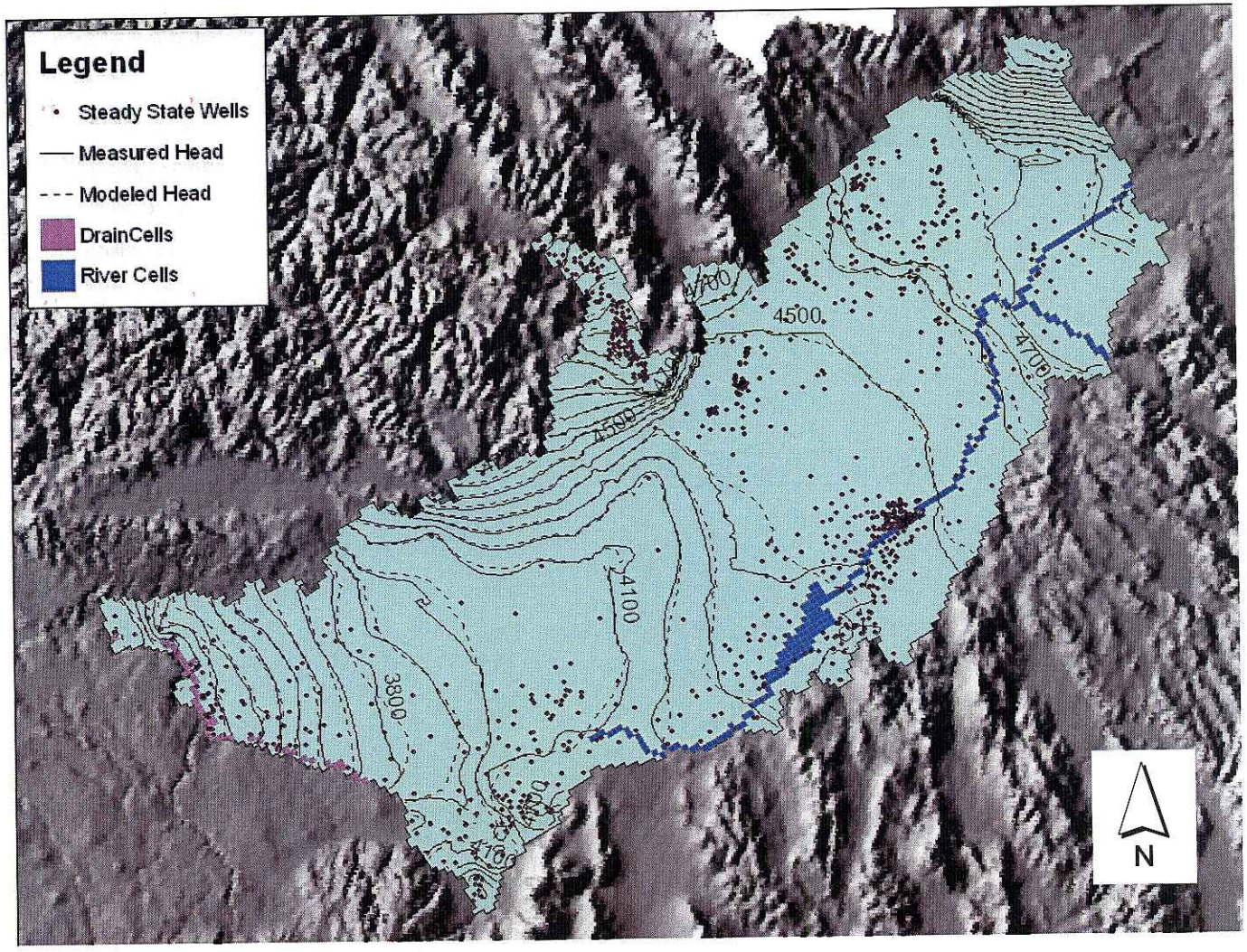


Figure 59. Steady state model-predicted versus observed aquifer potentiometric surface (100-ft. contours).

A&B 2988

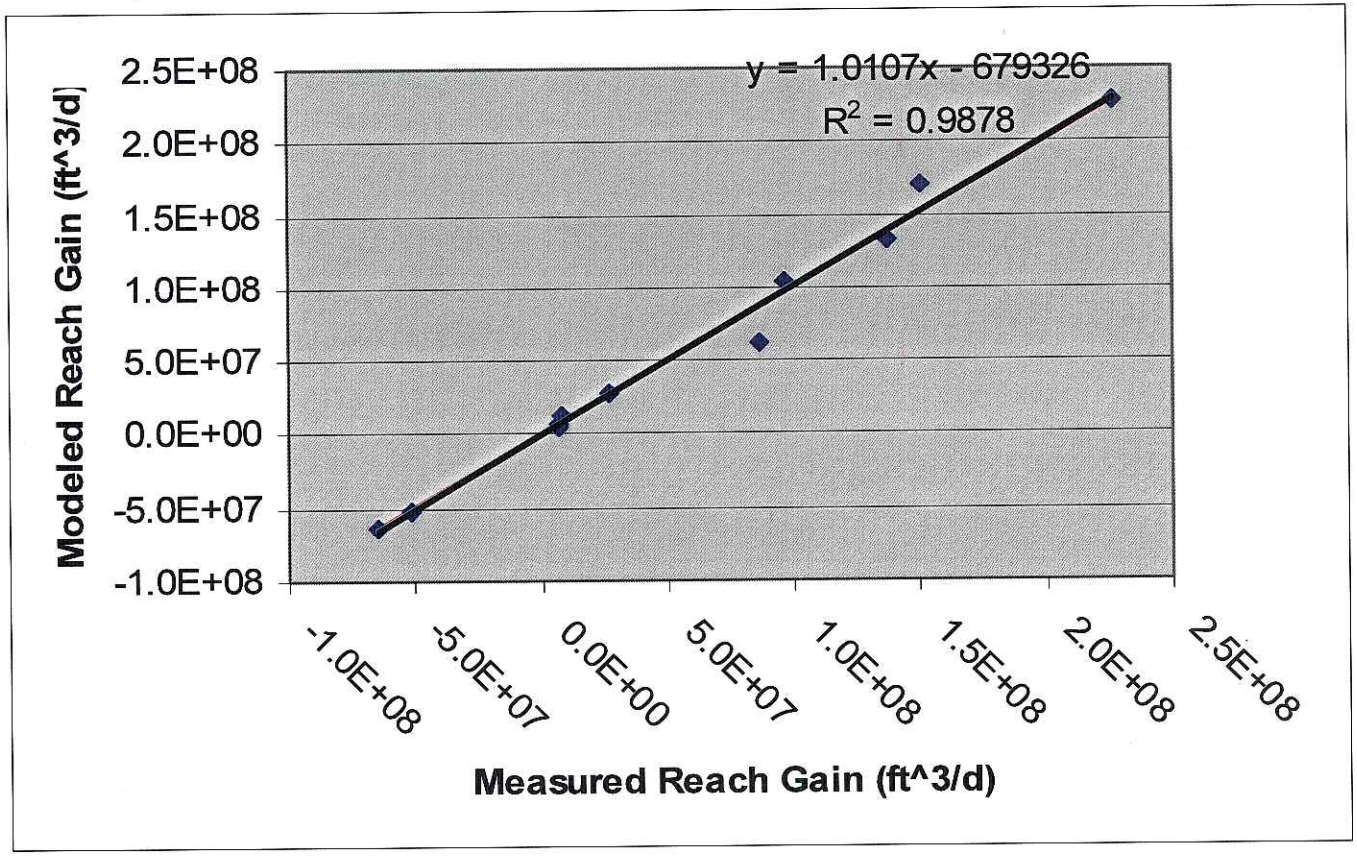


Figure 60. Scatter plot of model-predicted versus observed steady state river and spring fluxes ($ft^3/d$). (Positive value indicates reach gain.)

A&B 2989

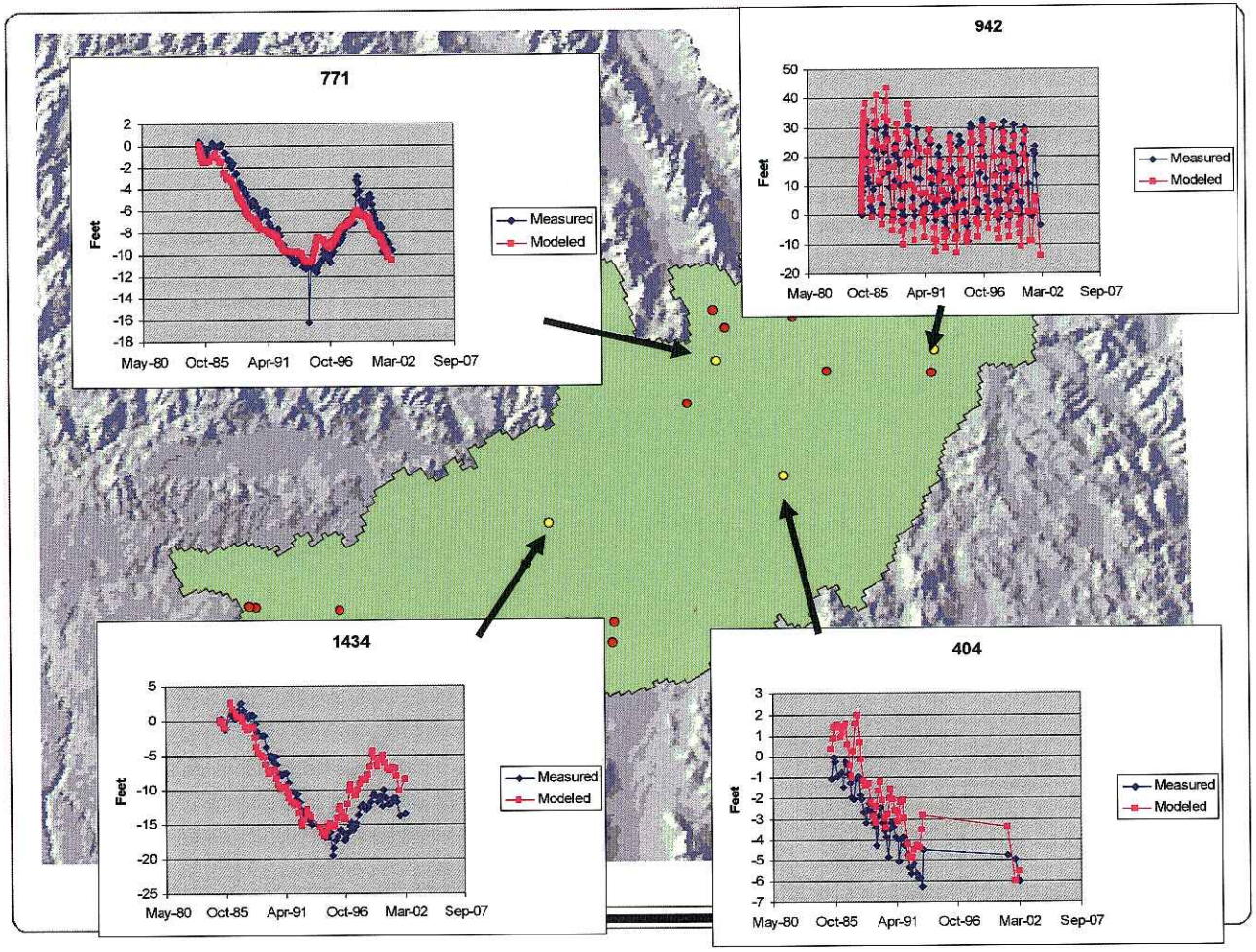


Figure 61. Selected seasonal well fits (1).

A&B 2990

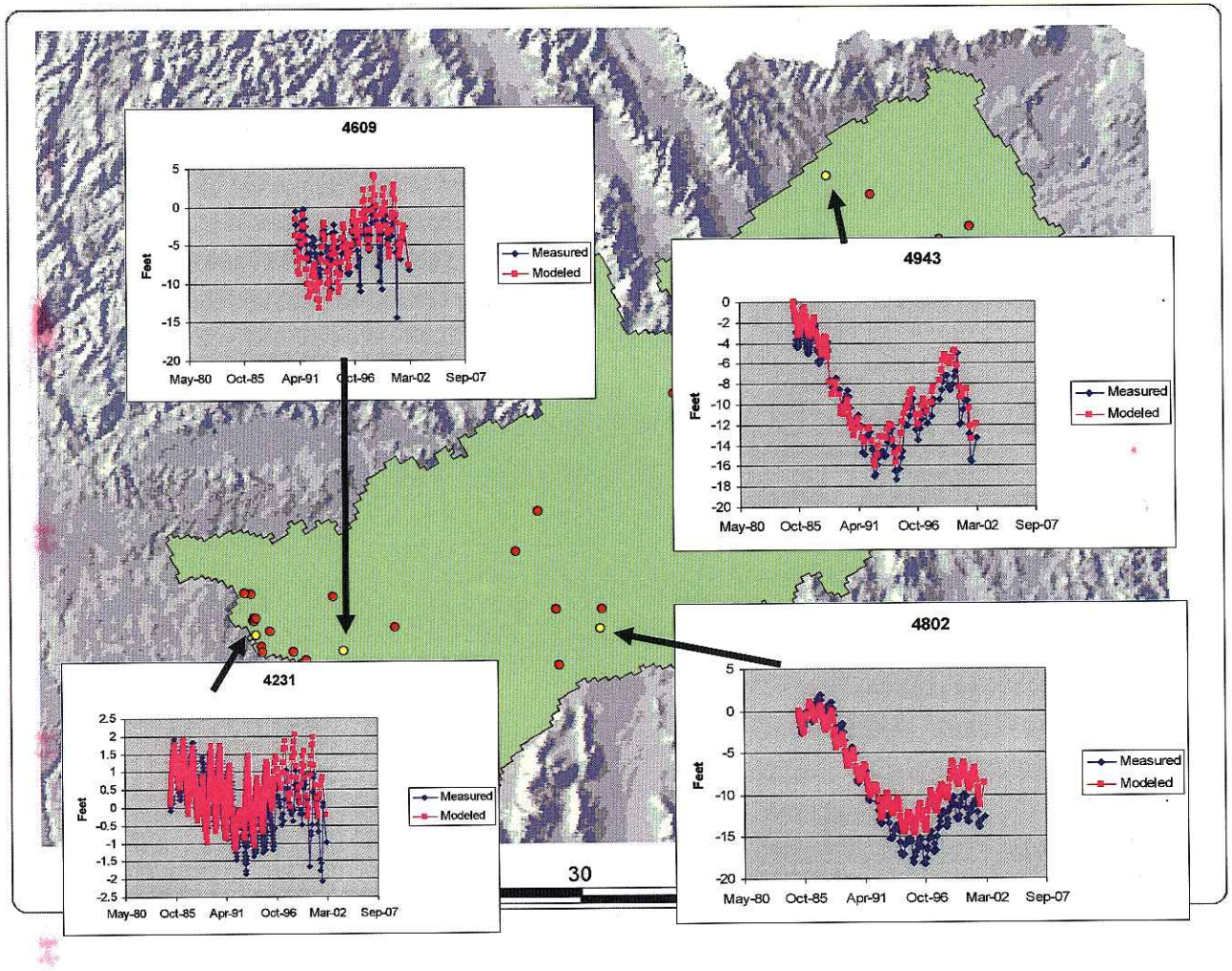


Figure 62. Selected seasonal well fits (2).

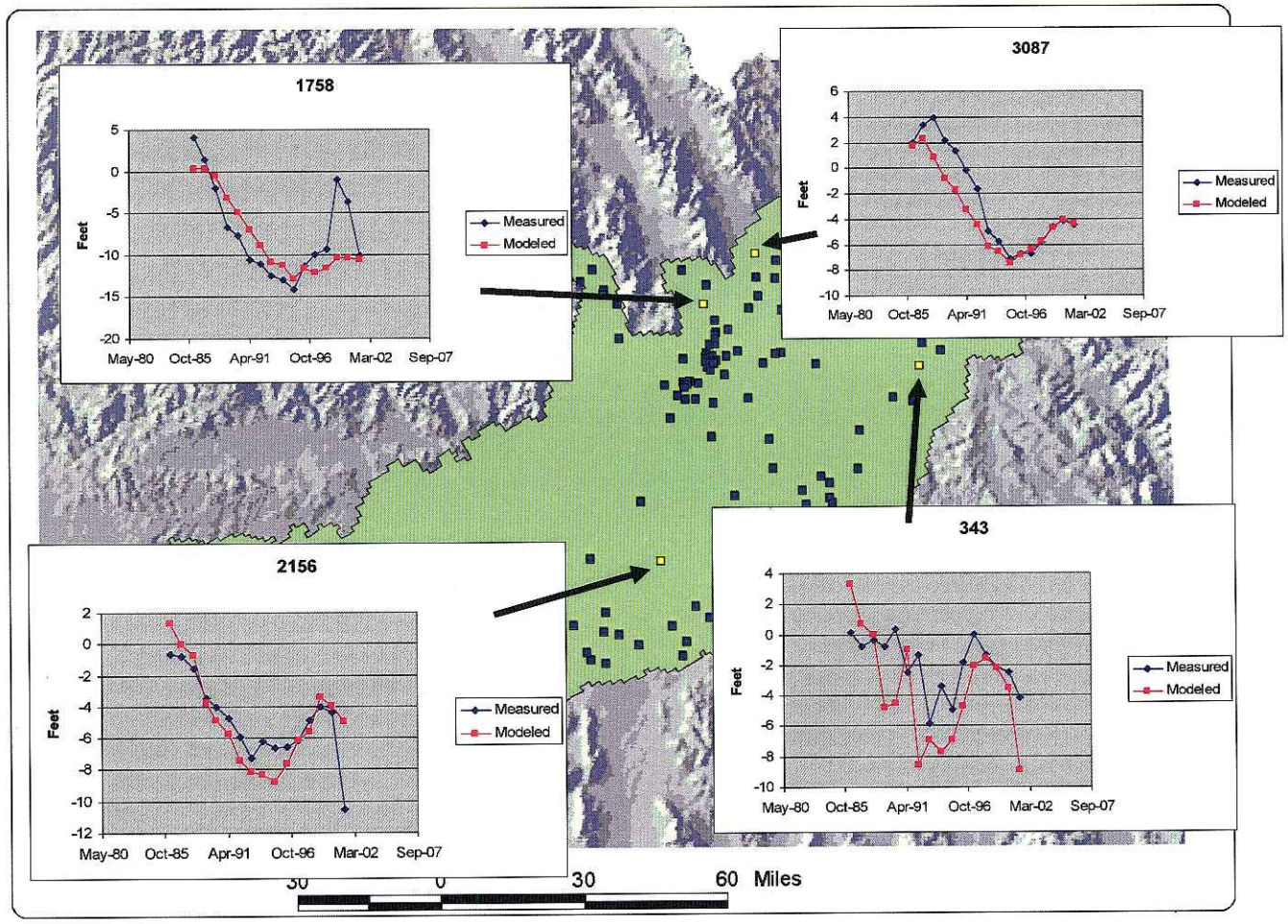


Figure 63. Selected trend well fits (1).

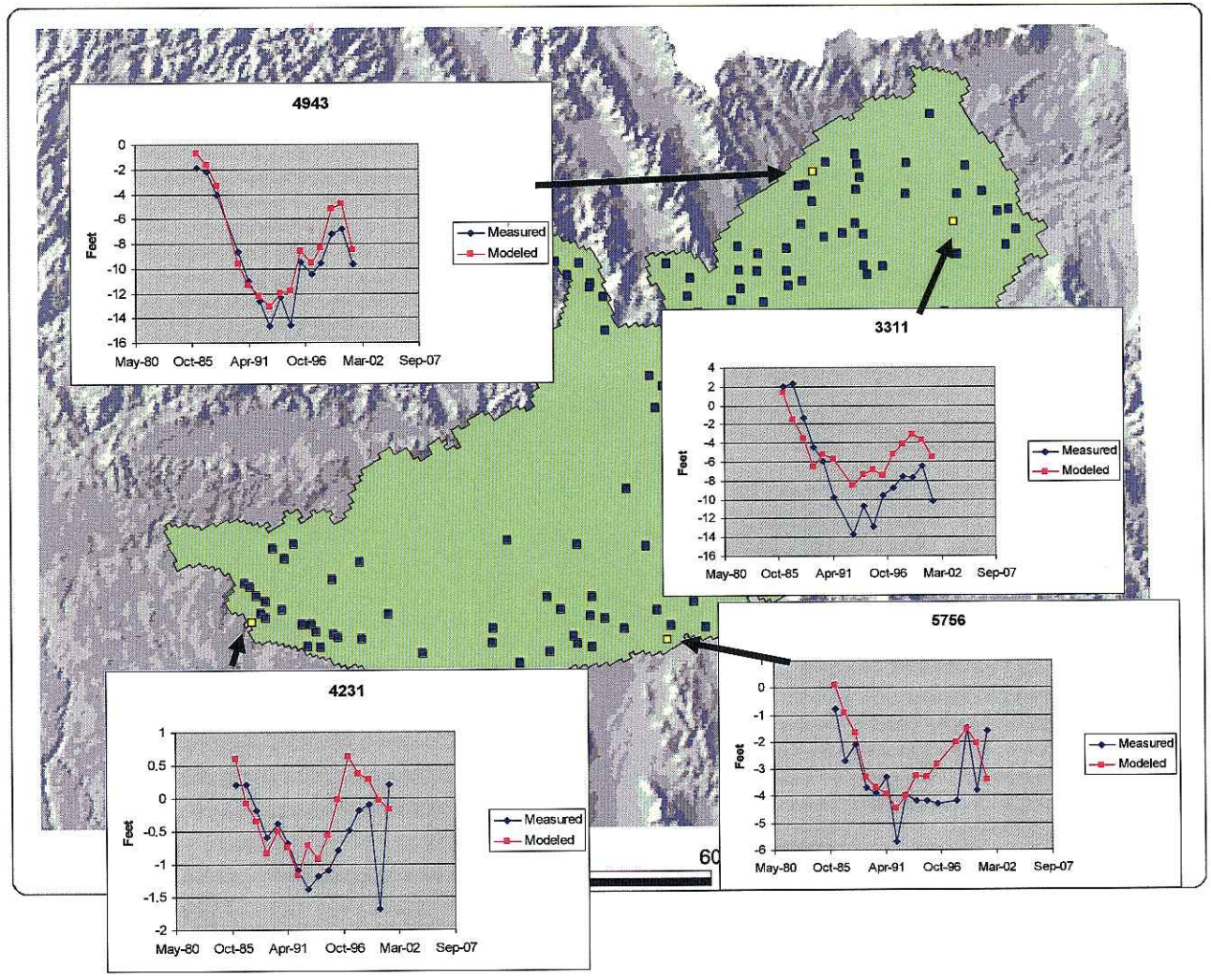


Figure 64. Selected trend well fits (2).

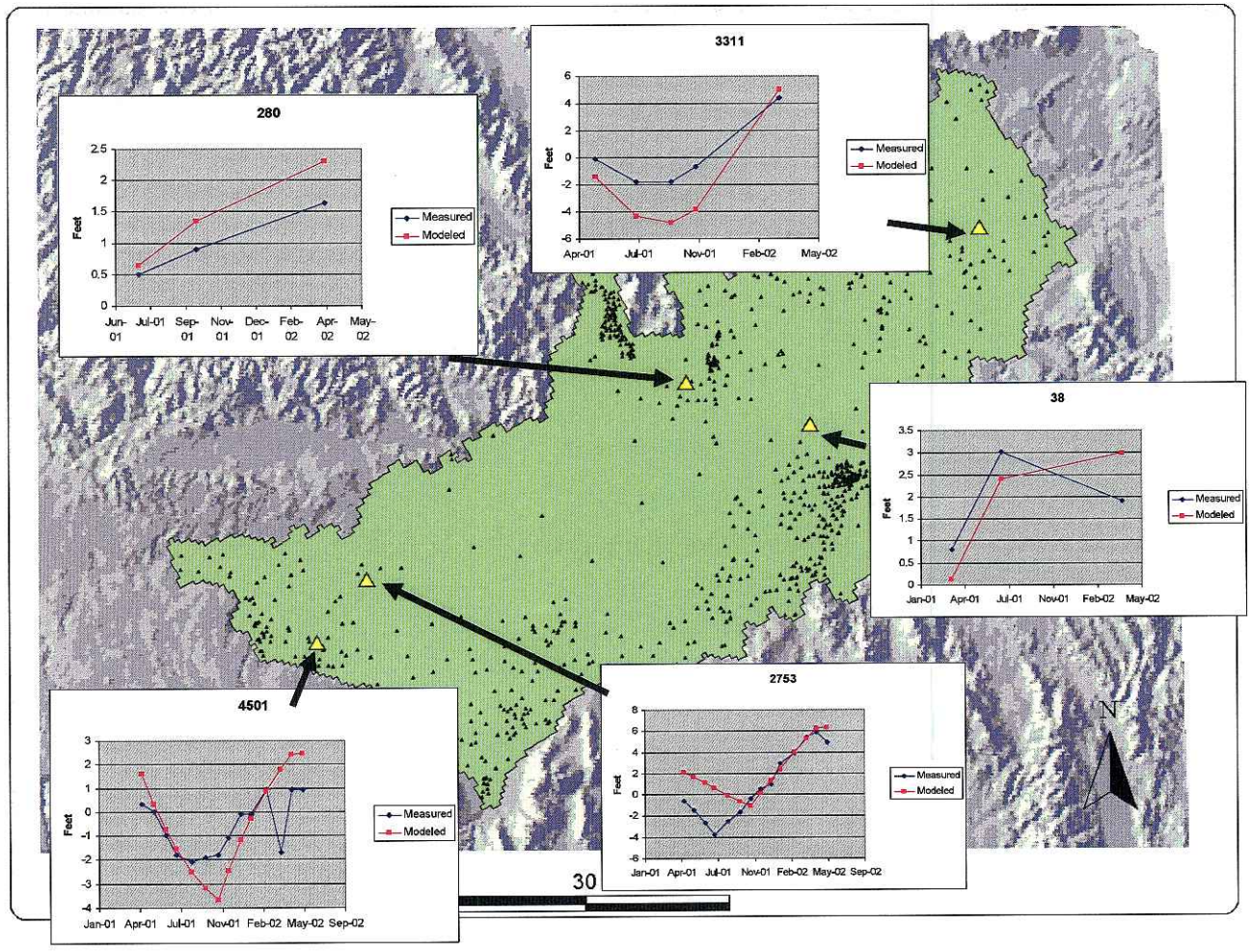


Figure 65. Selected mass measurement well fits.

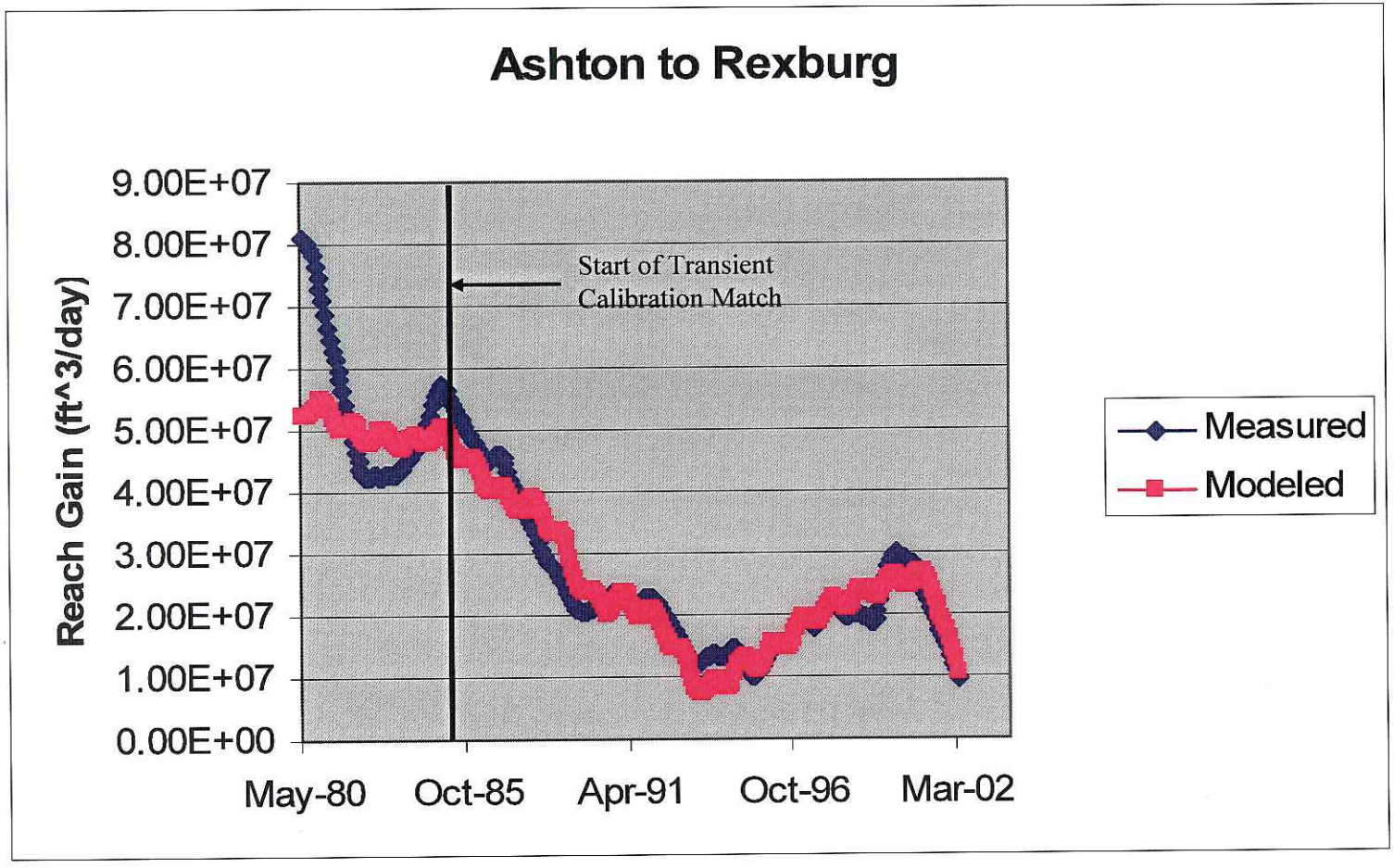


Figure 66. Modeled versus observed reach gain—Ashton to Rexburg reach, filtered data.

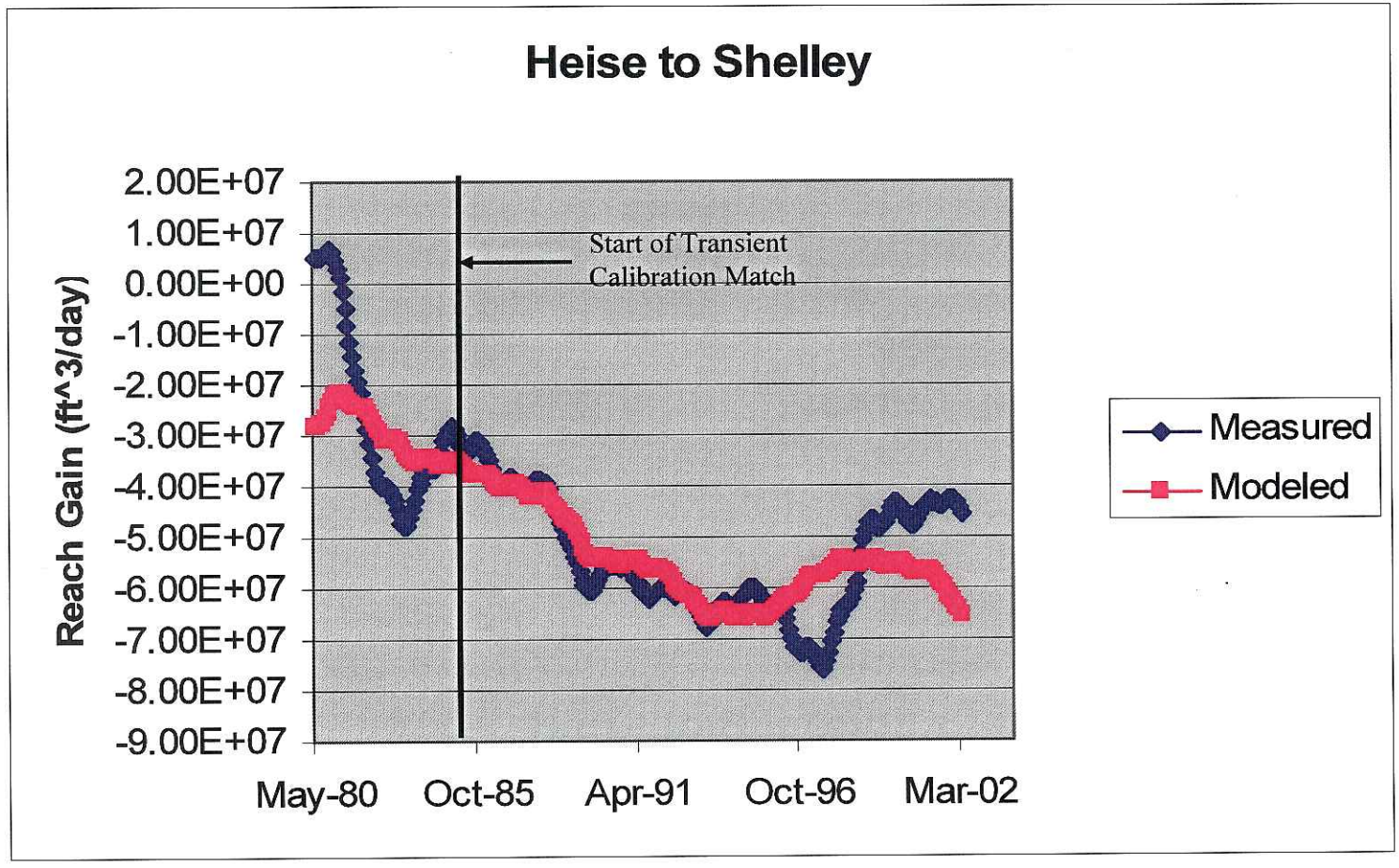


Figure 67. Modeled versus observed reach--Heise to Shelley reach, filtered data.

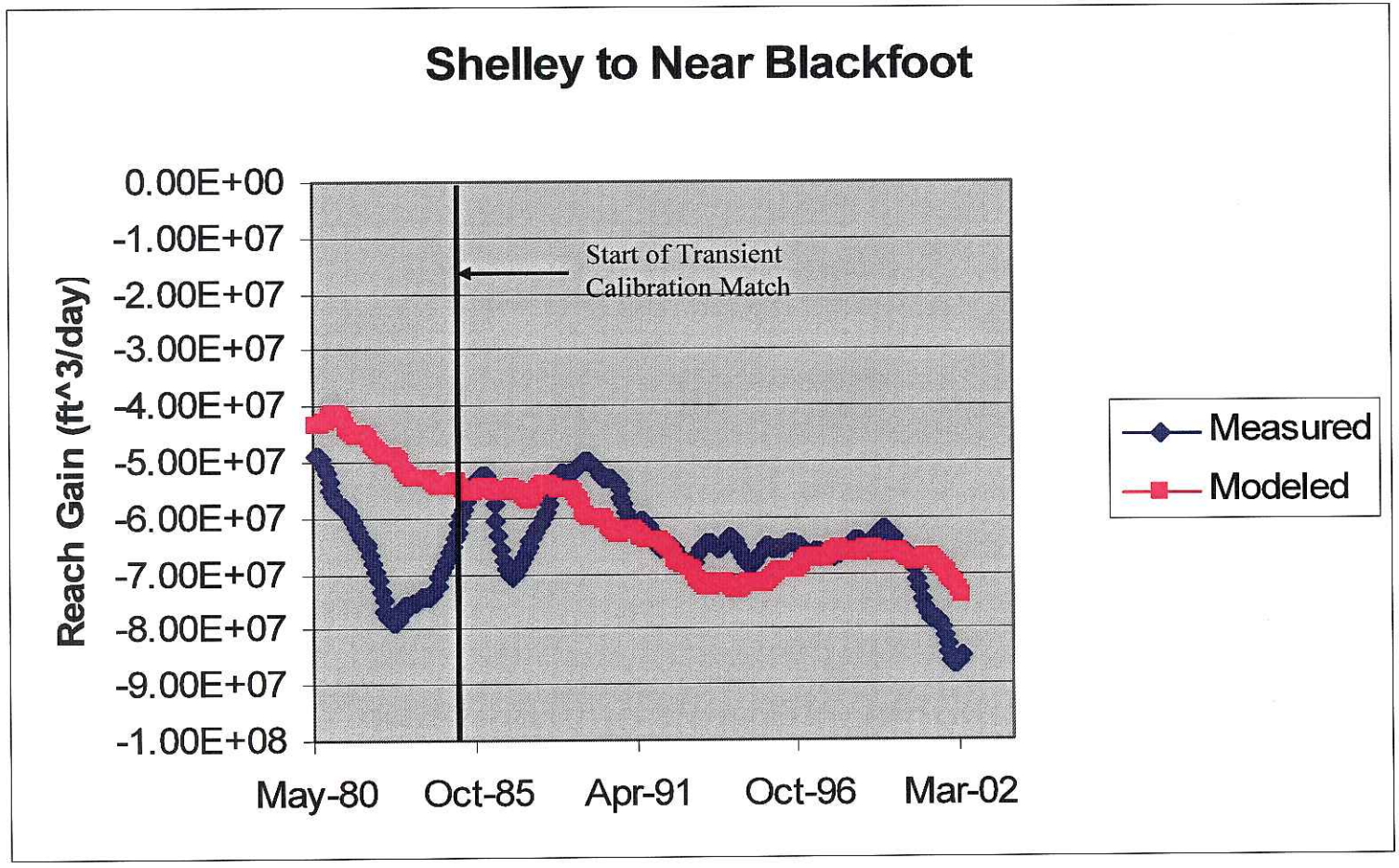


Figure 68. Modeled versus observed reach gain—Shelley to Near Blackfoot reach, filtered data.

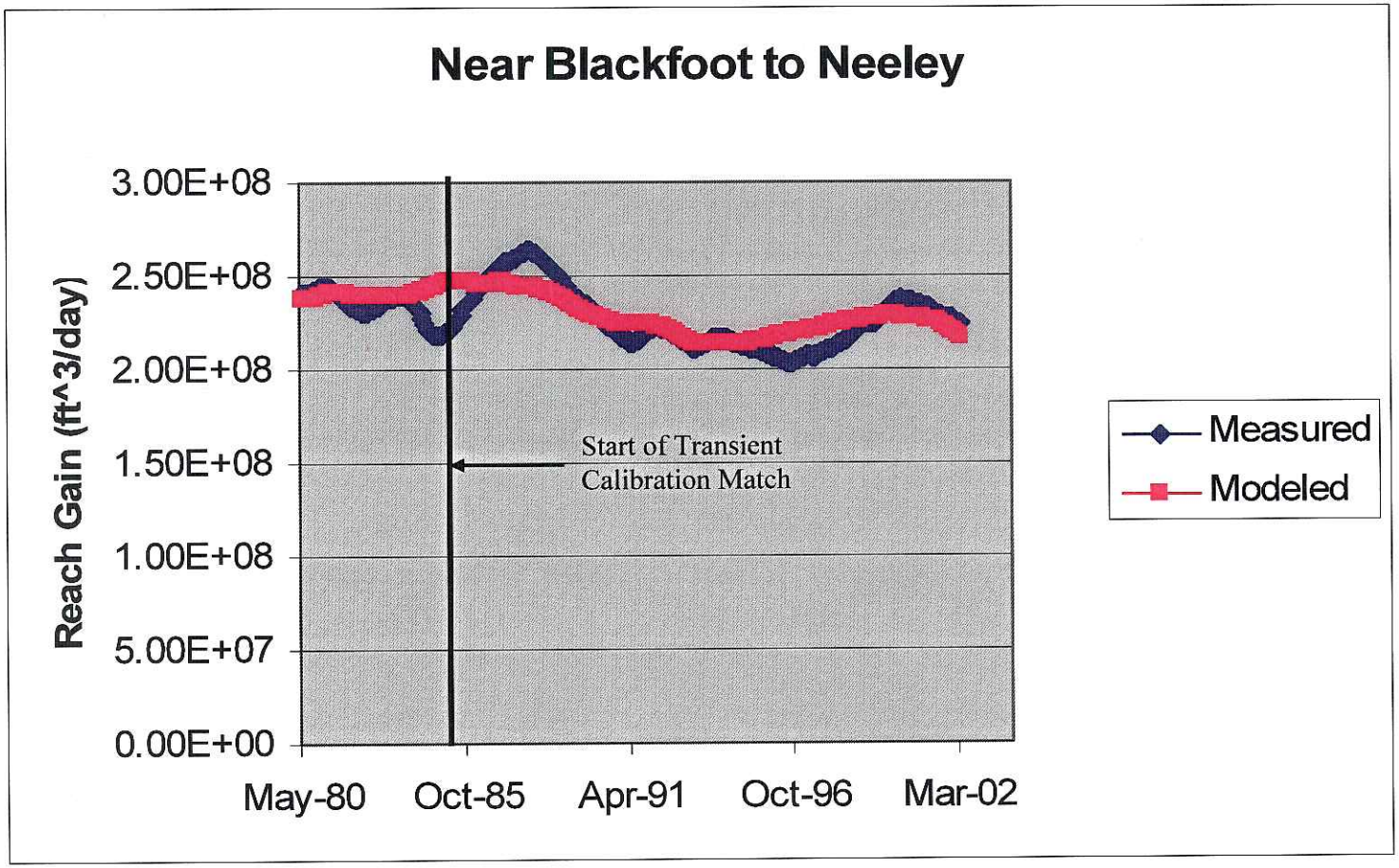


Figure 69. Modeled versus observed reach gain—Near Blackfoot to Neeley reach, filtered data.

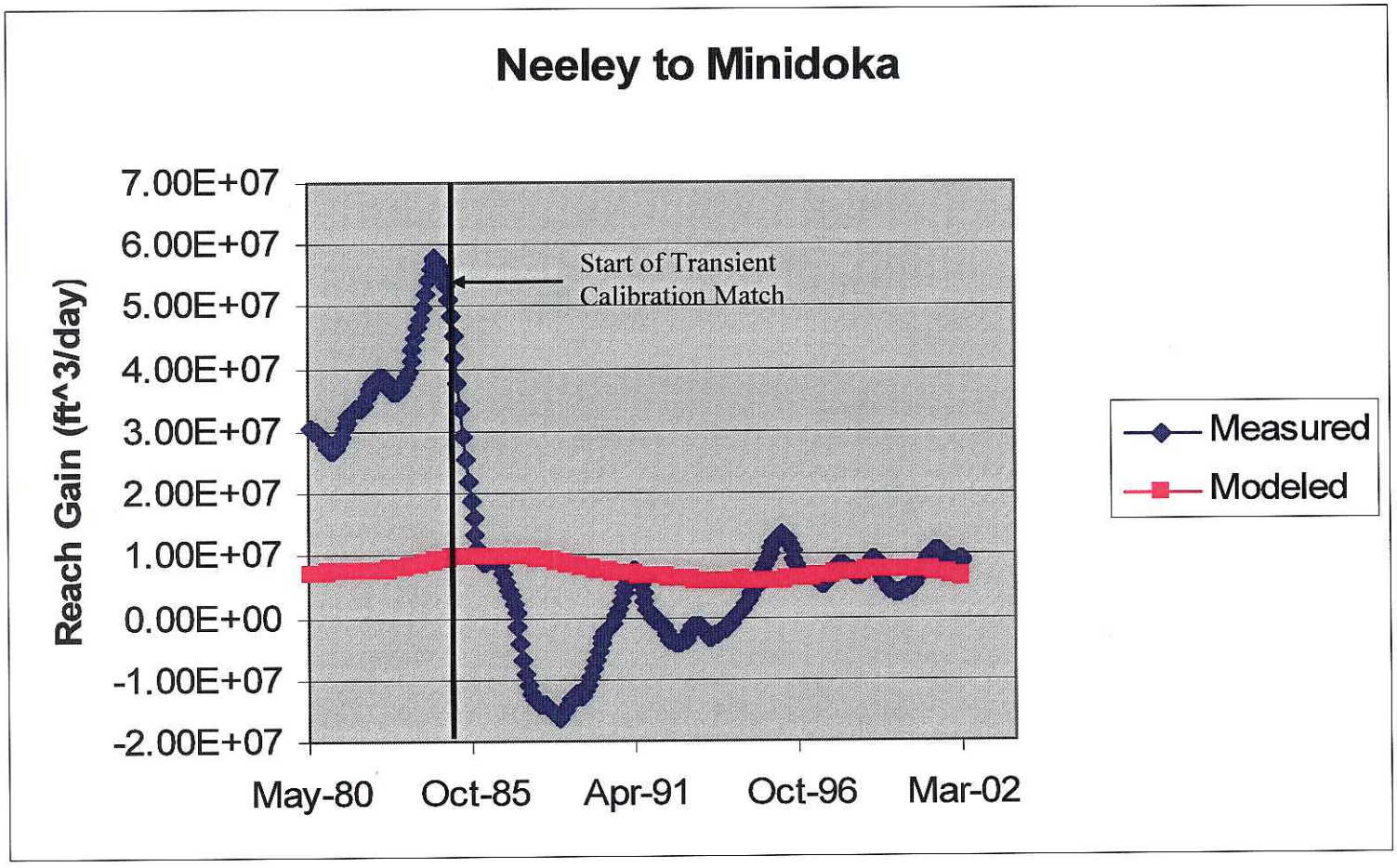


Figure 70. Modeled versus observed reach gain—Neeley to Minidoka reach, filtered data.

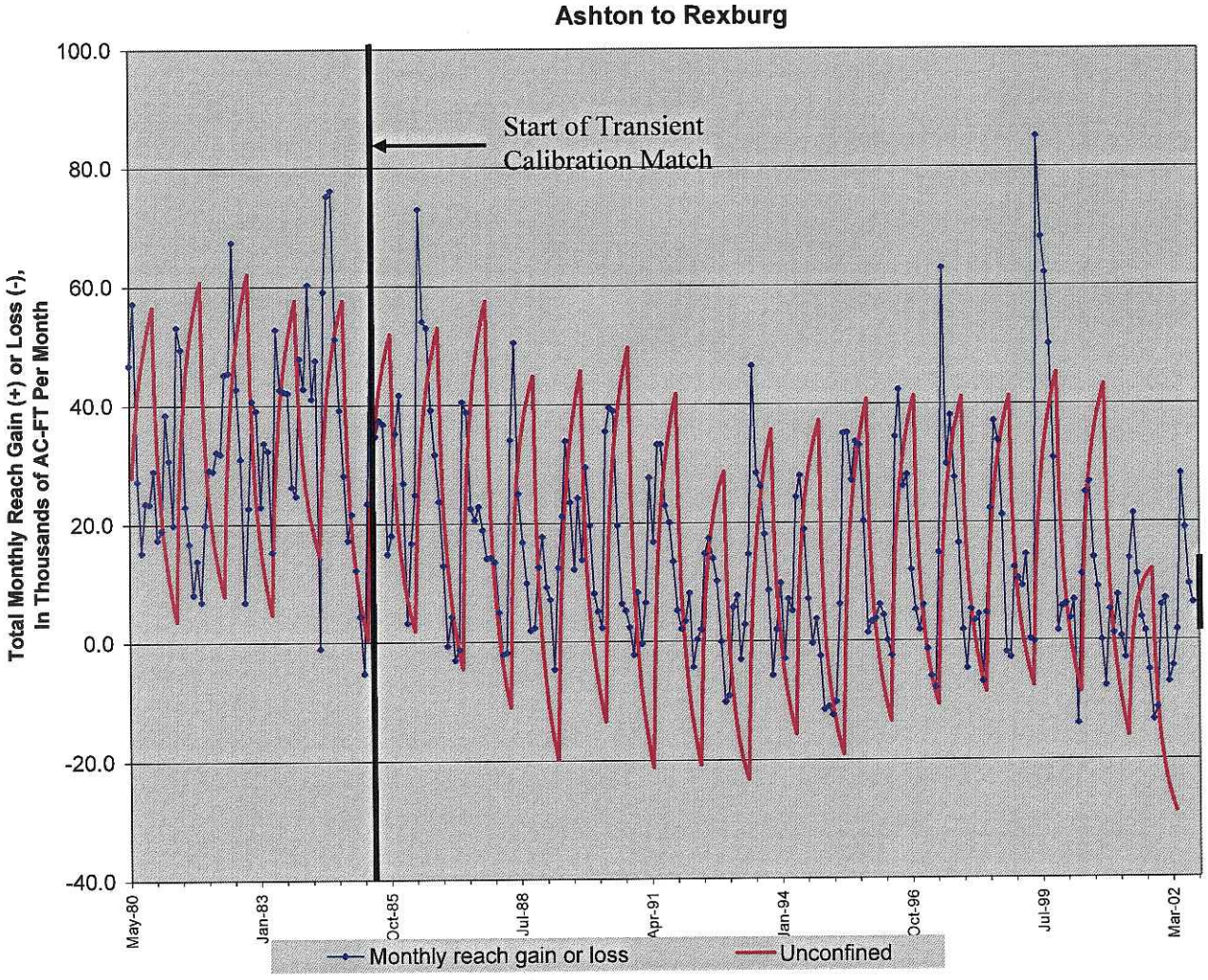


Figure 71. Modeled versus observed reach gain—Ashton to Rexburg reach, monthly unfiltered data.

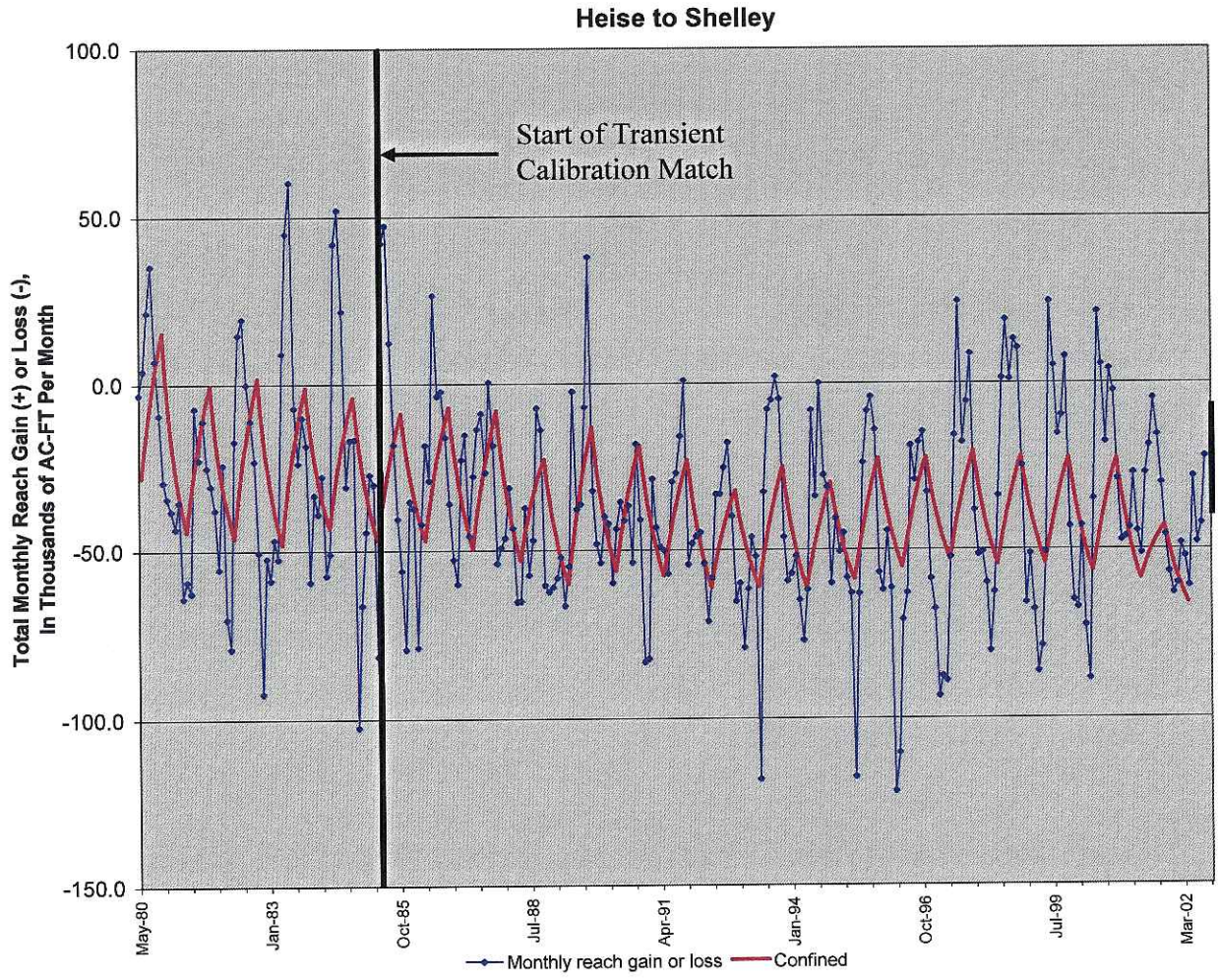


Figure 72. Modeled versus observed reach--Heise to Shelley reach, monthly unfiltered data.

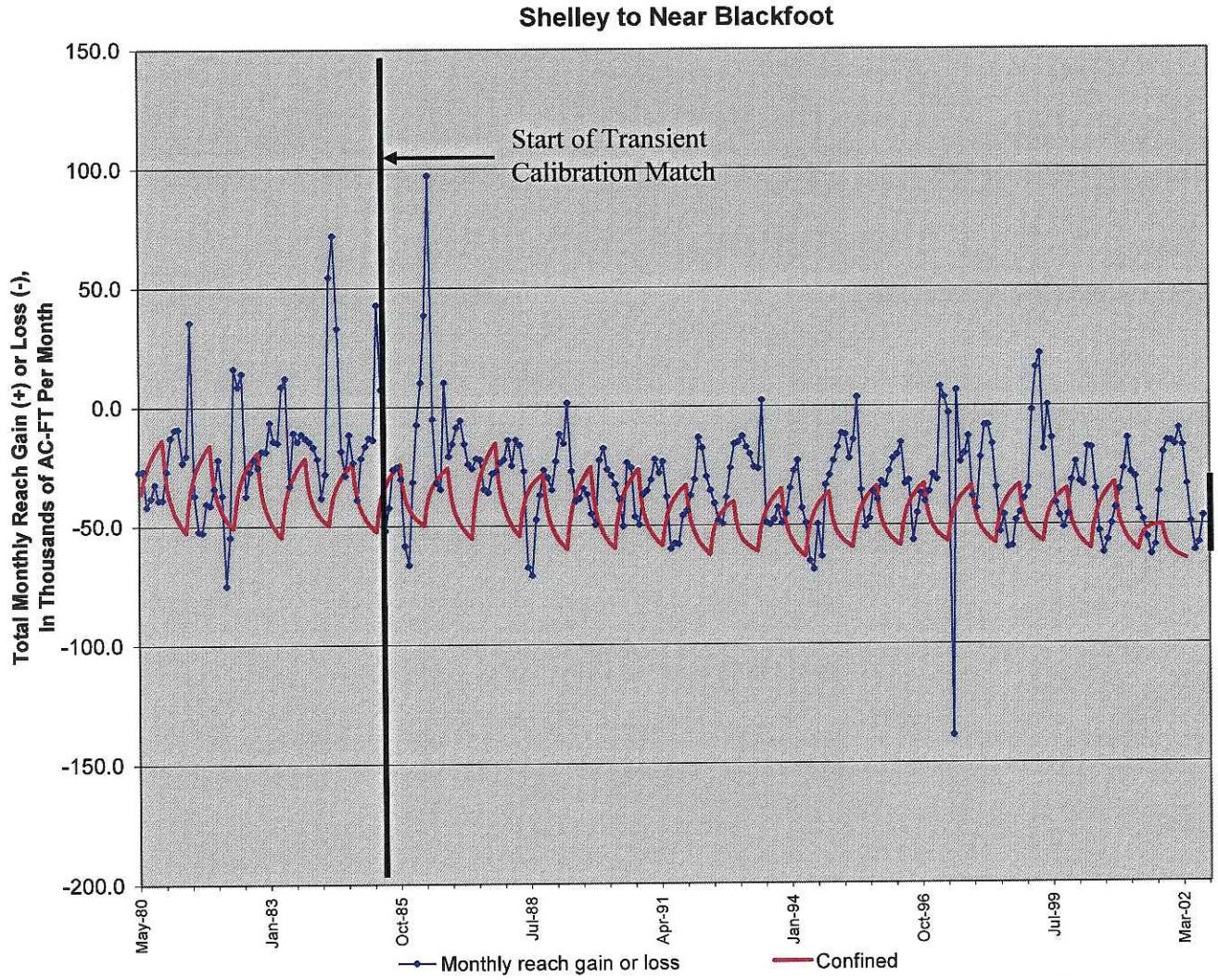


Figure 73. Modeled versus observed reach gain—Shelley to Near Blackfoot reach, monthly unfiltered data.

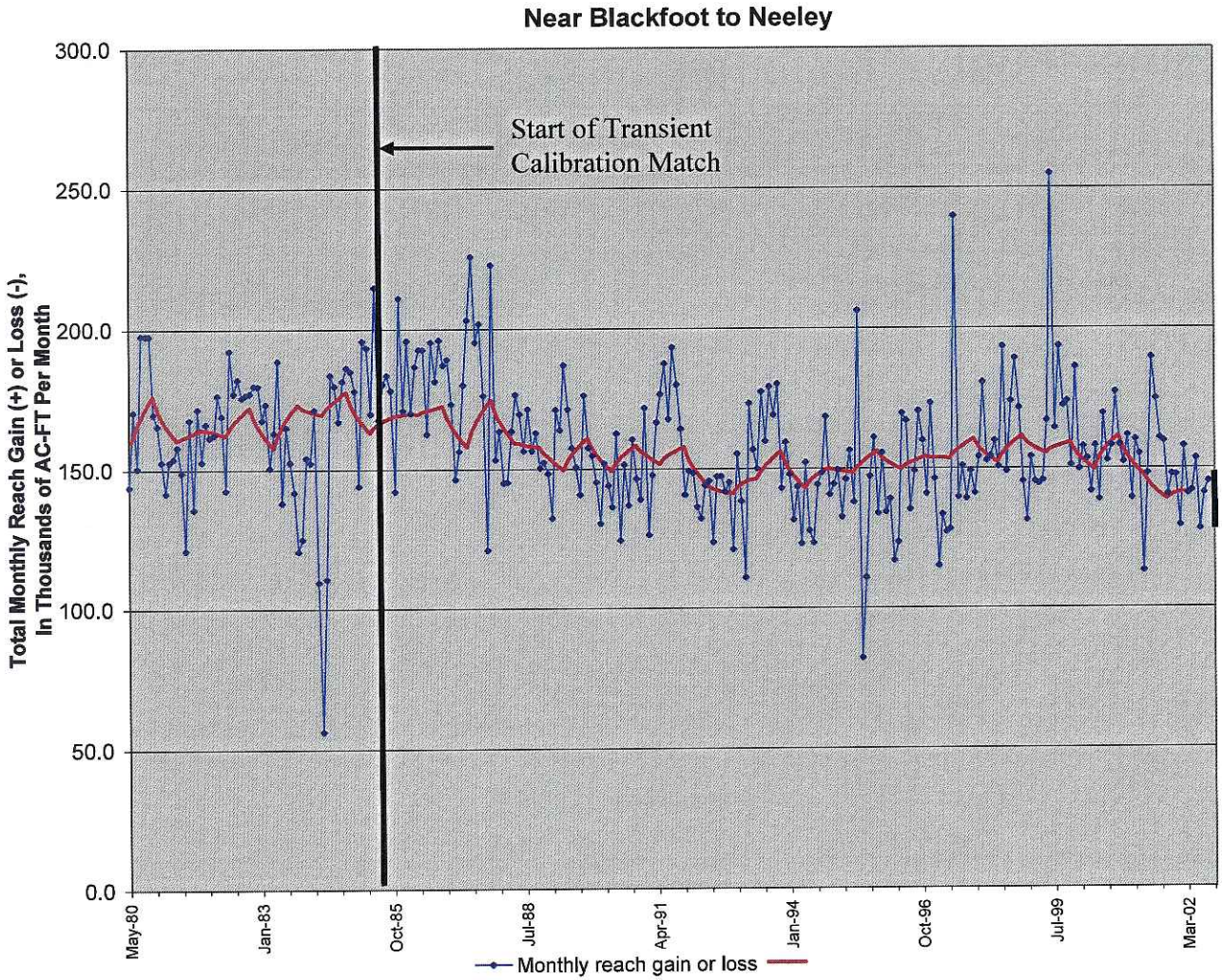


Figure 74. Modeled versus observed reach gain—Near Blackfoot to Neeley reach, monthly unfiltered data.

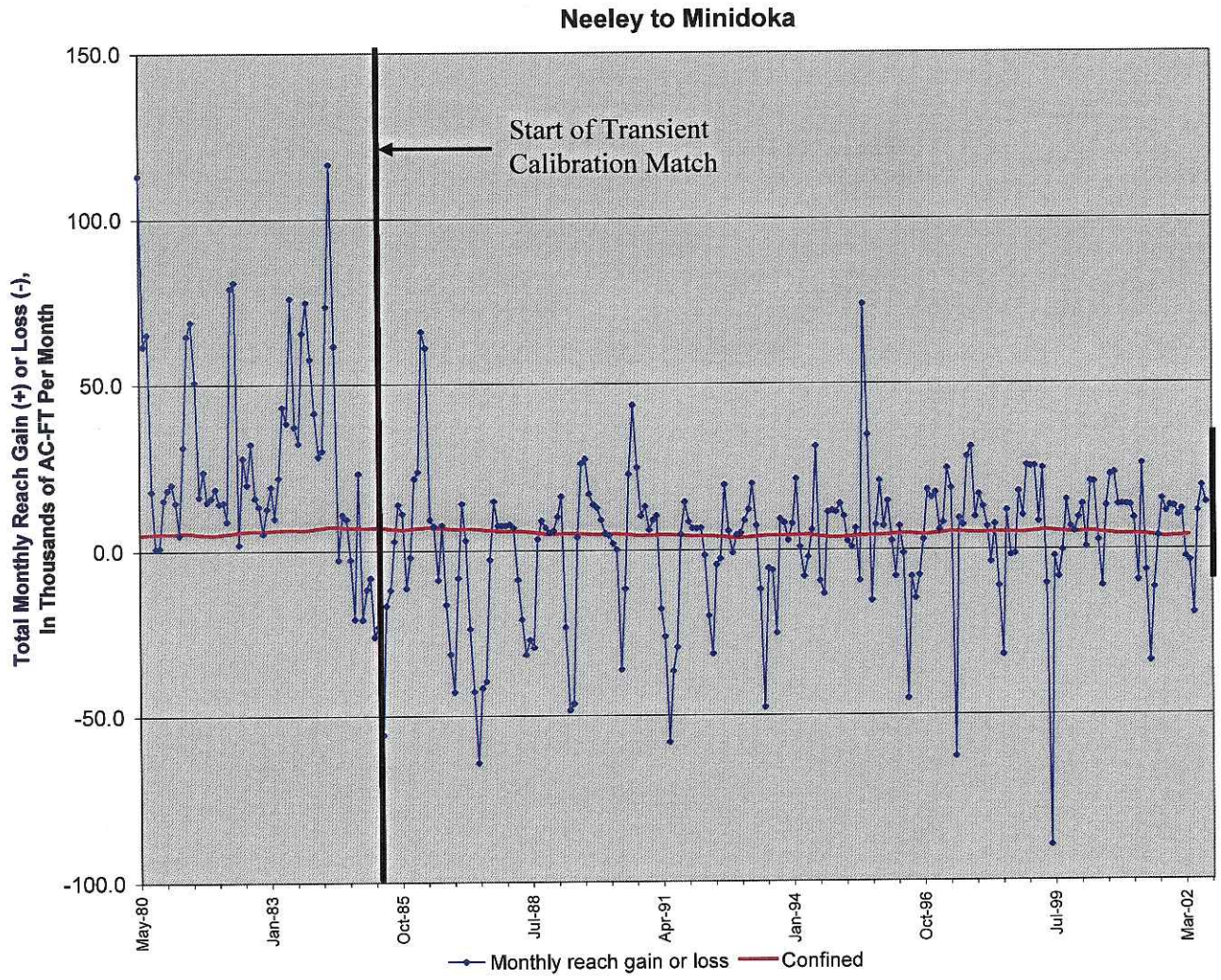


Figure 75. Modeled versus observed reach gain—Neeley to Minidoka reach, monthly unfiltered data.

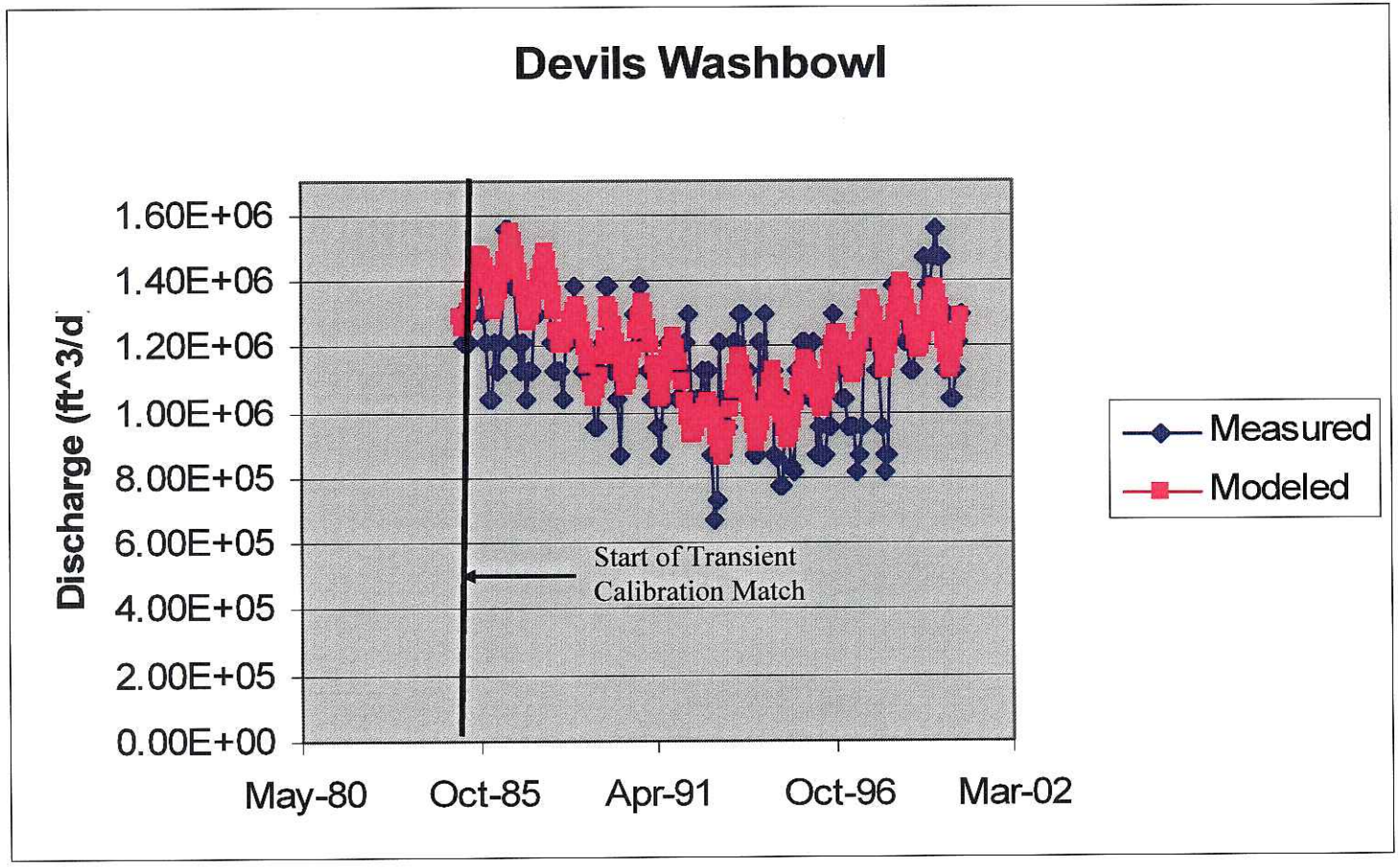


Figure 76. Modeled versus observed spring discharge—Devils Washbowl (ft^3/d).

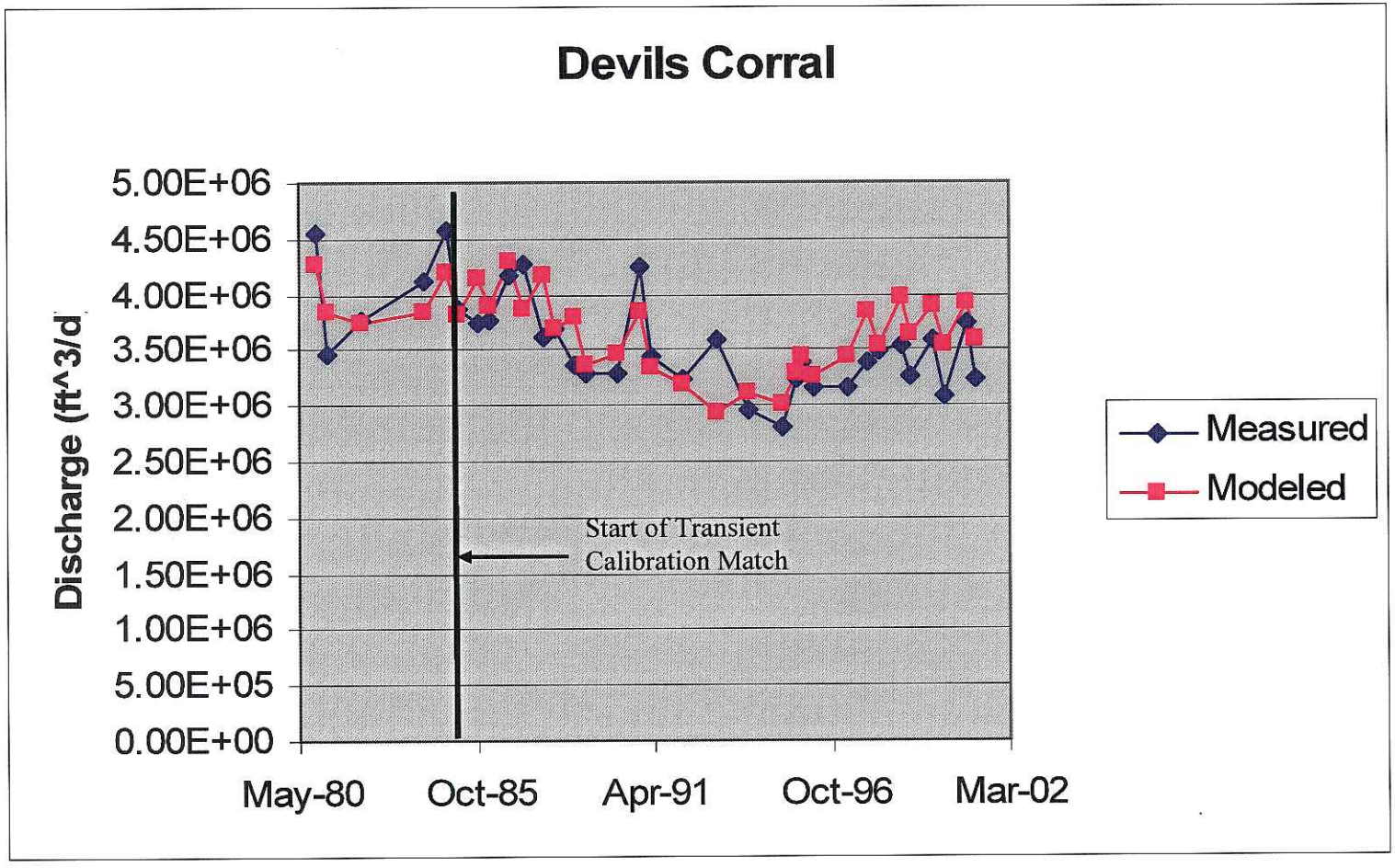


Figure 77. Modeled versus observed spring discharge—Devils Corral (ft^3/d).

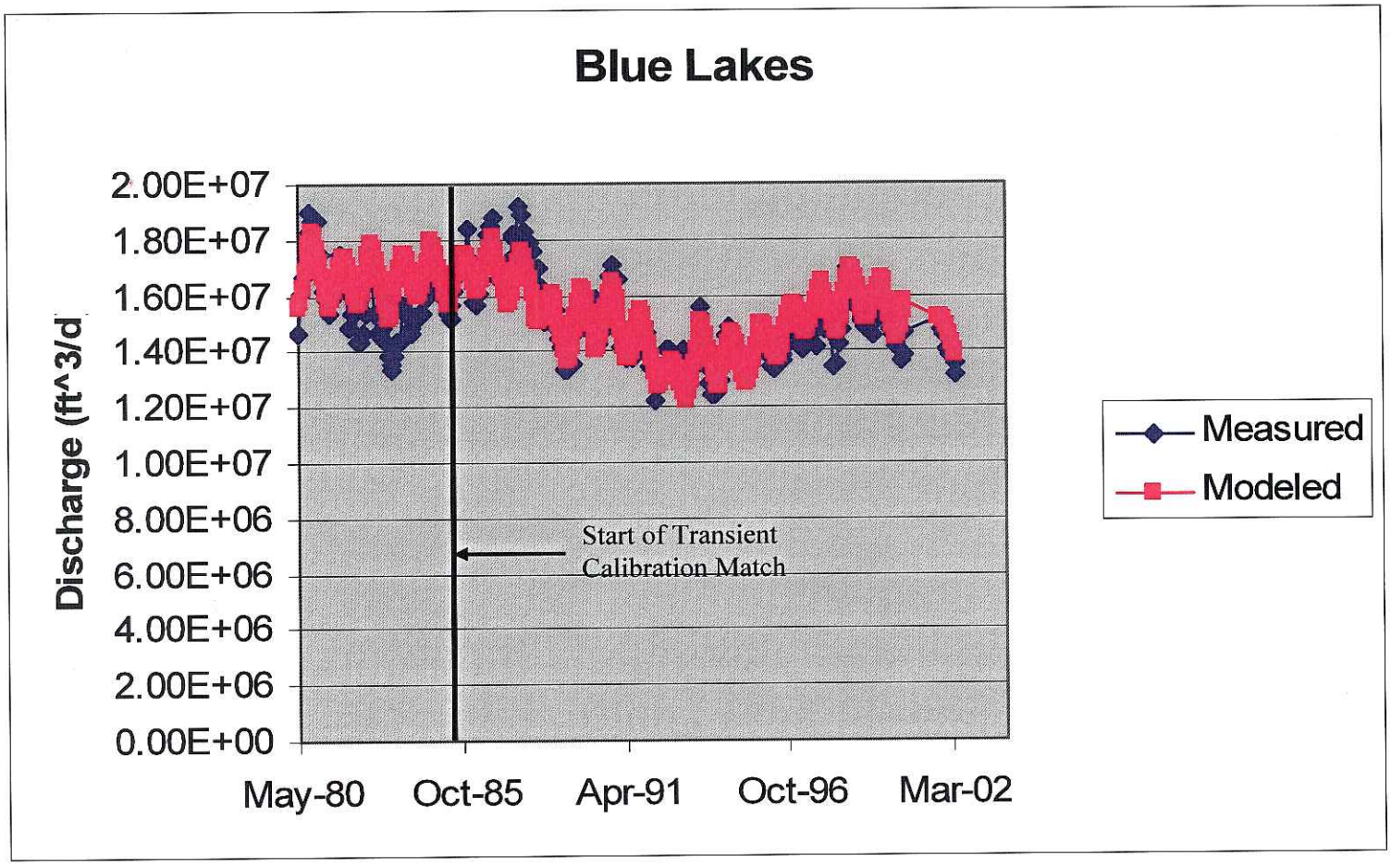


Figure 78. Modeled versus observed spring discharge—Blue Lakes (ft^3/d).

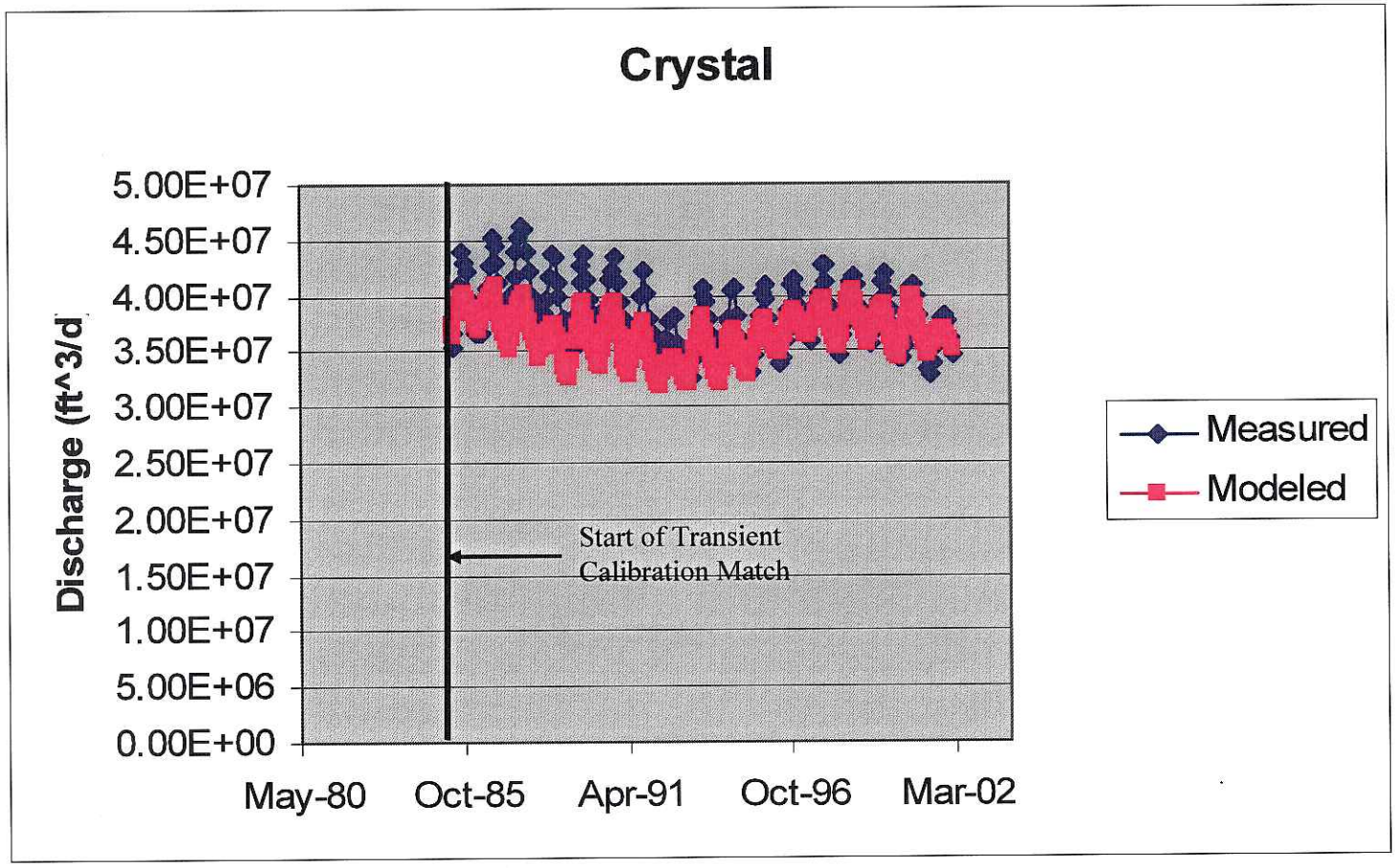


Figure 79. Modeled versus observed spring discharge—Crystal (ft^3/d).

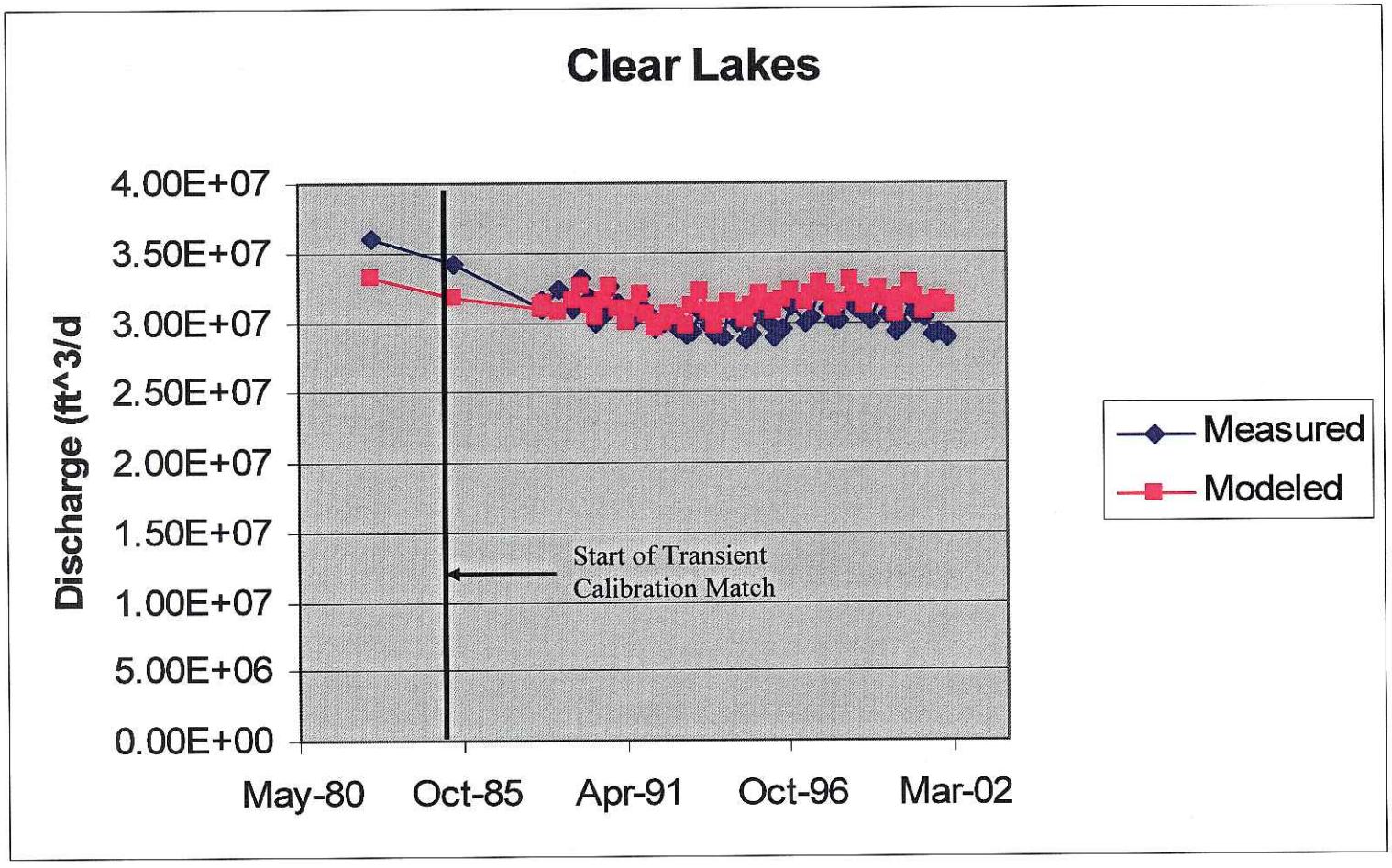


Figure 80. Modeled versus observed spring discharge—Clear Lakes (ft^3/d).

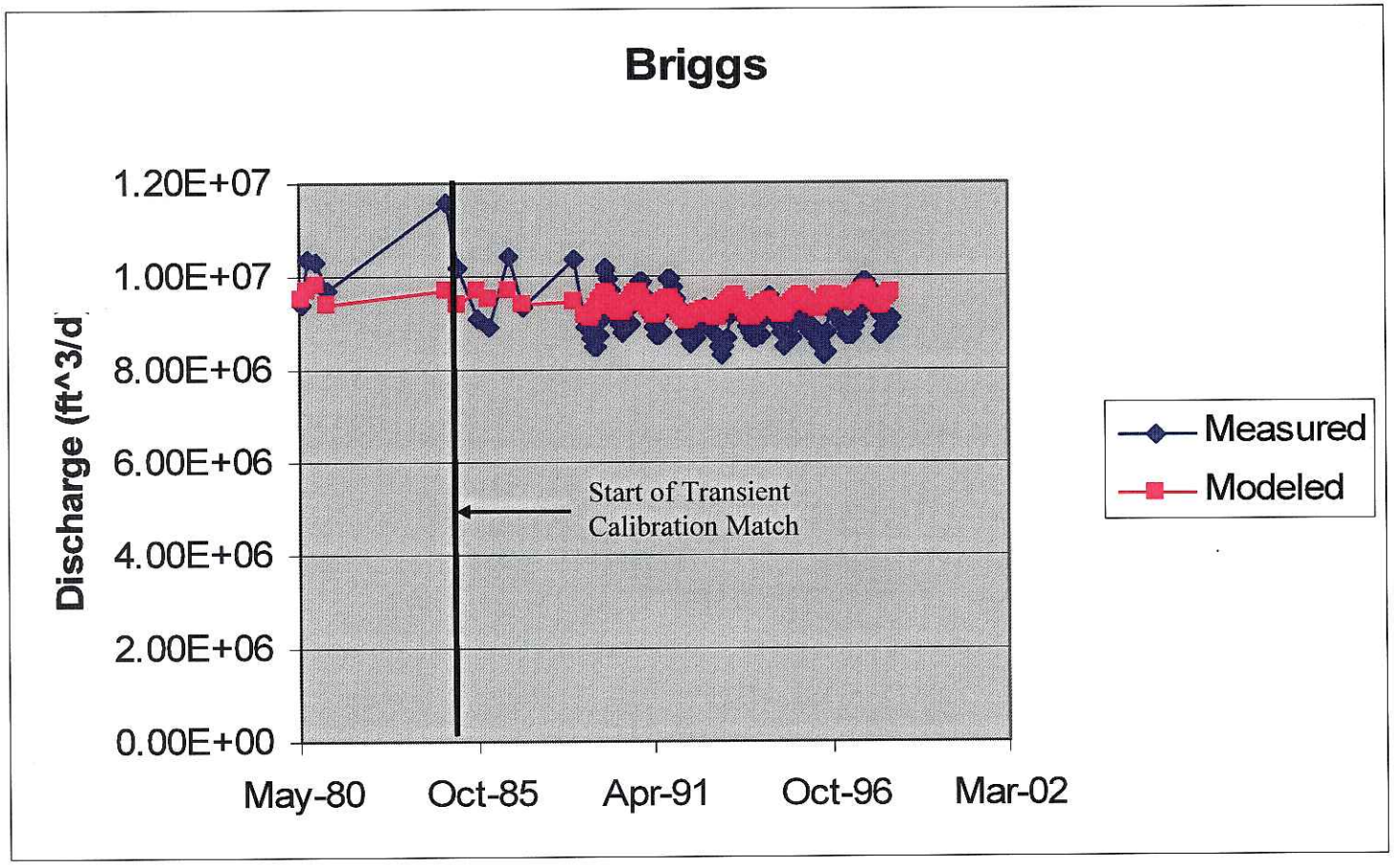


Figure 81. Modeled versus observed spring discharge—Briggs (ft^3/d).

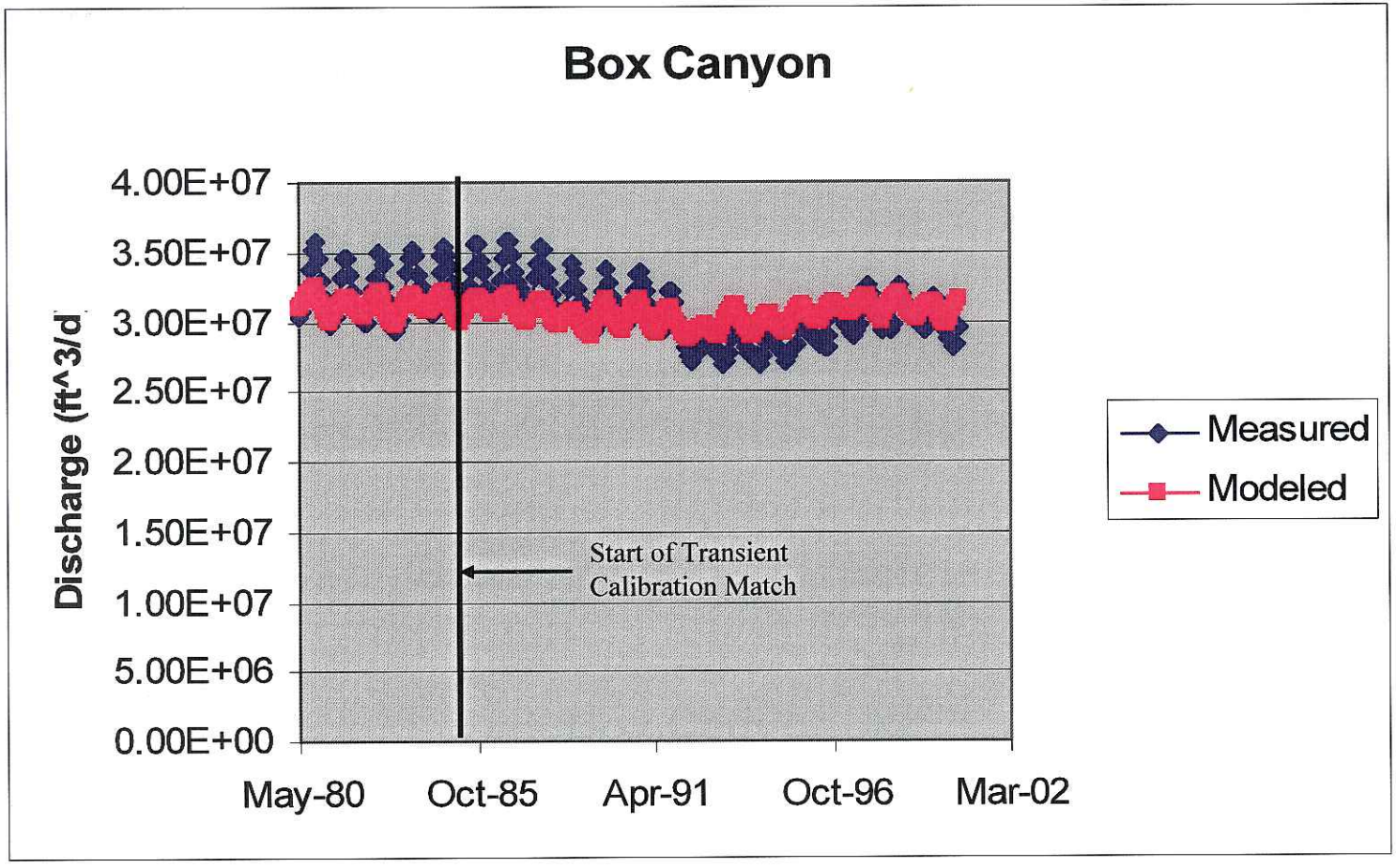


Figure 82. Modeled versus observed spring discharge—Box Canyon (ft^3/d).

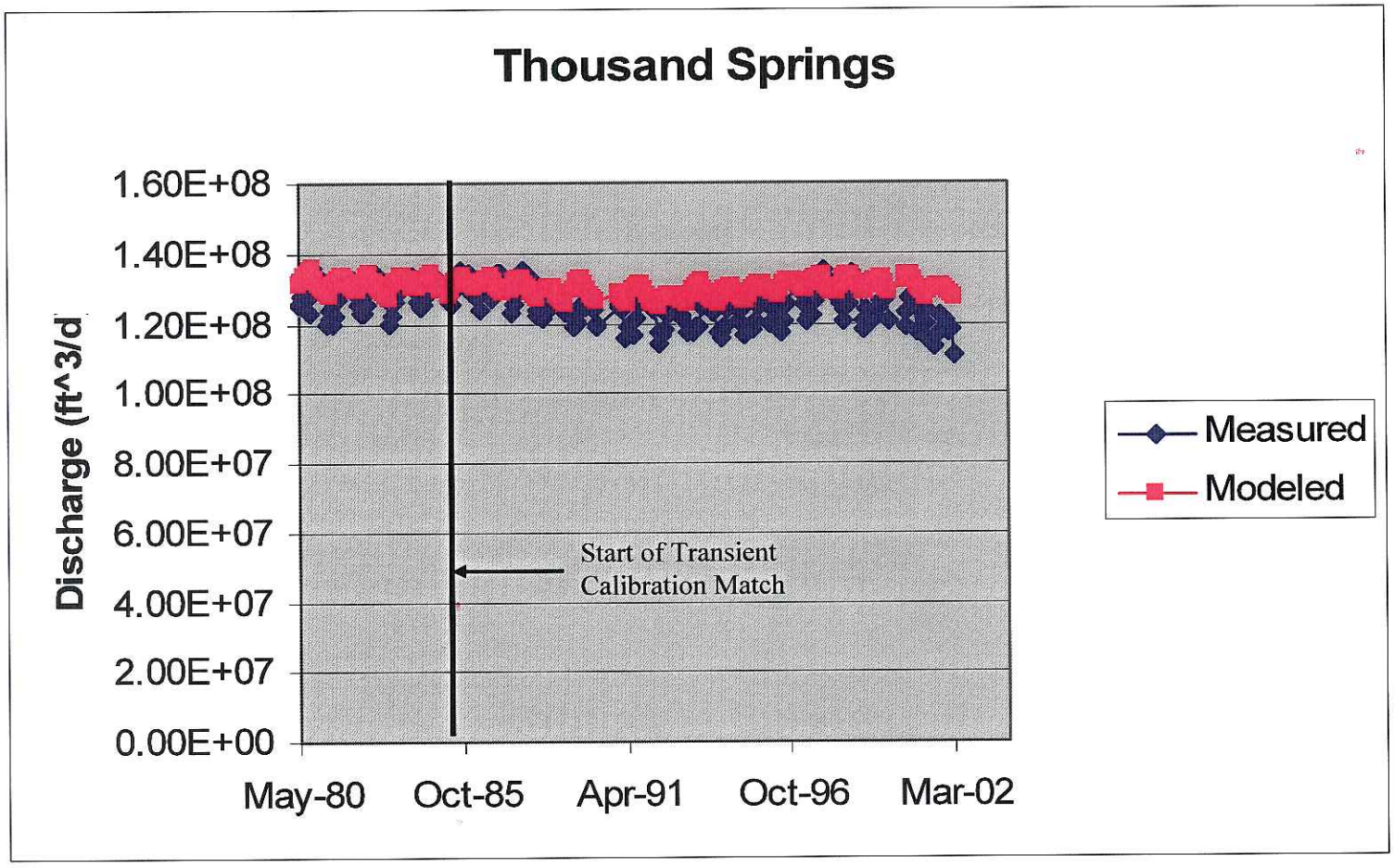


Figure 83. Modeled versus observed spring discharge—Thousand Springs (ft^3/d).

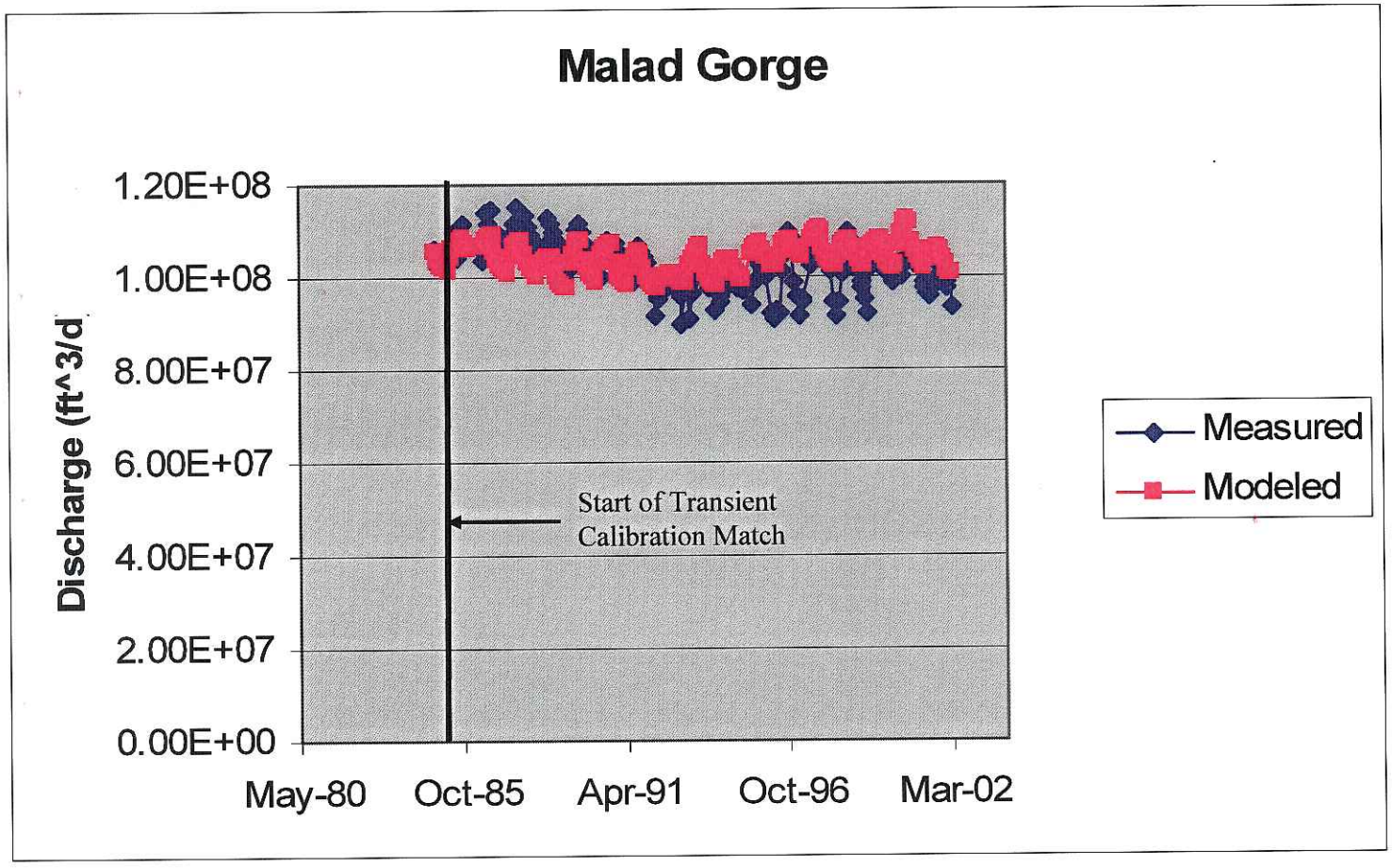


Figure 84. Modeled versus observed spring discharge—Malad (ft^3/d).

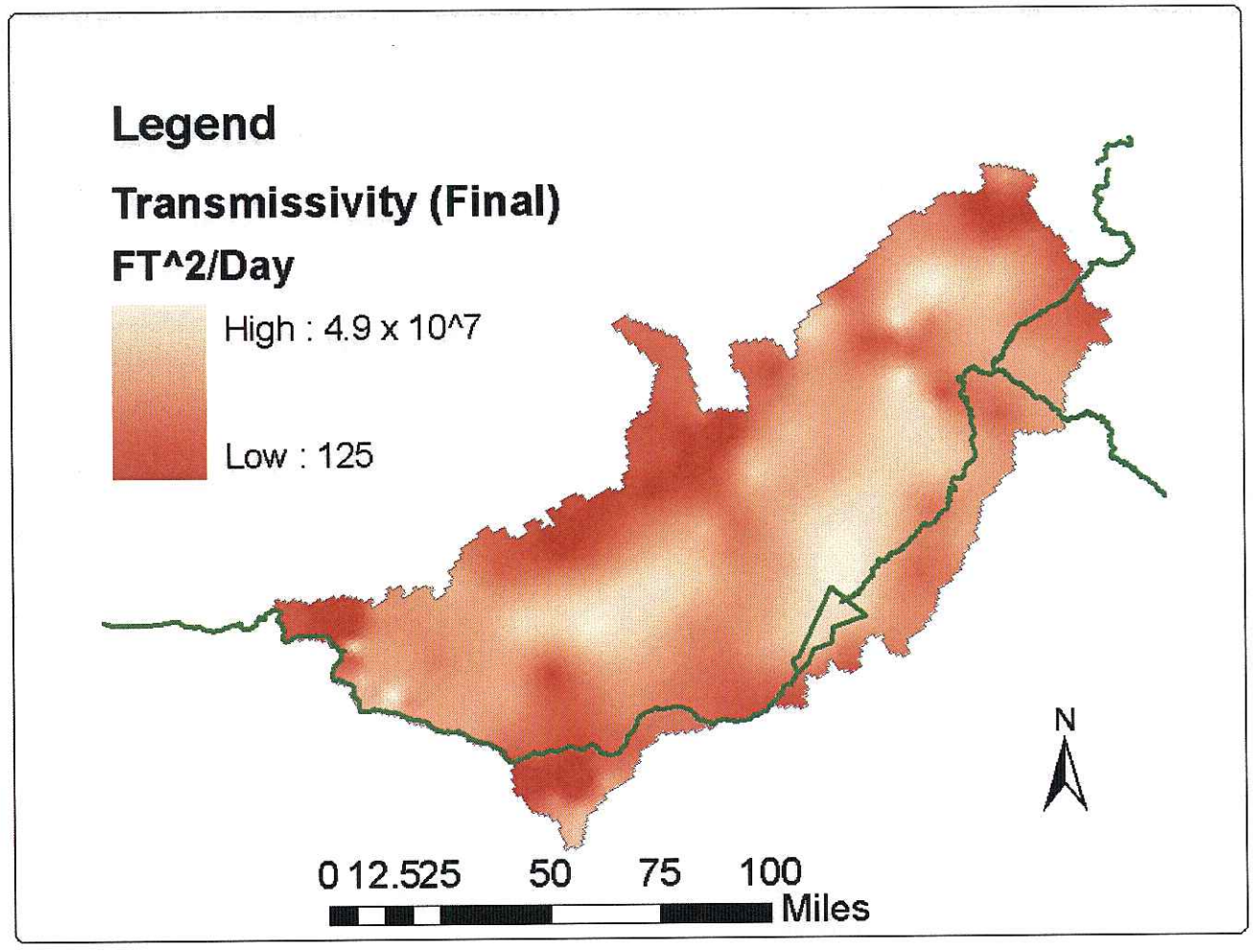


Figure 85. Transmissivity map from coupled steady state/transient calibration.

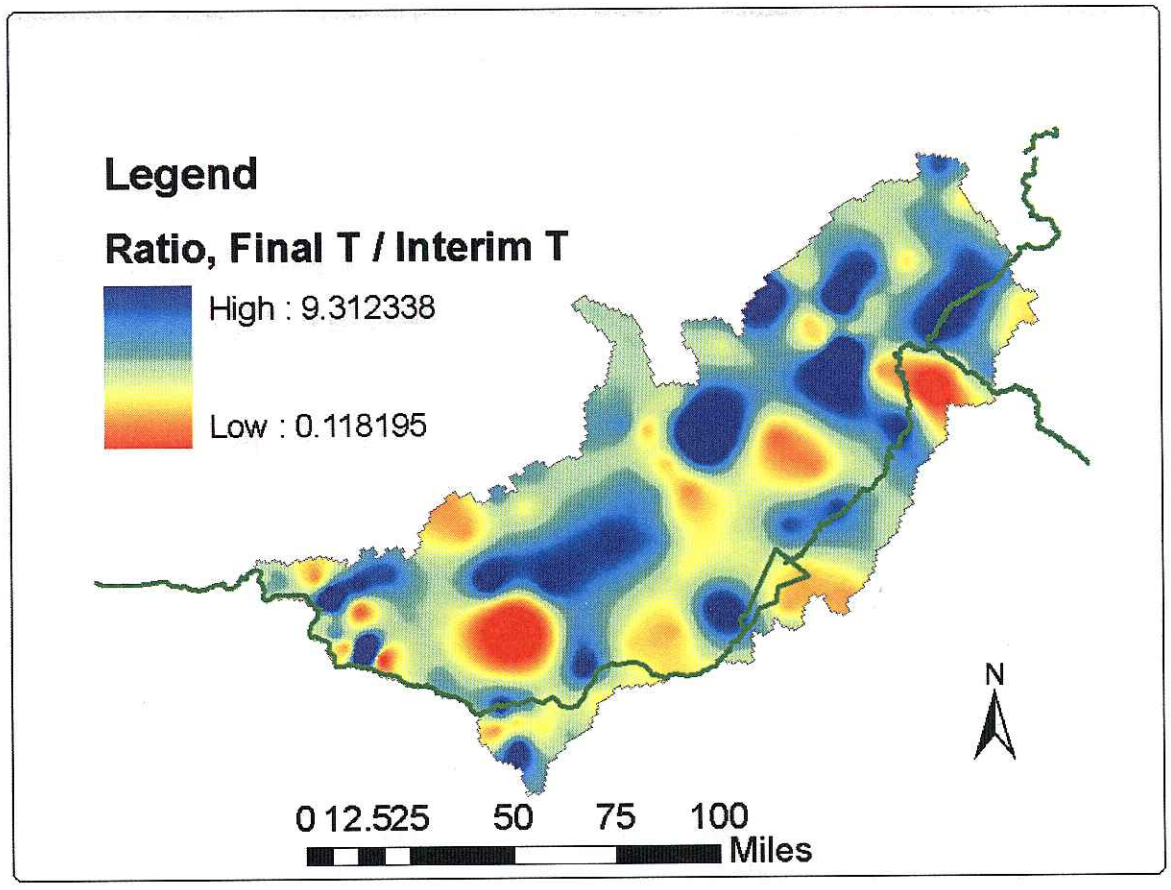


Figure 86. Ratio of final transmissivity to preliminary transmissivity.

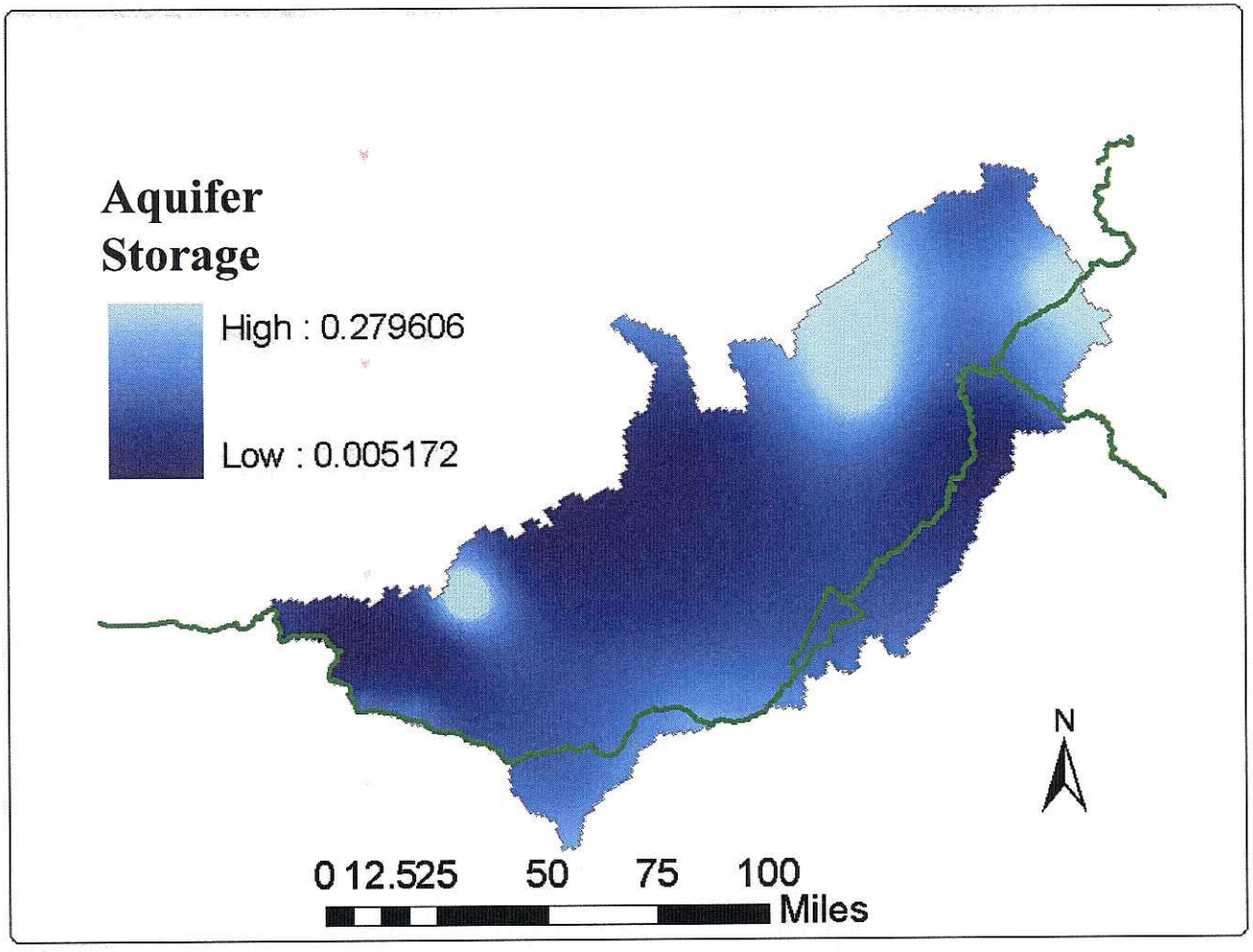


Figure 87. Map of aquifer storage.

# Appendix B Figures

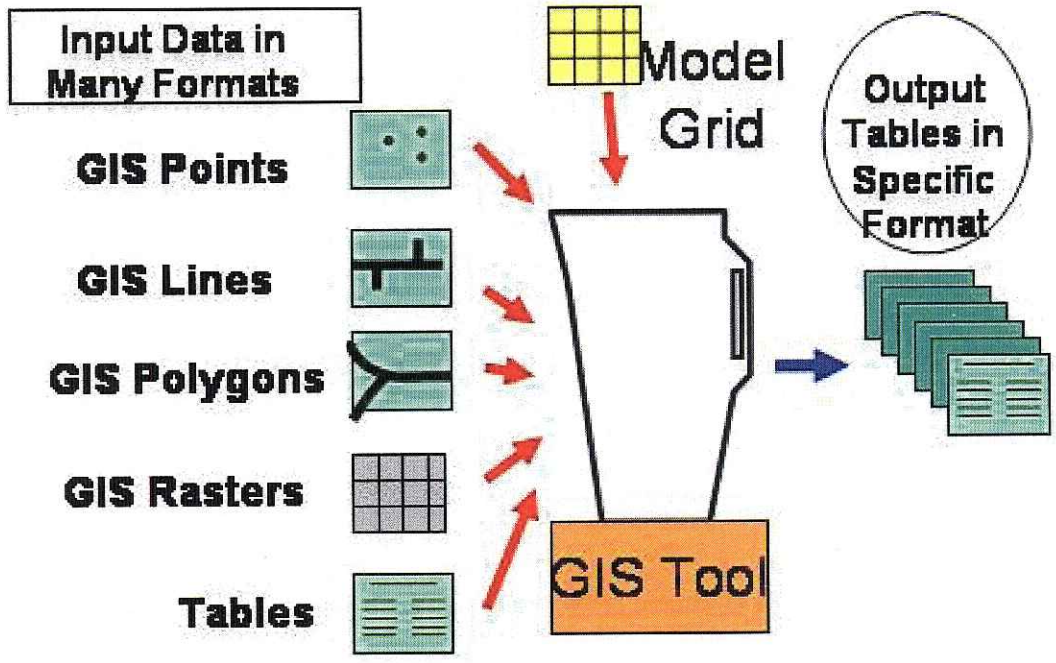


Figure B-1. Conceptual model of GIS component of the GIS/Fortran Recharge Tool.

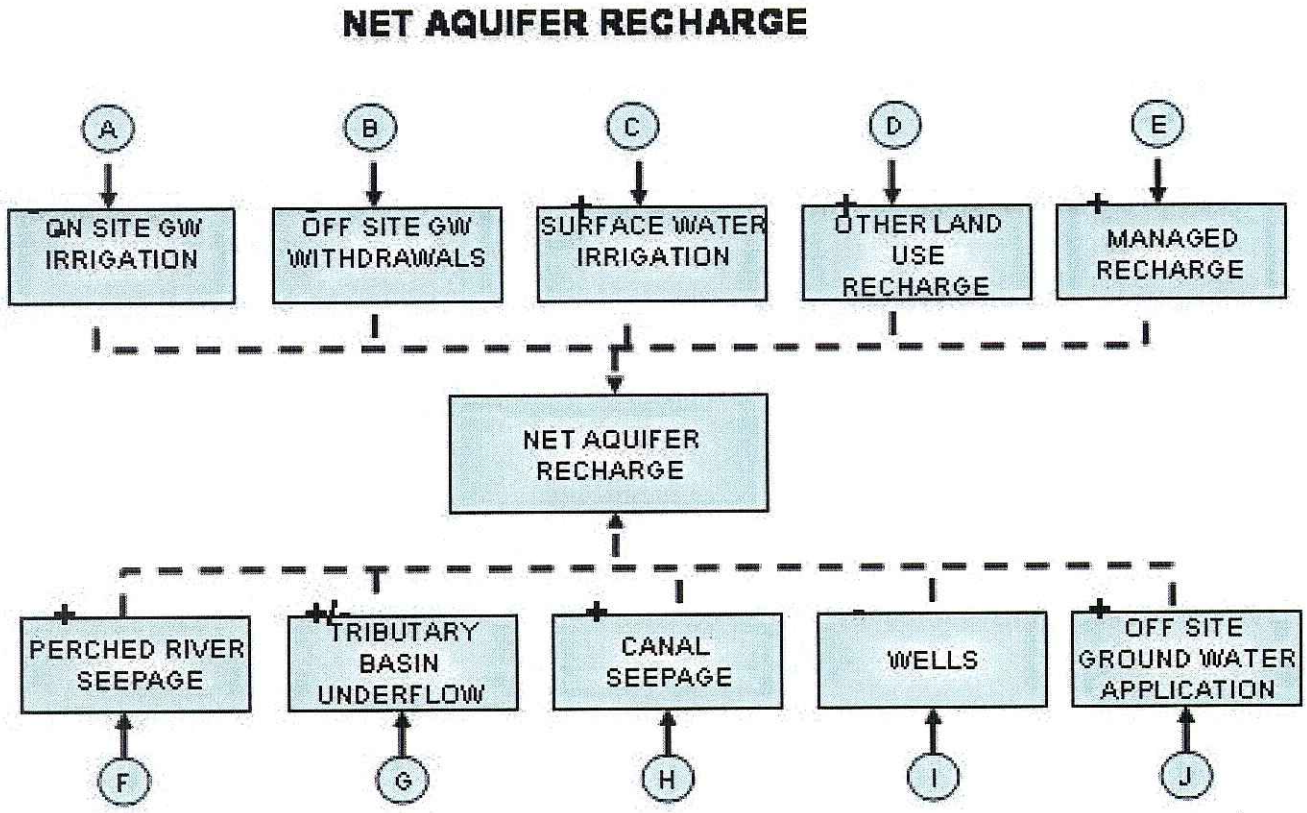


Figure B-2. Schematic of the components of recharge and discharge accounted for In the GIS/Fortran Recharge Tool.

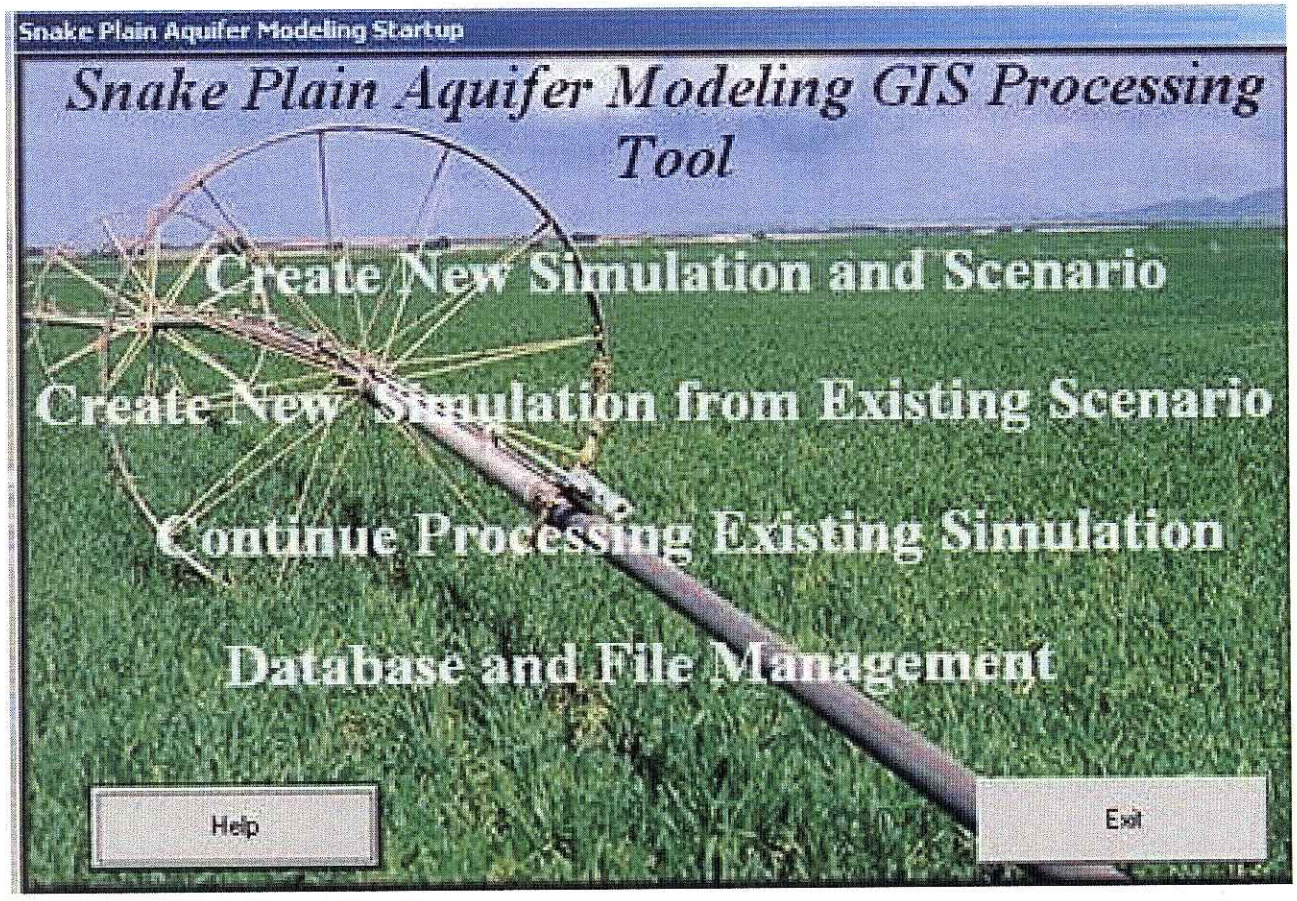


Figure B-3. User interface for the GIS/Fotran Recharge Tool.

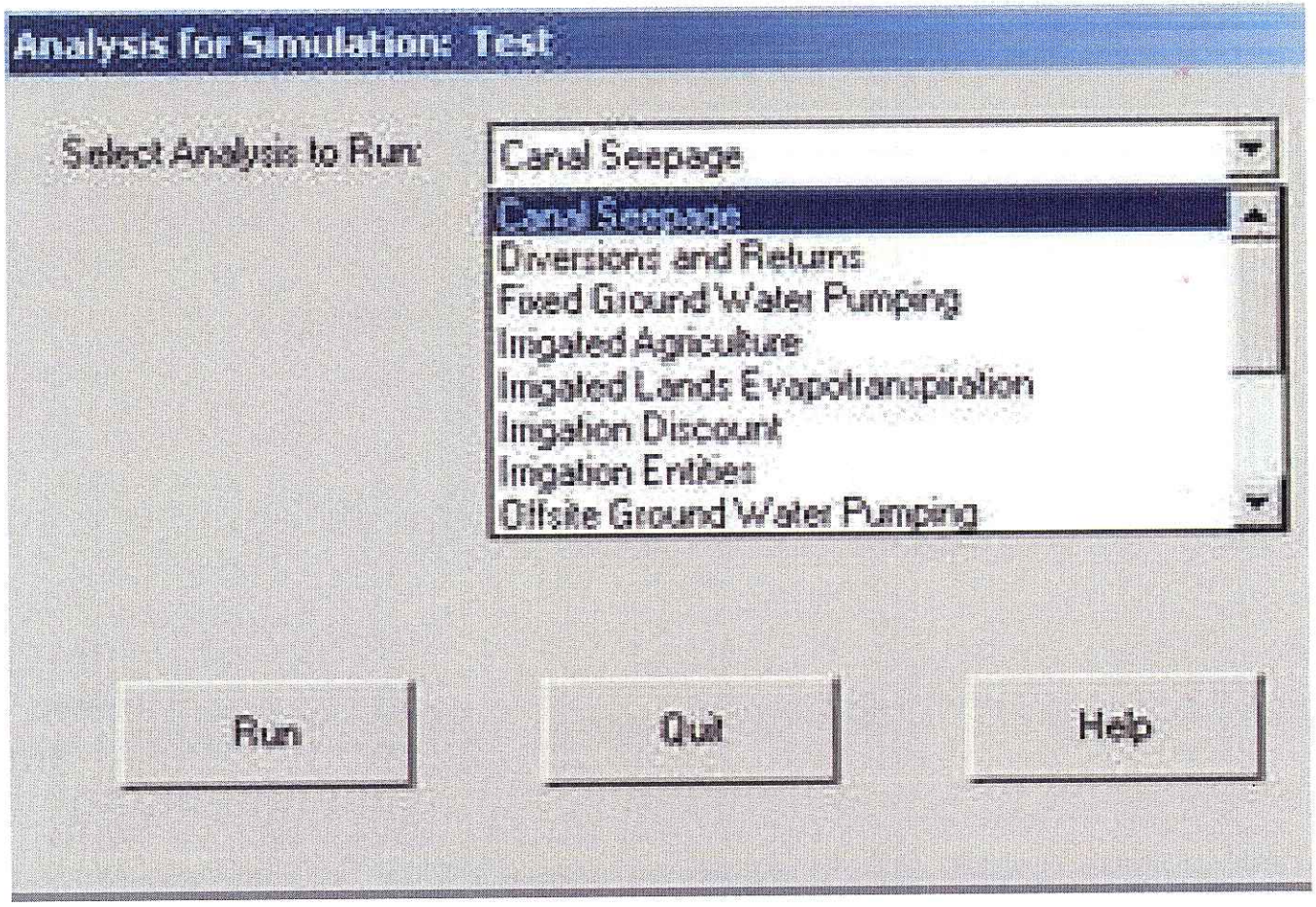


Figure B-4. User options available when building a scenario using the GIS/Fortran Recharge Tool.

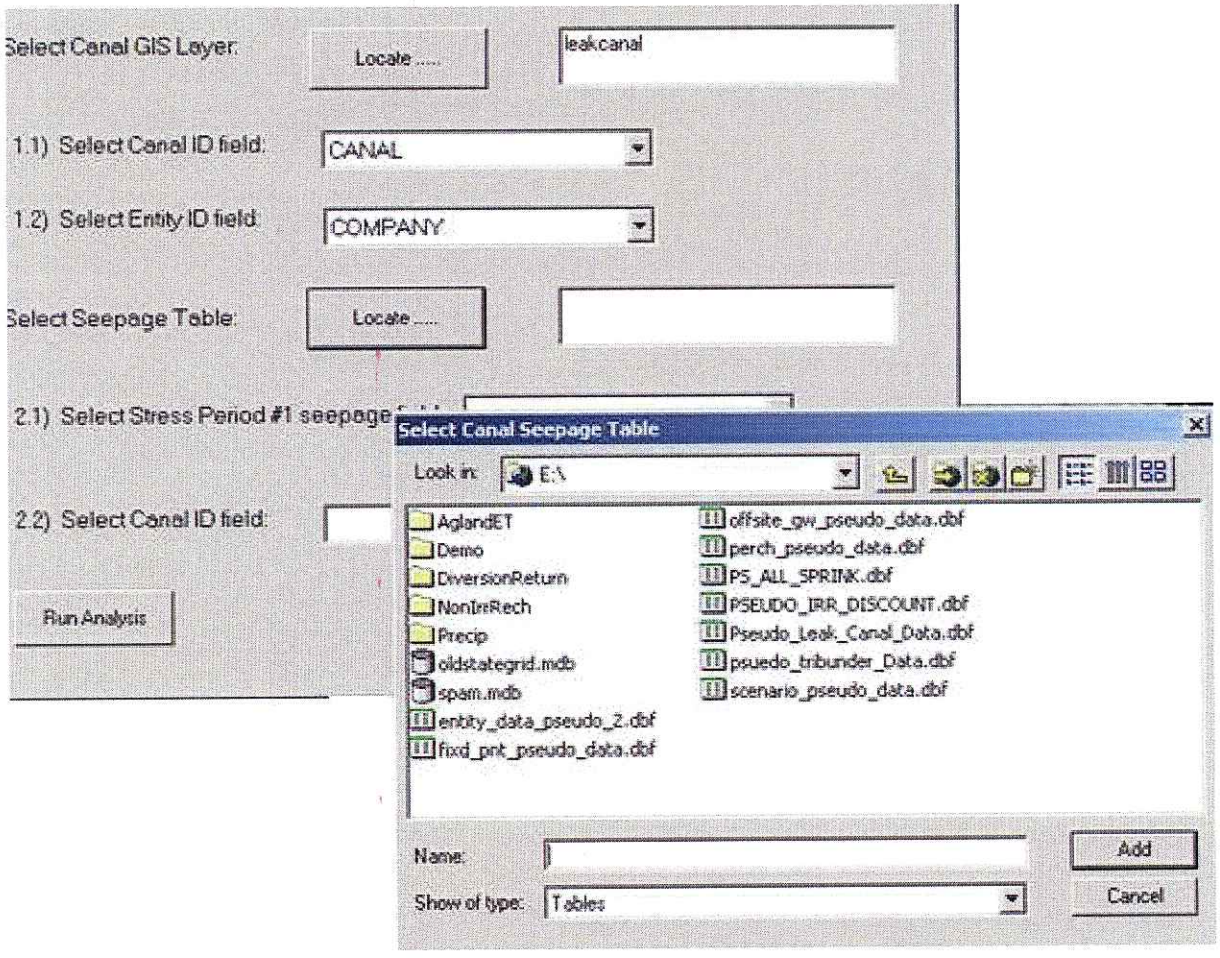


Figure B-5. Sample navigation window of the GIS/Fortran Recharge Program.

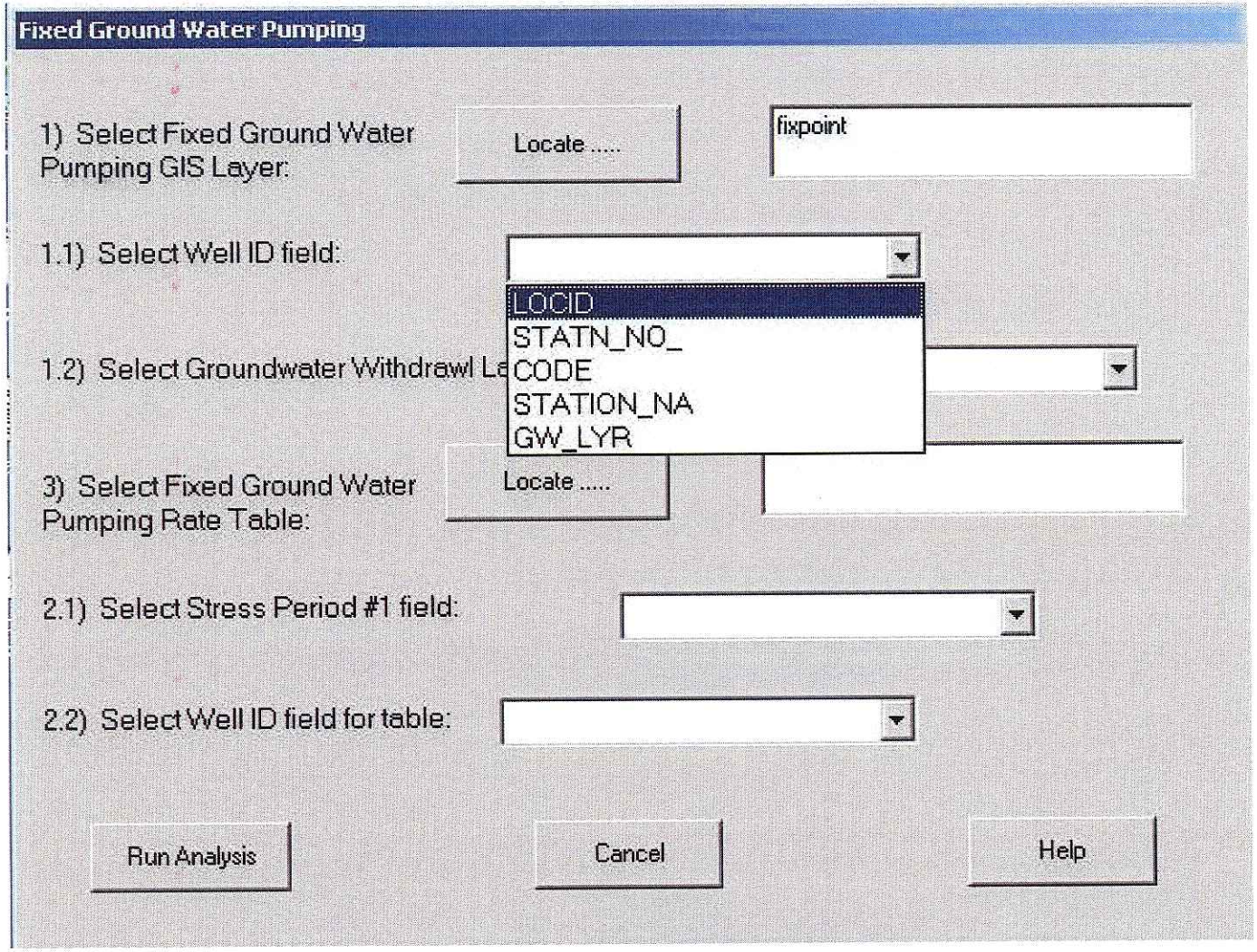


Figure B-6. Example of the data elements available for a specific user selection.

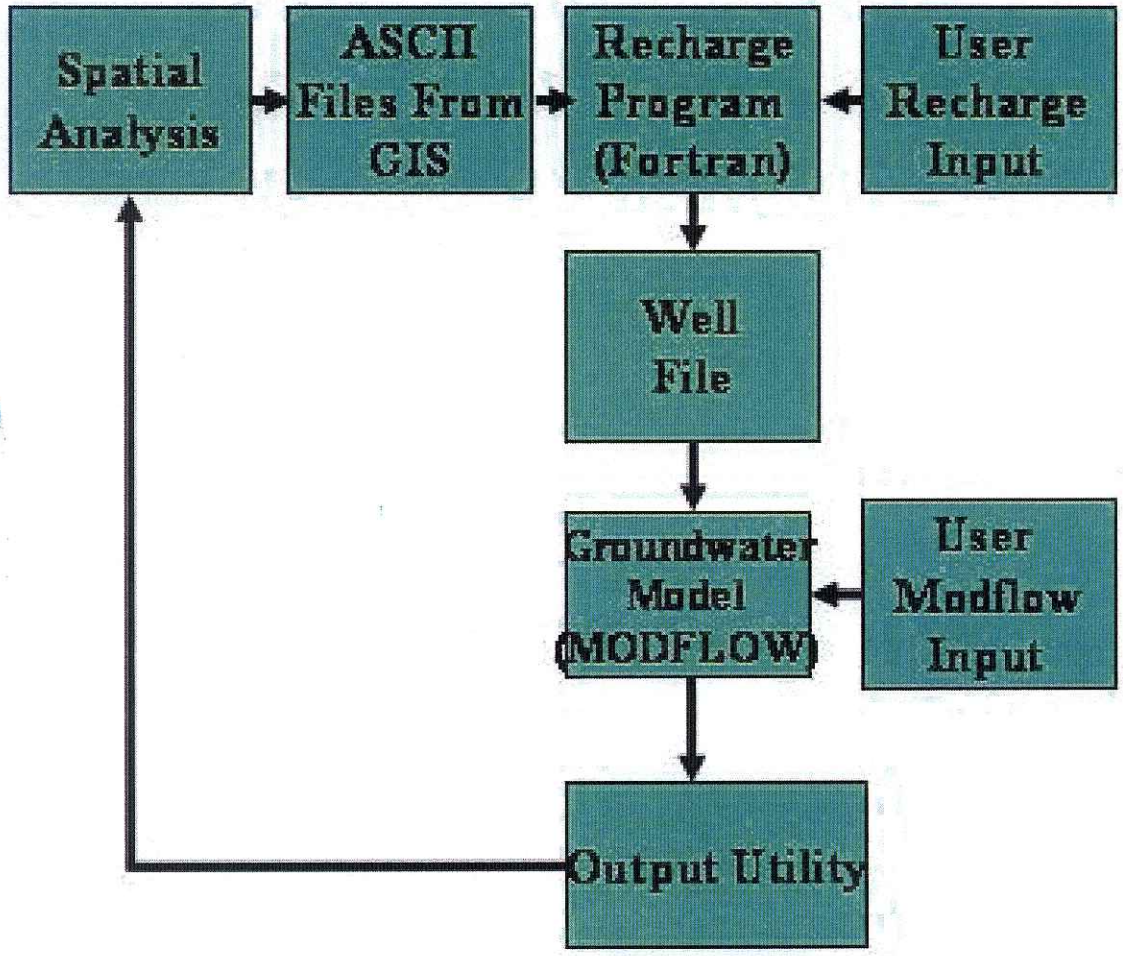


Figure B-7. Running the model without a parameter estimation routine. This schematic shows where the GIS and Fortran components of the recharge program fit in when running a model.

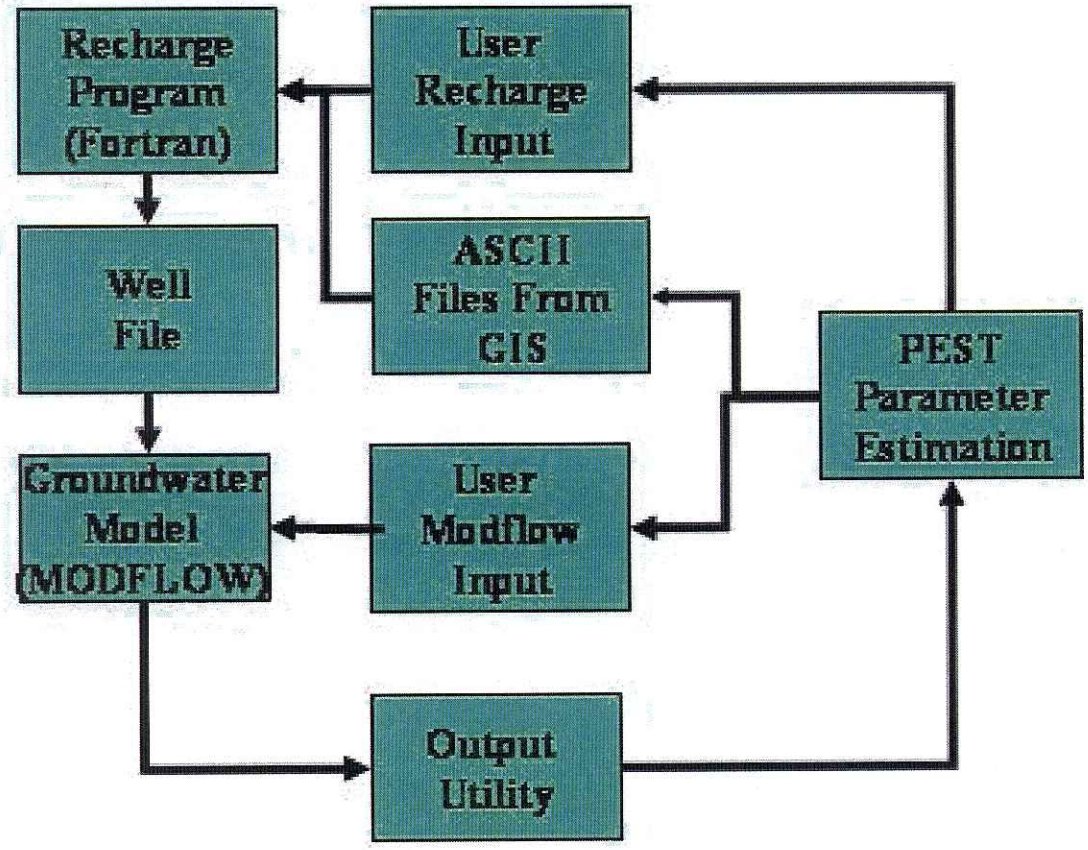


Figure B-8. Running the model with a parameter estimation package (PEST). This schematic shows how the Fortran component of the recharge program fits into the loop.